The Texas Medical Center Library

DigitalCommons@TMC

The University of Texas MD Anderson Cancer Center UTHealth Graduate School of Biomedical Sciences Dissertations and Theses (Open Access)

The University of Texas MD Anderson Cancer Center UTHealth Graduate School of Biomedical Sciences

12-2013

Novel Functions of Cetuximab in EGFR-targeted Therapy: Radiosensitization, Glycolysis Inhibition, and Cellular Redox Status Regulation

Haiquan Lu

Follow this and additional works at: https://digitalcommons.library.tmc.edu/utgsbs_dissertations

 Part of the Medicine and Health Sciences Commons

Recommended Citation

Lu, Haiquan, "Novel Functions of Cetuximab in EGFR-targeted Therapy: Radiosensitization, Glycolysis Inhibition, and Cellular Redox Status Regulation" (2013). *The University of Texas MD Anderson Cancer Center UTHealth Graduate School of Biomedical Sciences Dissertations and Theses (Open Access)*. 395.
https://digitalcommons.library.tmc.edu/utgsbs_dissertations/395

This Dissertation (PhD) is brought to you for free and open access by the The University of Texas MD Anderson Cancer Center UTHealth Graduate School of Biomedical Sciences at DigitalCommons@TMC. It has been accepted for inclusion in The University of Texas MD Anderson Cancer Center UTHealth Graduate School of Biomedical Sciences Dissertations and Theses (Open Access) by an authorized administrator of DigitalCommons@TMC. For more information, please contact digitalcommons@library.tmc.edu.

NOVEL FUNCTIONS OF CETUXIMAB IN EGFR-TARGETED THERAPY: RADIOSENSITIZATION, GLYCOLYSIS INHIBITION, AND CELLULAR REDOX STATUS REGULATION

By

Haiquan Lu, M.S.

APPROVED:

_____

Zhen Fan, M.D. Supervisory Professor

_____

Peng Huang, M.D., Ph.D.

_____

Jonathan M. Kurie, M.D.

_____

Chun Li, Ph.D.

_____

David J. McConkey, Ph.D.

APPROVED:

_____

Dean, The University of Texas

Graduate School of Biomedical Sciences at Houston

NOVEL FUNCTIONS OF CETUXIMAB IN EGFR-TARGETED THERAPY: RADIOSENSITIZATION, GLYCOLYSIS INHIBITION, AND CELLULAR REDOX STATUS REGULATION

A
DISSERTATION

Presented to the Faculty of
The University of Texas
Health Science Center at Houston
and
The University of Texas
MD Anderson Cancer Center
Graduate School of Biomedical Sciences
in Partial Fulfillment
of the Requirements
for the Degree of
DOCTOR OF PHILOSOPHY

by
Haiquan Lu, Master of Sciences
Houston, Texas

December, 2013

DEDICATION

To my beloved parents, whose encouragement and support gave me the confidence to accomplish all that I have today;

And to my darling wife, who always understood and supported me despite all the decisions I have made.

ACKNOWLEDGEMENTS

First and foremost, I would like to show my deepest appreciation to my mentor, Dr. Zhen Fan, who is not only an expert in the field of cancer target therapy, but also an outstanding teacher. Thanks for his unwavering and patient guidance and encouragement since the first time we have met, I learned how to be a scientist and finished my first step. His scientific curiosity and knowledge kept inspiring me in the past five years, and his devotion to science will be a paradigm for me in all my life.

I would like to express my special gratitude to some senior members in our lab. Without their help, I would never have reached fruition. When I joined in the lab, I did not have any lab experience before. Dr. Yang Lu, our lab manager, taught me many techniques with her great patience, starting from the most basic techniques such as cell culture and western blot. She made great efforts to organize all the orders and reagents in our lab and made our daily experiments hassle-free. Dr. Xinqun Li, an instructor in our lab, inspired me a lot with his smart ideas and impressive talks. Ke Liang, a research investigator in our lab, helped me a lot with his experience in radiation and animal work. All of them are so unselfishness that they are always willing to share their ideas and experience.

I would also like to thank all my friends and colleagues, including Midan Ai, Songbo Qiu, Jing Xu, Zhongguang Luo, Bharat K Chaganty, who helped me throughout all my research projects. And I would give my sincere thanks to my various committee members, Drs. Paul Chiao, Peng Huang, Jonathan M. Kurie, Chun Li, David J McConkey, Funda Meric-Bernstam, and Dos D. Sarbsssov, for their suggestions and continuous support on my project in the past five years.

Finally, I would like to thank all my friends and family members, for their continuous encouragement and support of my dreams. They shared all my happiness and more importantly, stayed with me and helped me out in every of my tough time. This was a work that would not be possible without them who stood on my side forever.

NOVEL FUNCTIONS OF CETUXIMAB IN EGFR-TARGETED THERAPY: RADIOSENSITIZATION, GLYCOLYSIS INHIBITION, AND CELLULAR REDOX STATUS REGULATION

Publication No. _____

Haiquan Lu, M.S.

Supervisory Professor: Zhen Fan, Ph.D.

Epidermal growth factor receptor (EGFR) is overexpressed in the majority of head and neck cancers. The anti-EGFR antibody cetuximab has been approved by the FDA for the treatment of head and neck cancers, however, only a small fraction of patients respond to cetuximab treatment. Further investigation to understand the mechanisms underlying cetuximab-mediated EGFR-targeted therapy and to develop novel therapeutic strategies to improve the efficacy of cetuximab is urgently needed. In the present study, we elucidated the mechanism of cetuximab in radiosensitization, and discovered novel functions of cetuximab in glycolysis inhibition and cellular redox status regulation. We found that cetuximab inhibits radiation-induced hypoxia inducible factor 1 (HIF-1), which is required for the radiosensitization role of cetuximab. We also found that cetuximab inhibits glycolysis in cancer cells through downregulation of HIF-1, which explains the cytostatic effect of cetuximab in the perspective of cancer metabolism. In addition, we discovered a novel function of cetuximab in decreasing the anti-oxidant capacity of cancer cells through downregulating glutamine transporter ASCT2, which is in an EGFR-kinase activity inhibition independent manner. Applications of these mechanism studies lead to findings of novel therapeutic targets to improve cetuximab

responses and/or overcome cetuximab resistance. We proved that targeting HIF-1 improves response of cetuximab-resistant cancer cells to the combination treatment of cetuximab and radiation, while targeting lactate dehydrogenase A (LDH-A) restores the role of cetuximab in cell cycle arrest in cetuximab-resistant cancer cells. Moreover, targeting pyruvate dehydrogenase kinase 1 (PDK1), in combination with cetuximab, leads to a synergetic and synthetic lethality in cancer cells, which bypasses most currently known cetuximab resistant mechanisms. In summary, our findings provide novel mechanistic insights into cetuximab-mediated EGFR targeted therapy and suggest novel therapeutic strategies for enhancing the response of cancer patients to cetuximab treatment.

TABLE OF CONTENTS

List of Figures

List of Tables

ABBREVIATIONS

1,9 PA	1,9-Anthrapyrazolone
ARNT	Aryl hydrocarbon receptor nuclear translocator
ATP	Adenosine-5'-triphosphate
bHLH	basic helix-loop-helix
CHX	Cycloheximide
DCA	Dicholoroacetate
EAA	Essential amino acid
ECAR	Extracellular acidification rates
EGF	Epidermal growth factor
EGFR	Epidermal growth factor receptor
ETC	Electron transport chain
FDA	Food and Drug Administration
FIH-1	Factor inhibiting HIF-1
GCS	γ-glutamylcysteine synthetase
GSH	Reduced form of glutathione
GSSG	Oxidative form of glutathione
HIF	Hypoxia inducible factor
HNSCC	Head and neck squamous cell carcinoma
HPV	human papillomavirus
HRE	Hypoxia response element
IR	Ionizing radiation
IVIS	in vivo imaging system

LDH-A	Lactate dehydrogenase A
NAC	N-acetyl-cysteine
NEAA	non-essential amino acid
OCR	Oxygen consumption rate
ODD	oxygen degradation dependent
PAS	PER-ARNT-SIM
PDH	Pyruvate dehydrogenase
PDK1	Pyruvate dehydrogenase kinase 1
PEITC	Phenethyl isothiocyanate
PHD	Prolyl hydroxylase domain
PTB	phosphotyrosine binding
ROS	Reactive oxygen species
SH2	Src homology 2
SOD	Superoxide dismutase
TAD	Transactivation domain
TGFα	Transforming growth factor α
TMRM	Tetramethyl rhodamine methyl ester
VHL	von Hippel–Lindau
Y	Tyrosine

Chapter 1 Introduction

1.1 Head and neck squamous cell carcinoma (HNSCC)

Head and neck cancer is a biologically similar group of epithelial cancers. Primary tumors can occur in the lip, oral cavity, nasal cavity, paranasal sinuses, pharynx, and larynx. Head and neck cancer is the sixth leading type of cancer by incident with about 600,000 new cases each year worldwide [1]. The majority of head and neck cancers are squamous cell carcinoma. The five-year survival rate for patients with HNSCC is approximately 40-50% [2]. The most important risk factors for head and neck cancers are alcohol consumption and tobacco use, which have a synergetic effect [3, 4]. Human papillomavirus (HPV) infection is also considered to be a risk factor [5].

1.2 Conventional therapy and targeted therapy in HNSCC

Conventional treatments for HNSCC include surgery, radiotherapy, chemotherapy, and in combination chemo-radiotherapy [6, 7]. For patients at stage I/II when they are diagnosed, they are treated with either surgery or radiotherapy [8]. Patients with recurrent or metastatic HNSCC will be treated with chemotherapy plus radiotherapy as the standard of care [9, 10].

Current conventional therapies are often nonselective and are associated with systemic toxicities that often reduce compliance and prevent timely completion of therapy. Targeted therapies in HNSCC may minimize toxicity rates and improve survival. Potential targeted therapies in HNSCC mainly target cellular pathways of carcinogenesis [11, 12]. The signaling pathways deregulated in HNSCC and certain key components are being targeted with biological agents (Table 1).

Targeting Agent	Drug	Clinical development phase
EGFR MAbs	Cetuximab, Panitumumab	Approved, Phase III
EGFR tyrosine kinase inhibitors	Gefitinib, Erlotinib	Phase III
VEGFR inhibitors	Bevacizumab, Vandetanib	Phase III, Phase II
Multiple kinase inhibitors	Sorafenib, Sunitinib, Lapatinib	Phase II
Src kinase inhibitor	Dasatinib	Phase II
mTOR inhibitors	Everolimus, Temsirolimus	Phase II
COX inhibitor	Celecoxib	Phase I
CDK inhibitors	Seliciclib, Flavopiridol	Phase I
Heat shock protein inhibitor	Tanespimycin	Phase I
Proteasome inhibitor	Bortezomib	Phase II
Histone acetylation inhibitors	Vorinostat, Romidepsin	Phase II

Table 1. Targeted biological drugs under development.

1.3 Epidermal growth factor receptor (EGFR)

The epidermal growth factor receptor (EGFR) is a 170-kd transmembrane glycoprotein and belongs to human EGF receptor (HER) family [13]. It is composed of an extracellular domain that provides ligand-binding sites, a single transmembrane domain and a cytosolic region that contains a juxtamembrane domain, a tyrosine kinase domain and a C-terminal tail segment. EGFR is activated by binding with its specific ligands, including epidermal growth factor (EGF) and transforming growth factor α (TGFα) [14]. Binding with ligands causes the structural changes of EGFR extracellular domain and leads to dimerization of two receptor monomers. Receptor dimerization leads to activation of intrinsic tyrosine kinase domains and subsequent autophosphorylations on multiple tyrosine (Y) residues of the C-terminal tail segments, including Y992, Y1045, Y1068, Y1086, Y1148 and Y1173 [15]. These tyrosine autophosphorylations create docking motifs for different cytosolic signaling molecules containing SH2 (Src homology 2) and PTB (phosphotyrosine binding) domains. Through recruiting these molecules, EGFR initiates several downstream signaling cascades including the RAS-RAF-MEK-ERK pathway, the PI3K-AKT pathway, the PLCγ-PKC pathway, and the STATs pathway (Figure 1) [16]. Activation of these cell signalings finally modulates cell proliferation, migration, adhesion, invasion, cell cycle progression and differentiation.

More than 90% of HNSCCs express a high level of EGFR on the cell surface [17, 18]. Overexpression of EGFR has been correlated with more aggressive phenotype, increased resistance to standard chemotherapy and radiation, and poorer clinical outcome [19-25]. EGFR signaling network has emerged as a key target in HNSCC.

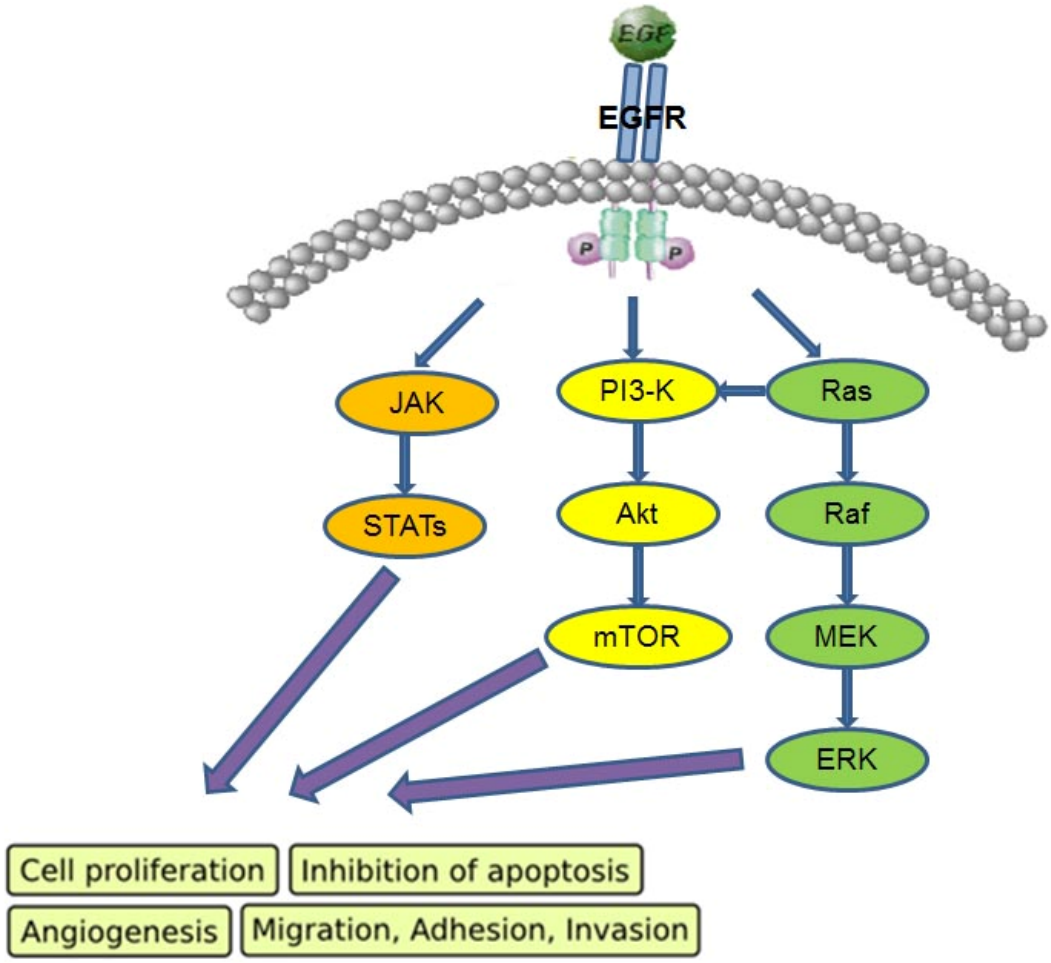

Figure 1. Downstream signaling cascade of EGFR.

1.4 Cetuximab

Cetuximab (Erbitux®) is a human-murine chimeric monoclonal antibody directly against human EGFR [26]. Cetuximab binds with EGFR competitively with EGF and TGF-α, and its affinity for the receptor is 5- to 10-fold higher than that of endogenous ligands [26, 27]. Binding of cetuximab to EGFR inhibits ligand-induced dimerization and activation of the receptor [28]. Furthermore, it stimulates internalization and degradation of the receptor [29], resulting in a decreased responsiveness of EGFR-bearing cells to endogenous ligands. Cetuximab-induced blockade of receptor-dependent signal transduction pathways leads to a number of antitumor effects that have been demonstrated in preclinical studies, including inhibition of cell growth and survival, and inhibition of angiogenesis and metastasis [30-35].

In randomized, open-label, multinational, phase III clinical trials, cetuximab plus radiotherapy significantly improved the duration of locoregional control (primary endpoint) compared with radiotherapy alone in patients with locally advanced HNSCC (Bonner trial) [23], while cetuximab plus first-line platinum-based chemotherapy significantly improved overall survival (primary endpoint) compared with first-line platinum-based chemotherapy alone in patients with recurrent and/or metastatic HNSCC (EXTREME trial) [36]. Based on the results above, cetuximab was approved by the FDA in March 2006 for use in combination with radiation therapy for treating HNSCC or as a single agent in HNSCC patients who have had prior platinum-based therapy.

1.5 Hypoxia inducible factors (HIFs)

It has been estimated that 50–60% of solid tumors contain hypoxic tissues that develop as a result of an imbalance between limited oxygen supply and fast consumption in proliferating tumors [37]. Tumor hypoxia has been known to contribute to tumor radioresistance and poor clinical outcomes of human cancers for over half century [38, 39]. Hypoxia inducible factors (HIFs) are essential mediators of the cellular oxygen-signaling pathway [40]. HIFs are the members of the PAS (PER-ARNT-SIM) family of basic helix-loop-helix (bHLH) transcription factors. To date, three HIFs (HIF-1, -2, and -3) have been identified that regulate transcriptional programs in response to hypoxia (Figure 2).

The active HIF transcription factors are heterodimers composed of an oxygen-sensitive α subunit and a constitutively expressed β subunit, also known as ARNT. All α subunit of HIFs have bHLH, PAS, and ODD (oxygen degradation dependent) domain, and share 50-60% homology with each other. ARNT is the general binding partner for all three α subunits of HIFs [41, 42]. ARNT does not have an ODD domain, and is therefore constitutively expressed in all tissues under aerobic conditions.

Under normoxic condition, HIFs are degradation by the von Hippel–Lindau (VHL) tumor suppressor, pVHL, the substrate recognition component of an E3 ubiquitin ligase complex that interacts with HIF-α in an oxygen-dependent manner [43]. Prolyl-4-hydroxylase domain (PHD)-containing proteins hydroxylate conserved proline residues within the HIF-α-ODD domain and mediate pVHL binding and degradation of HIF-α [44, 45]. Under hypoxic condition, HIF-α subunits are stabilized and translocate to the nucleus, where they form heterodimer with β subunit and bind to hypoxia response

elements (HREs) of HIF target genes (Figure 3). Once stabilized, the HIF heterodimer activates transcription by recruiting the transcriptional activators p300 and CBP. The interaction between HIF and p300/CBP is also regulated in an oxygen-dependent manner by factor inhibiting HIF-1 (FIH-1) [46]. FIH hydroxylates asparagine residues located within the HIF-α C-terminal transactivation domain (CTAD) and prevents p300/CBP binding [47].

The activities of HIFs can also be regulated through its protein synthesis pathway in an oxygen-independent manner. Growth factors binding to tyrosine kinase receptor will activate PI3K-Akt-mTOR pathway and MAPK pathway [48-50]. Activation of these two pathways will cause the activation of p70 S6 kinase (S6K), and inactivation of the eukaryotic translation initiation factor 4E (eIF-4E) binding protein (4E-BP1), and lead to the increase of translation rate of a subset of mRNA to protein, including HIFs.

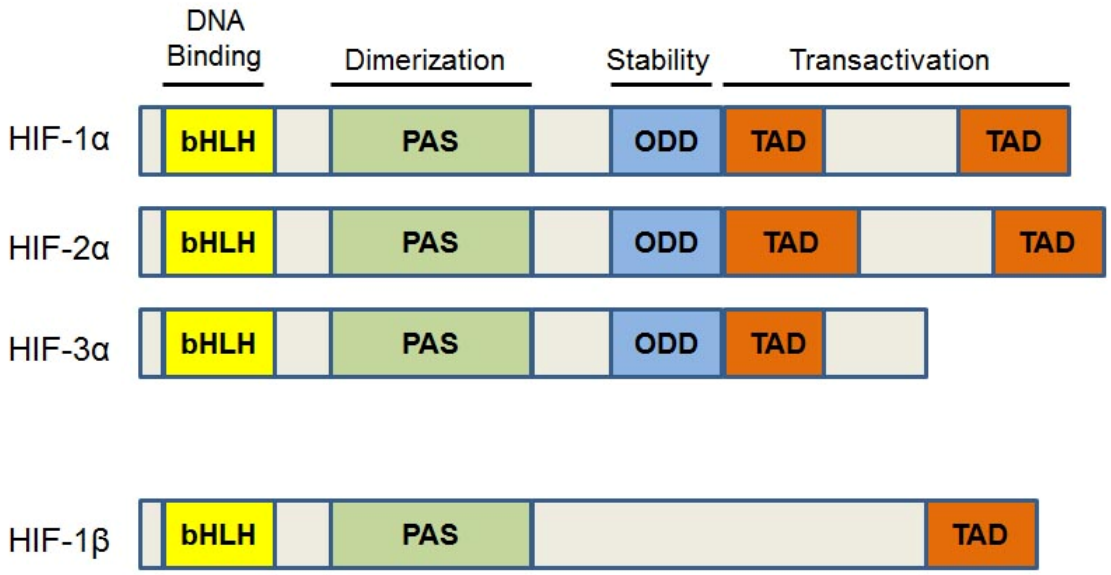

Figure 2. Schematic representation of HIF family member protein domains.

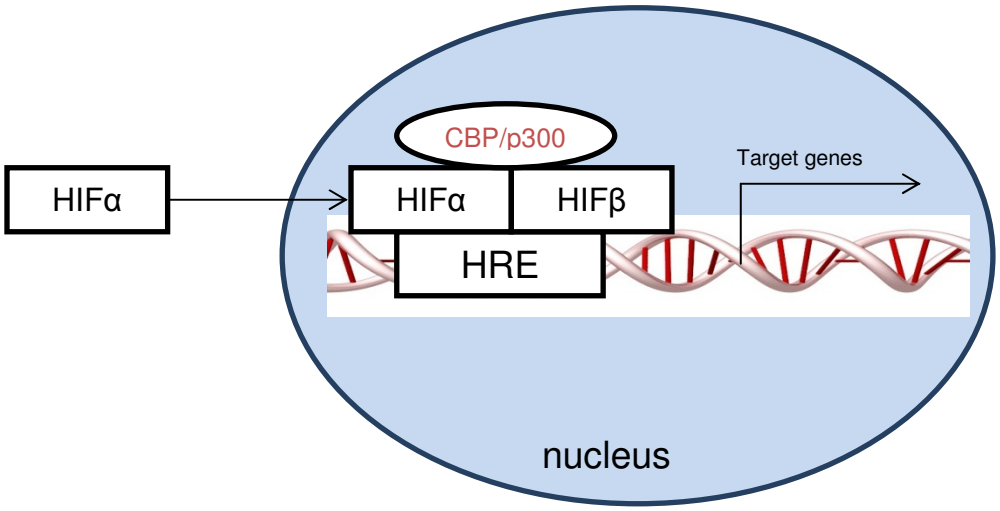

Figure 3. Activation of HIFs by hypoxia.

1.6 HIF-1 function in cancer

HIF-1 was the first HIF family members to be cloned and is the best understood isoform [51]. It is considered to be the master regulator of cellular responses to hypoxia [52]. As described in 1.5, HIF-1 is a heterodimer that consists of a constitutively expressed HIF-1β subunit and a HIF-1α subunit, the expression of which is highly regulated. As a transcription factor, HIF-1 directly regulates more than 100 genes that are related with tumorigenesis, including key steps in glucose metabolism, angiogenesis, erythropoiesis, proliferation, metastasis, and apoptosis. Table 2 lists some of direct downstream targets of HIF-1.

Metabolism	**Angiogenesis**	**Erythropoiesis**	**Proliferation**	**Metastasis**
GLUT1/3	VEGF	EPO	Cyclin G2	KRT14/18/19
HK1/2	VEGFR	CP	IGF-BP	VIM
ENO1	ENG	TF	TGF-α	MIC2
GAPDH	HO1	TFR	WAF1	CATHD
PFKBF3	NOS2		ADM	FN1
PFKL	PAI1		NIP3	MMP2
PGK1			MDR	c-MET
PKM				LRP1
TP1				
ALDA				
LEP				
LDHA				

Table 2. HIF-1 target genes and their roles in cancer.

1.7 Warburg effect

As early as 1920s, Otto Warburg observed that tumor cells rapidly use glucose and convert the majority of it to lactate [53, 54]. After revision and expansion by tumor biologists in the past century, it is widely accepted that cancer cells adopt a new form of metabolism. In contrast with normal cells, cancer cells prefer to convert glucose to lactate, even in the presence of abundant oxygen. This phenomenon, an emerging hallmark of cancer and fast proliferating cells, is so called aerobic glycolysis, or Warburg effect (Figure 4). Because of low efficiency of glycolysis in generating ATP, the reliance of tumor cells on glycolysis for energy production causes them to consume more glucose [55].

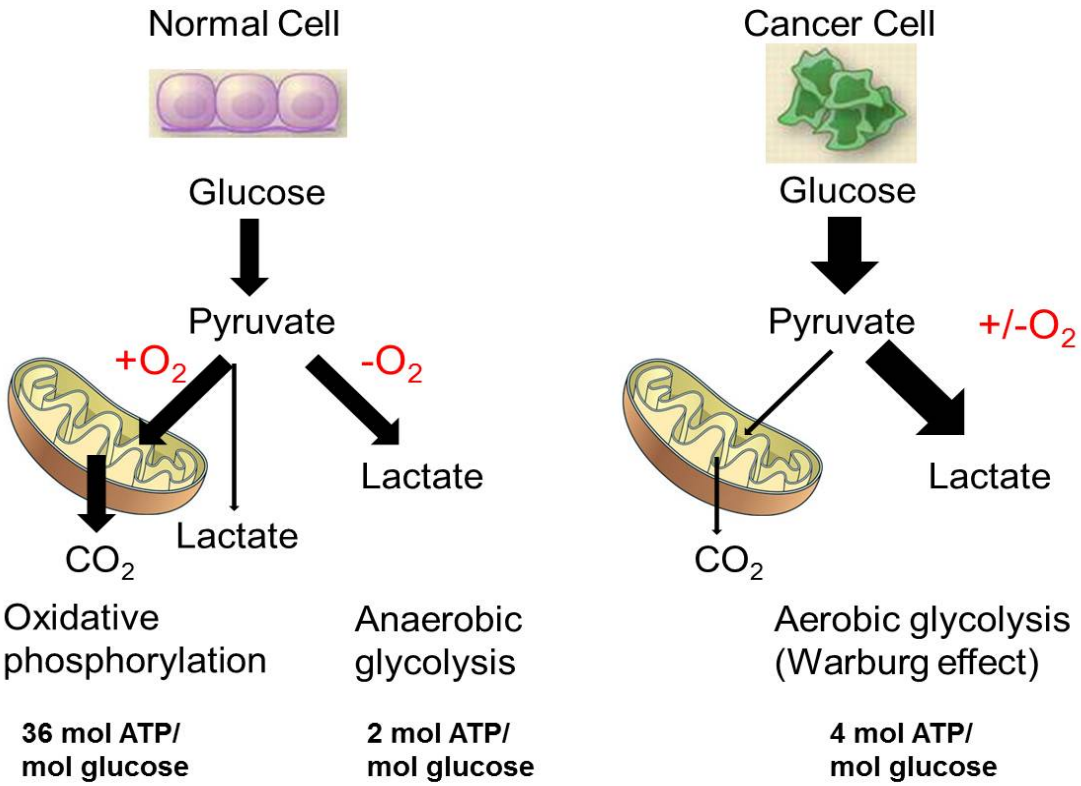

Figure 4. Schematic representation of Warburg effect.

1.8 Regulation of Warburg effect by HIF-1

Although the reasons for altered cancer metabolism are complex and are not fully understood, activation of HIF-1 in cancer cells is considered to be one of the principal molecular mechanisms underlying Warburg effect. Activation of HIF-1 and HIF-1 transcriptional program has two major effects on metabolism in cancer cells (Figure 5). First, HIF-1 promotes glycolysis through activating genes involved in glucose uptake, enzymes for glycolysis, conversion of pyruvate to lactate, and lactate export [56-63]. Second, HIF-1 inhibits mitochondrial function and decrease the rate of oxidative phosphorylation [64-67]. Activation of HIF-1 switched glucose metabolism from oxidative phosphorylation towards aerobic glycolysis.

As the rate of glycolysis increases in cancer cells, more pyruvate, the product of glycolysis, is produced. Two critical HIF-1 targets that contribute to HIF-1-regulated metabolic changes in cancer are lactate dehydrogenase A (LDH-A) and pyruvate dehydrogenase kinase 1 (PDK1), both of which are directly related with pyruvate conversion. LDH-A is induced by HIF-1 and this enzyme converts pyruvate to lactate. Activation of LDH-A by HIF-1 will increase the conversion of pyruvate to lactate. PDK1 phosphorylates and negatively regulates the E1 subunit of the mitochondrial enzyme pyruvate dehydrogenase (PDH), which catalyses the broken down of pyruvate to acetyl-CoA and CO_2. Through activating PDK1 and inactivating PDH, HIF-1 blocks the flow of pyruvate into mitochondria and leads to a reduction in oxidative phosphorylation.

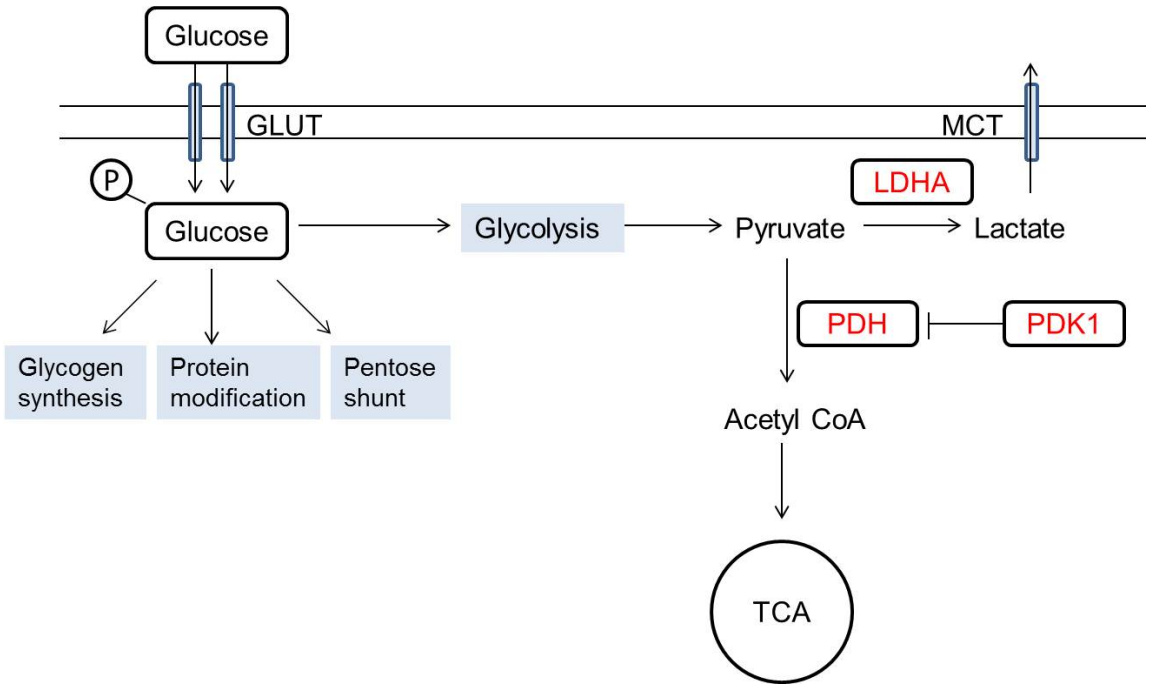

Figure 5. HIF-1 mediated regulation of cancer cell metabolism.

1.9 Reactive oxygen species (ROS) and cellular redox homeostasis

One of the major advantages cancer cells prefer aerobic glycolysis to oxidative phosphorylation as the energy source is to avoid overproduction of reactive oxygen species [68]. Cellular ROS are generated endogenously as in the process of mitochondrial oxidative phosphorylation, through which molecular oxygen (O_2) is reduced to form superoxide anion ($O_2^{\bullet -}$), and then converted to hydrogen peroxide (H_2O_2) through the action of superoxide dismutases (SODs) [69]. ROS is majorly produced in Complex I, II, and III of electron transport chain (ETC), where electrons can prematurely reduce oxygen [70].

The level of intracellular ROS is tightly controlled, or the term redox homeostasis is used. Low levels of mitochondrial ROS production are required for proliferation and differentiation. An induction in ROS production will lead to adaptive programs including the transcriptional upregulation of antioxidant genes. Overproduction of ROS will lead to the initiation of senescence and apoptosis. The highest levels of cellular ROS will cause non-signaling, irreversible damage to cellular components (Figure 6)

Since cancer cells have elevated ROS generation and are under increased intrinsic oxidative stress, they are more dependent on antioxidants for cell survival and more vulnerable to further oxidative insults induced by agents that generate ROS or decrease the cellular antioxidant capacity. It is a convincing therapeutic approach to induce preferential cancer cell death by a ROS-mediated mechanism based on the different redox states in normal and malignant cells.

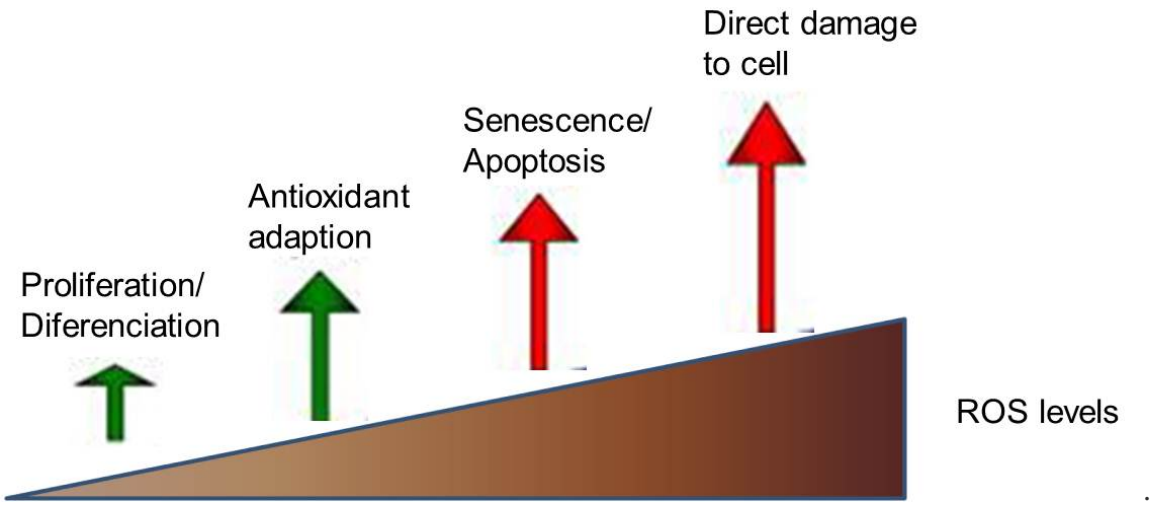

Figure 6. Mitochondrial ROS levels dictate biological outcomes.

1.10 Glutathione and its synthesis

Glutathione (γ-glutamyl-cysteinyl-glycine) is a tripeptide enzymatically formed by glycine, cysteine, and glutamate, and is the most abundant non-protein thiol in mammalian cells [71]. The reduced form of glutathione GSH and the oxidative form of glutathione GSSG is the major couple to maintain intracellular redox homeostasis. GSH acts as a reducing agent and is the major ROS-scavenging system in cells. The important redox-modulating enzymes, including the peroxidases, peroxiredoxins and thiol reductases, rely on GSH as their source of reducing equivalents [72].

The synthesis of glutathione from glutamate, cysteine, and glycine is catalyzed sequentially by two cytosolic enzymes, γ-glutamylcysteine synthetase (GCS) and GSH synthetase [73]. Traditionally, the availability of cysteine and the activity of GCS were considered as the rate-limit step for the synthesis of glutathione [74]. Recent data showed that glycine deprivation also significantly decrease the intracellular GSH level [75]. In addition, the formation of GSH is also relied on glutamine, because glutamine metabolism produces glutamate and glutamate pool is necessary for cells to acquire cysteine [76].

1.11 Glutamine metabolism

Glutamine is the most abundant amino acid in the plasma. In cell culture, tumor cells metabolize glutamine at rates far in excess of any other amino acid [77]. Glutamine supports cell survival, growth and proliferation through metabolic and non-metabolic mechanisms [76]. After its import through surface transporters, glutamine is either exported in exchange with the import of essential amino acids (EAAs) or converted to glutamate catalyzed by the mitochondrial enzyme glutaminase. The γ-nitrogen of glutamine provides nitrogen for nucleotide and hexosamine biosynthesis. Glutamate can be converted to some other non-essential amino acid (NEAA), or metabolized as a respiratory substrate through glutaminolysis, or work as a precursor for the synthesis of GSH.

Chapter 2 Materials and Methods

2.1 Cell lines and cell culture

HNSCC cell lines HN5, FaDu, UMSCC1, OSC19, TU167, and Sqcc/Y1, UMSCC2, UMSCC22A, UMSCC22B, MDA1986, and HN30 were maintained in Dulbecco's modified Eagle's medium (DMEM)/F12 medium supplemented with 10% fetal bovine serum, 2 mM glutamine, 100 units/mL penicillin, and 100 μg/mL streptomycin under conditions of 5% CO2 at 37 °C in an incubator. Cetuximab acquired resistant HN5-R and FaDu-R cells were generated by exposing parental HN5 and FaDu cells to cetuximab containing media for more than 1 year with stepwise increases in concentration up to 20 nM. HN5-HIF-1α-ΔODD and FaDu-HIF-1α-ΔODD cells were established by transfecting parental HN5 and FaDu cells with pcDNA3.1 construct containing a HIF-1α oxygen-dependent degradation domain deletion mutant (referred to as HIF-1α-ΔODD) using Lipofectamine 2000 (Life Technologies, Carlsbad, CA) and maintained in medium containing 500 μg/mL neomycin. Immortalized nontransformed NOM9-TK human head and neck epithelial cells were maintained in serum-free keratinocyte basal growth medium supplemented with components in KGM SingleQuots kit including bovine pituitary extract, recombinant human EGF, insulin, hydrocortisone, and gentamicin sulfate (Lonza, Inc.,Walkersville, MD).

2.2 Reagents

Cetuximab was provided by ImClone System, an Eli Lilly company (New York, NY), 1-methyl-1, 9 pyrazoloanthrone (1-methyl 1, 9 PA) was purchased from

CalBiochem/EMD Chemicals, Inc. (Gibbstown, NJ), oxamate and dicholoroacetate were purchased from Sigma-Aldrich (St. Louis, MO).

2.3 Western blot analysis

Cultured cells were lysed in a lysis buffer containing 50 mM TrisHCl (pH 7.4), 150 mM NaCl, 0.5% NP-40, 50 mM NaF, 1 mM Na_3VO_4, 1 mM phenylmethylsulfonyl fluoride, 25 μg/ml aprotinin, and 25 μg/ml leupeptin and kept on ice for 15 min. The lysates were cleared by centrifugation, and the supernatants were collected. Equal amounts of protein lysate, as determined using the Pierce Coomassie Plus colorimetric protein assay (Thermo Fisher Scientific), were separated by SDS–PAGE, blotted onto nitrocellulose, and probed with the intended primary antibodies (Table 3). The signals were visualized using the enhanced chemiluminescence detection kit (Amersham Biosciences, Piscataway, NJ).

Primary Antibody	Vendor
EGFR-Y1068p	Cell Signaling Technology
EGFR	Sigma-Aldrich
Akt-S473p	Cell Signaling Technology
Akt	Cell Signaling Technology
Erk-T202/Y204p	Cell Signaling Technology
Erk	Santa Cruz Biotechnology
Ras	Cell Signaling Technology
HIF-1α	BD Transduction Laboratories
LDH-A	Cell Signaling Technology
PDK1	Enzo Life Sciences
PDH-S293p	Novus Biologicals
PDH	Cell Signaling Technology
PARP	Cell Signaling Technology
cleaved Caspase-3	Cell Signaling Technology
Caspase-3	Cell Signaling Technology
Rab5	Abcam
Rab11	Abcam
ASCT2	Santa Cruz Biotechnology
xCT	Santa Cruz Biotechnology
β-actin	Sigma-Aldrich

Table 3. List of antibodies.

2.4 cDNA construct, siRNA and transfection

The pcDNA3.1 expression constructs containing HIF-1α-ΔODD were kindly provided by Dr. L. Eric Huang (University of Utah), and the pcDNA3.1 expression constructs containing pBI-GL-V6L were kindly provided by Dr. Van Meir EG (Emory University). The RasG12V and ASCT2 cDNAs were subcloned to pcDNA3.1 expression vector (Invitrogen, Carlsbad, CA). The siRNA oligonucleotide duplexes targeting HIF-1α, LDHA, PDK1, ASCT2, EGFR, Rab5 and Rab11 are listed in Table 4. The cDNA constructs and the siRNA oligonucleotides were transfected into the targeted cells with Lipofectamine 2000 according to the manufacturer's instructions.

Target Gene	Target DNA Sequence	Vender
HIF-1α (in Chapter 3)	AACTGATGACCAGCAACTTGA	Qiagen
HIF-1α (in Chapter 4)	#1: CAAAGTTCACCTGAGCCTA	Sigma-Aldrich
	#2: GATTAACTCAGTTTGAACT	Sigma-Aldrich
LDH-A	#1: GGAGAAAGCCGTCTTAATT	Sigma-Aldrich
	#2: GATTAAGGGTCTTTACGGA	Sigma-Aldrich
	#3: CAGATTTAGGGACTGATAA	Sigma-Aldrich
PDK1	#1: GGATGAAATTGCACCTATT	Sigma-Aldrich
	#2: GTCCAGGAGACTGTGTCAT	Sigma-Aldrich
	#3: TGCTAGGCGTCTGTGTGAT	Sigma-Aldrich
ASCT2	#1: GTCAGCAGCCTTTCGCTCA	Sigma-Aldrich
	#2: CCAAGCACATCAGCCGTTT	Sigma-Aldrich
	#3: GAGGATGTGGGTTTACTCT	Sigma-Aldrich
EGFR	#1: GAGGAAATATGTACTACGA	Sigma-Aldrich
	#2: CTATGTGCAGAGGAATTAT	Sigma-Aldrich
	#3: GACATAGTCAGCAGTGACT	Sigma-Aldrich
Rab5	ON-TARGET plus SMART pool	Dharmacon
Rab11	ON-TARGET plus SMART pool	Dharmacon

Table 4. List of siRNA.

2.5 Luciferase activity assay

Luciferase activity was measured following the instruction with a luciferase activity assay kit from Promega (Madison, WI). Briefly, cultured cells were lysed in lysis buffer provided in the kit. Cell lysates were cleared by centrifugation, and the supernatants were collected. Protein concentration was determined by Lowry protein assay. Protein samples (20 μg each in 20 μl of lysis buffer) were added into wells of an opaque-side, clear-bottom, 96-well microplate and then mixed with 80 μl in each well of the luciferase assay reagent. Luciferase activity was read immediately with a FLUOstar Omega luminescence microplate reader (BMG Labtech).

2.6 MTT proliferation assay

Cells were cultured in 24-well plates with 0.5 mL/well of medium containing 0.5% FBS at 37°C. At the end of the desired treatment in cell culture, cells were incubated for an additional 2 hours after addition of 50 μL/well of 10 mg/mL 3-(4,5-dimethylthiazol-2-yl)-2,5-diphenyltetrazolium bromide (MTT). Cells were then lysed with a lysis buffer (500 μL/well) containing 20% SDS in dimethyl formamide/H2O (1:1, v/v; pH 4.7) at 37°C for at least 6 hours. The relative number of surviving cells in each group was determined by measuring the optical density (OD) of the cell lysates at an absorbance wavelength of 570 nm. The OD value in each treatment group was then expressed as a percentage of the OD value in the untreated control cells, and plotted against treatments.

2.7 Clonogenic survival assay

In the experiments for radiation response, cells were seeded on 60-mm dishes and experienced irradiation at room temperature with γ-rays generated from a high-dose-rate ^{137}Cs unit (4.5 Gy/min). The irradiated cells were then sub-seeded in triplicate into 10-

cm dishes, with densities varying from 500 to 3000 cells/dish according to the dose of γ-rays the cells received (to yield 50–300 colonies per dish finally). In the experiments for responses to cetuximab and PDK1 targeting, the cells were seeded in triplicate into 6-cm dishes, with densities varying from 250 to 1000 cells/dish. The cells were cultured in a 37 °C, 5% CO_2 incubator for 8–20 days depending on the growth rate of the cells. Individual colonies (>50 cells/colony) were fixed and stained with a solution containing 0.2% crystal violet in 10% ethanol for 30 minutes and counted. The surviving fraction, expressed as a function of irradiation, was calculated as follows: surviving fraction = colonies counted/(cell numbers seeded × plating efficiency), where plating efficiency is the percentage of cells seeded that grow into colonies under a specific culture condition of a given cell line.

2.8 Metabolic flux assay

The bioenergetic flux of cells in response to cetuximab treatment or HIF-1α siRNA was determined using the Seahorse XF96 extracellular flux analyzer (Seahorse Biosciences). For cetuximab treatment, cells were plated at 2×10^4 cells/well in XF96 plates and incubated at 37°C under conditions of 5% CO2 with DMEM/F12 cell culture medium containing 10% FBS for 24 hours. The medium was then changed to low serum (0.5% FBS) medium for serum starvation for another 24 hours. The cells were treated with and without 20 nM cetuximab for 10 hours in 0.5% FBS medium. The medium was then replaced with unbuffered DMEM XF assay medium (pH adjusted to 7.4 using 1N sodium hydroxide) supplemented with 2 mM glutamine and 1 g/L glucose, plus or minus 20 nM cetuximab. For HIF-1α siRNA treatment, cells were experienced with control siRNA or HIF-1α siRNA as described in 2.4. After 48 hours, cells were plated at 2×10^4

cells/well in XF96 plates and incubated at 37°C under conditions of 5% CO2 with DMEM/F12 cell culture medium containing 10% FBS for another 24 hours. The medium was then replaced with the same unbuffered DMEM XF assay medium as described above. After medium changes, the cells were placed in a 37°C, CO2-free incubator for 1 hour. The basal oxygen consumption rate and extracellular acidification rate were then determined by using the XF96 plate reader with the standard program recommended by the manufacturer.

2.9 Glucose consumption assay

Cells were seeded into 6-well plates at 5×10^5 cells/well in 3 mL of phenol-red-free cell culture medium containing 0.5% FBS and 1 g/L glucose. At indicated times after treatment, an aliquot of 50 μL of conditioned medium was collected from each well and diluted with 950 μL of distilled water (1:20). The glucose concentration in the diluted medium was measured using the Glucose (GO) assay kit from Sigma-Aldrich according to the manufacturer's instructions. Briefly, samples were mixed with the glucose assay reagent provided in the assay kit and incubated at 37°C for 30 minutes. 12N sulfuric acid was added to each well to stop the reaction and OD values at 540 nm in each well were measured for comparison with the standard control of glucose. Glucose consumption was calculated by subtracting the concentration of glucose remaining in the medium at the indicated time point from the concentration of glucose present in fresh cell culture medium. Glucose consumption is expressed as mg/10^6 cells after indicated time periods.

2.10 Lactate production assay

Cells were seeded into 6-well plates at 5×10^5 cells/well in 3 mL of serum-free cell culture medium containing 0.5% FBS and 1 g/L glucose. At indicated times after

treatment, an aliquot of 50 μL of conditioned medium was collected from each well and diluted with 950 μL of distilled water (1:20). The lactate concentration in the diluted medium was measured using the Lactate Assay Kit from BioVision Inc. (Milpitas, CA). Briefly, the sample was mixed with reaction reagent provided in the assay kit and incubated at 37 °C for 30 minutes before measurement of the OD value at 570 nm for comparison with the standard control of lactate. The levels of lactate are expressed as nmol/10^6 cells after indicated time periods.

2.11 Intracellular ATP assay

Intracellular ATP levels were determined with the ATP bioluminescent assay (Sigma-Aldrich). Briefly, cells were seeded into 6-well plates at 5×10^5 cells/well and treated with or without 20 nM cetuximab for 4 hours in low-glucose (1 g/L) medium supplemented with 0.5% FBS. Cells were then harvested and resuspended in 1 mL of PBS. An aliquot of 50 μL of cell suspension was mixed with 100 μL of ATP-releasing reagent and 50 μL of water in each well of a 96-well plate. The samples (100 μL) in each well were then transferred to another 96-well plate pre-filled with 100 μL of ATP assay mix in each well. The amount of light emitted in each well was immediately measured under a luminometer (FLUOstar Omega).

2.12 LDH-A activity assay

LDH-A activities were measured using a colorimetric LDH Activity Assay Kit (BioVision, Inc.) based on a reaction that converts NAD to NADH by LDH-A in a specific time period. Briefly, after desired treatments, cell pellets were collected and homogenized on ice in 0.5 mL of cold assay buffer. Supernatants were collected by centrifugation. Protein concentrations were determined by using the Pierce Coomassie

Plus colorimetric protein assay. 50 μL of aliquots (volume adjusted using assay buffer) containing equal amounts of protein and 50 μL of reaction reagent (48 μL of assay buffer and 2 μL of LDH-A substrate mix solution) were added into each well of a 96-well plate and the plates were read under a microreader at 450 nm immediately (T0) and 10 minutes after the reaction (T1). LDH-A activity was expressed by an increase in OD values (T1-T0). Relative LDH-A activities in cells of untreated and treated groups were expressed as percentage of the LDH-A activity in cells of untreated group after 4 hours in culture, which was arbitrarily set as 100.

2.13 Flow cytometry analysis for cell cycle

After desired treatments, cells were harvested by trypsin and fixed in 70% ethanol overnight. After centrifugation and washing with PBS, cells were stained with propidium iodide (50 μg/mL) and RNaseA (20 μg/mL) on ice for 30 minutes and then subjected to flow cytometric analysis with an LSRFortessa cell analyzer (BD Biosciences). Cell cycle distribution data were analyzed with FlowJo software, version 10.

2.14 Cell death assay

Cell death was measured by using the Cell Death Detection ELISA, a colorimetric ELISA kit (Roche Diagnostics Corp., Indianapolis, IN) that quantitatively measures cytoplasmic histone-associated DNA fragments (mononucleosomes and oligonucleosomes). The procedure was performed exactly according to the manufacturer's instructions.

2.15 ROS detection

Intracellular ROS was measured by using the total ROS detection kit (Enzo Life Sciences, Plymouth Meeting, PA) according to the manufacturer's instructions. Briefly,

cells were seeded in 12-well plate at around 40-60% confluency. After indicated treatment, cells were either stained directly with ROS detection solution at 37 °C for 1 hour and analyzed using fluorescence microscopy equipped with standard green filter, or trypsinized and resuspended in eppendorf tubes, and stained with ROS detection solution at 37 °C for 1 hour and analyzed with an LSRFortessa cell analyzer (BD Biosciences).

2.16 Mitochondrial membrane potential assay

Mitochondrial membrane potential (ψm) was measured by staining with fluorescent dye tetramethylrhodamine methyl ester (TMRM). For fluorescence microscopy, cells were seeded in 12-well plate at around 60-80 confluency. After indicated treatment, cells were stained with TMRM and counterstained with Hoechst at 37 °C for 30 minutes, and analyzed with fluorescence microscopy equipped with standard red and blue filter, respectively. For quantitative analysis, cells were seeded in clear-bottom, opaque-walled 96-well plate at around 60-80 confluency. After indicated treatment, cells were stained with TMRM and counterstained with Hoechst at 37 °C for 30 minutes, and relative TMRM was determined by ratio of the reading at 590 nm (TMRM) over 460 nm (Hoechst) wavelength with a fluorescence plate reader.

2.17 Glutamine uptake assay

After indicated treatment, cells were trypsinized and incubated with 0.5 mL of glutamine-deficient medium containing 5 μCi/mL radiolabelled ^{3}H-glutamine at 37 °C for 5 minutes. After incubation, cells were spun down and washed three times with ice-cold PBS, after which cells were lysed with 200 μL of a 0.2% SDS/0.2 N sodium hydroxide (NaOH) solution, incubated for 1 h, neutralized with 20 μL of 1 N hydrochloric acid (HCl), and analyzed with Beckman scintillation counter LS6500.

Relative glutamine uptake in cells of treated groups was expressed as percentage of the glutamine uptake in cells of untreated group.

2.18 Intracellular glutathione assay

Intracellular glutathione was measured using glutathione assay kit (Cayman Chemical), based on the enzymatic recycling catalyzed by glutathione reductase and the reaction of GSH with 5,5′-dithio-bis-2-nitrobenzoic acid (DTNB) to produce a yellow product, which was quantified by a spectrometer. After indicated treatments, cells were collected, sonicated and deproteinated by precipitation with an equal volume of 10% metaphosphoric acid (Sigma-Aldrich). The precipitated proteins were removed by centrifugation at 3,000g for 5 min. The supernatant was collected, neutralized and assayed for GSH and GSSG using the Cayman glutathione assay kit according to the procedures recommended by the manufacturer.

2.19 Immunoprecipitation

Indicated cells were lysed in a lysis buffer containing 50 mM TrisHCl (pH 7.4), 150 mM NaCl, 0.5% NP-40, 50 mM NaF, 1 mM Na_3VO_4, 1 mM phenylmethylsulfonyl fluoride, 25 μg/ml aprotinin, and 25 μg/ml leupeptin and kept on ice for 15 min. The lysates were cleared by centrifugation, and the supernatants were collected. Protein concentration was determined as described in 2.3. Protein extracts containing 500 μg protein were subsequently incubated for 1 hour at room temperature with the anti-EGFR monoclonal antibody cetuximab (4 μg), rabbit anti-ASCT2 antibody (4 μg), or with nonspecific normal mouse immunoglobulin G (IgG) (4 μg), and then incubated with 10 μl protein A beads for 10 hours at 4 °C. The precipitates were washed three times with a

lysis buffer and then denatured by heating in sample buffer. Immunoprecipitates were analyzed by Western blot as described for indicated antibodies as described in 2.3.

2.20 Animal studies and imaging of tumor bioluminescence

Bioluminescent sublines of FaDu, FaDu-R, and UMSCC1 were established by infection with virus containing luciferase reporter gene. Female nude mice at 4-6 month old were inoculated with FaDu, FaDu-R, HN5, HN5-R, or UMSCC1 cells (1×10^7 cells/mouse in 100 μl serum-free medium) subcutaneously on their right flanks. When tumors were well established at the volume of 150-250 mm^3, the nude mice that had developed tumors were divided into six groups (6-7 mice in each group) with similar average tumor volume, and treated with vehicle, cetuximab (0.25 mg/mouse, bi-weekly), DCA (50 mg/kg/day or 250 mg/kg/day, daily), or combination of cetuximab and DCA for 21 days. Tumor volume was measured twice a week with a digital caliper, and calculated using the formula $\pi/6 \times ab^2$ (a: length; b: width, $a > b$). For bioluminescent sublines, tumors were also monitored using the Xenogen in vitro imaging system in living animals at day 21 from treatment start date, after intraperitoneal injection of D-luciferin (3.3 mg/100 μl) and induction of anesthesia by inhalation of 2.5% isoflurane. After the end of treatment, measurement of tumor volume was continued in each group until the group had less than 4 mice.

2.21 Statistical analysis

Student's t-test was used in all statistical analyses. The data are presented as mean ± standard deviation in all *in vitro* experiments, and are presented as mean ± standard error of the mean in animal experiments. P values < 0.05 were considered statistically significant.

Chapter 3 Cetuximab sensitizes HNSCC to radiation through inhibiting radiation-induced upregulation of HIF-1α

3.1 Introduction

Radiation is an important therapy for patients with locally advanced and inoperable HNSCC. However, about 50% of patients treated with definitive radiotherapy with or without chemotherapy experience local recurrence or even remote metastasis [2, 78]. Because of prior radiotherapy, these patients usually cannot tolerate additional radiotherapy treatment, and most of whom eventually died of tumor local progression or remote metastasis with poor life qualities. Approximately 90% of HNSCCs express a high level of EGFR [17, 18]. Overexpression of EGFR confers HNSCC resistant to radiation [19-22, 79, 80]. Cetuximab improved the radiosensitivity of HNSCC in preclinical models [20, 32], and the combination of radiotherapy plus cetuximab resulted in prolonged survival in a pivotal phase III trial [23, 81]. Cetuximab has been approved by the Food and Drug Administration for treatment of HNSCC in combination with radiotherapy. However, the mechanisms underlying cetuximab-mediated radiosensitization of HNSCC are not fully understood.

Tumor hypoxia has been known to contribute to tumor radioresistance and poor clinical outcomes of human cancers for over half a century [38, 39]. During radiotherapy, oxygen is required to generate free oxygen radicals that induce DNA damage and kill tumor cells [82, 83]. Hypoxia-inducible factor-1 (HIF-1), the master regulator of tumor response to hypoxia, has recently been implicated in regulating radiation response in several preclinical and clinical studies [84-87]. Our lab previously reported that cetuximab downregulates HIF-1α, the regulatory subunit of HIF-1, by inhibiting new

HIF-1α protein synthesis [87]. Data from our lab also indicated that response of cancer cells to cetuximab correlates with downregulation of HIF-1α by cetuximab, and downregulation of HIF-1α by cetuximab is required to mediate cetuximab-induced antitumor activity [88, 89].

In this study, we hypothesized that cetuximab sensitizes HNSCC cells to radiation through inhibiting radiation-induced upregulation of HIF-1α. To test this hypothesis, we explored the effects of experimental elevation and experimental downregulation of HIF-1α on radiation responses. We tested the effect of HIF-1α overexpression on anti-tumor roles of cetuximab as a monotherapy and in combination with radiotherapy. We also analyzed the impact of small molecular HIF-1α inhibitor in restoring the role of cetuximab in radiosensitization in cetuximab-resistant HNSCC cell lines. Our findings not only validated HIF-1α as an important target for sensitizing cetuximab plus radiotherapy, but also developed a novel strategy to improve the clinical response of HNSCC to radiotherapy.

3.2 Results

3.2.1 Treatment with ionizing radiation upregulates HIF-1α through *de novo* protein synthesis in HNSCC cell lines

To examine whether radiation treatment can upregulate HIF-1α in HNSCC cell lines, two HNSCC cell lines, FaDu and HN5, both of which display inhibited proliferation in response to cetuximab treatment, were subjected to 3 Gy ionizing radiation for indicated time. We found that the expression levels of HIF-1α were upregulated, examined by western blot analysis (Figure 7A), and the transcriptional activities of HIF-1 were increased, examined by a hypoxia response element (HRE) luciferase reporter assay (Figure 7B) in both HN5 and FaDu cells after treatment of ionizing radiation in normoxic culture.

To investigate the mechanism underlying radiation-induced HIF-1α in HNSCC cells, we employed pharmacologic inhibitor of protein synthesis, cycloheximide, to determine its effect on HIF-1α expression in HN5 and FaDu cells after radiation treatment. We found that addition of cycloheximide immediately after radiation effectively inhibited radiation-induced regulation of HIF-1α expression (Figure 7C), suggesting that the radiation-induced upregulation of HIF-1α involves *de novo* protein synthesis.

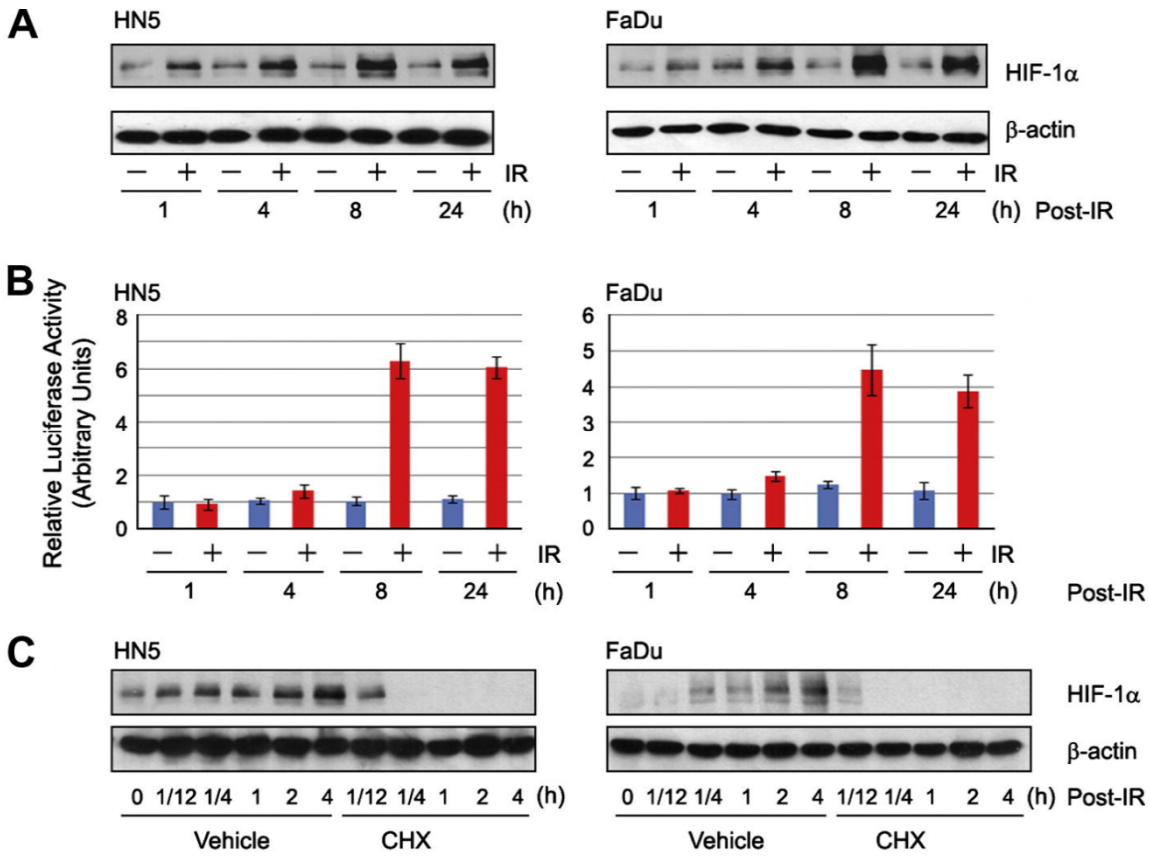

Figure 7. Ionizing radiation upregulates HIF-1α through *de novo* protein synthesis in HNSCC cells. (A) HN5 and FaDu cells were irradiated with 3 Gy of ionizing radiation (IR) or not and then cultured for the indicated time periods. At each time point, the irradiated cells and the accompanying unirradiated cells were collected for detection of the level of HIF-1α protein by Western blot analysis. The level of β-actin was used as an internal control of equal protein loading in each lane. (B) HN5 and FaDu cells were transiently transfected with pBI-GL-V6L construct for 24 h prior to irradiation. The cells were then irradiated and collected as described in A for measurement of the transcriptional activity of HIF-1 on HRE-luciferase reporter by a luciferase activity assay as described in materials and methods. (C) HN5 and FaDu cells were irradiated with 3 Gy of ionizing radiation, and 10 μM cycloheximide (CHX) or vehicle (DMSO) was added immediately after irradiation. Cells were harvested at each indicated time point for measurement of the level of HIF-1α protein by Western blot analysis.

3.2.2 Overexpression of HIF-1α renders HNSCC cells radio-resistant, whereas silencing of HIF-1α sensitizes HNSCC cells to radiation

To determine the role of HIF-1α in mediating cell response to radiation, we examined cell responses to radiation through experimentally changing the level of HIF-1α in HN5 and FaDu cells. Since wild-type HIF-1α is instable in normoxia, we transfected HN5 and FaDu cells with a HIF-1α mutant with deletion of the oxygen-dependent degradation domain (HIF-1α-ΔODD), which is degradation-resistant in normoxic culture and retains the majority of transcriptional activity of HIF-1α. We found that overexpression of HIF-1α-ΔODD conferred resistant to radiation in both HN5 and FaDu cells, as measured by clonogenic survival assays (Figure 8A and B). In contrast, silencing of HIF-1α expression by HIF-1α siRNA for 48 h before radiation treatment sensitized responses to radiation in HN5 and FaDu cells (Figure 8C and D). These findings indicated that HIF-1α plays an important role in conferring resistance to radiation.

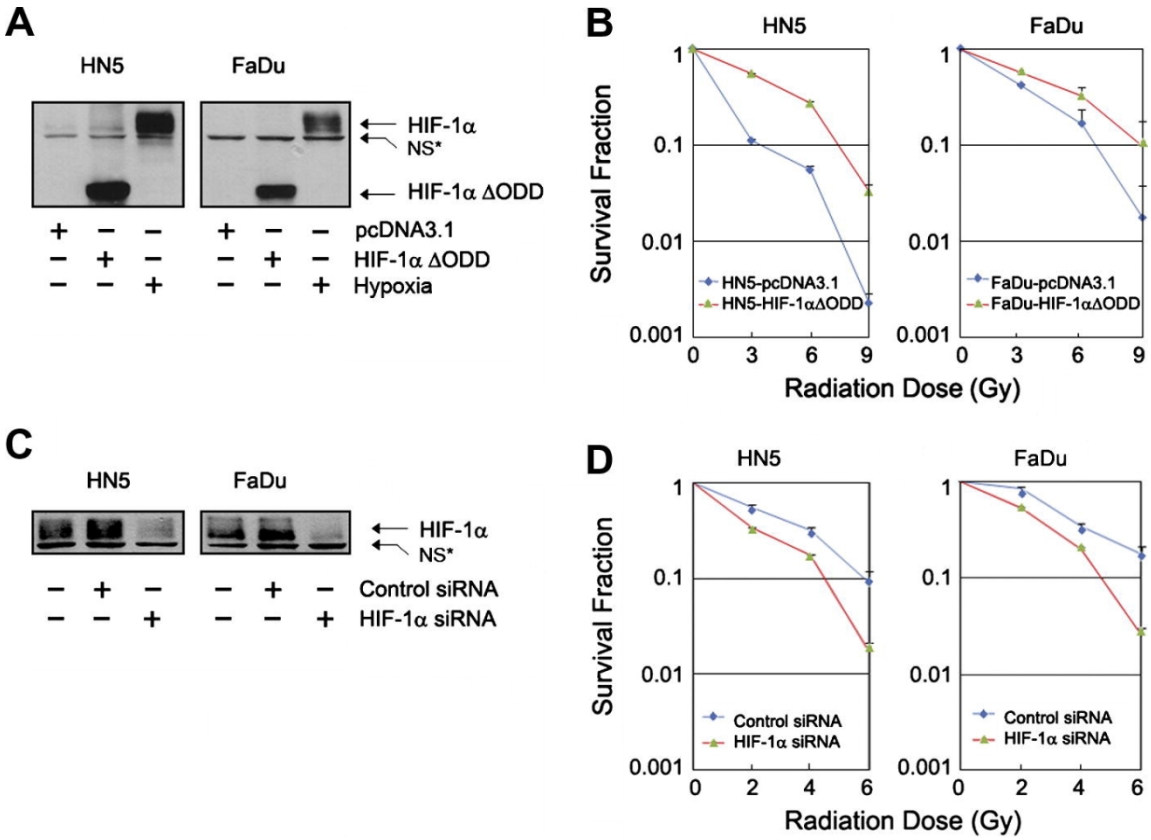

Figure 8. Role of HIF-1α in mediating HNSCC cell response to radiation-induced clonogenic survival inhibition. (A) and (B) HN5 and FaDu cells were transiently transfected with HIF-1α-ΔODD construct or control vector (pcDNA3.1) for 48 h. In (A), the cells were harvested for detection of HIF-1α-ΔODD expression by Western blot analysis. A nonspecific band below HIF-1α serves as a reference of equal protein loading in each lane. In (B), the cells were irradiated with the indicated doses of radiation and subjected to a clonogenic survival assay as described in materials and methods. (C) and (D) HN5 and FaDu cells were transiently transfected with HIF-1α-specific siRNA or control siRNA for 48 h. In (C), the cells were harvested for detection of the basal level of HIF-1α by Western blot analysis. A nonspecific band below HIF-1α serves as a reference of equal protein loading in each lane. In (D), the cells were irradiated with the indicated doses of radiation and subjected to a clonogenic survival assay as described in materials and methods. *NS: nonspecific band.

3.2.3 Cetuximab inhibits radiation-induced upregulation of HIF-1α in HNSCC cells, leading to radiosensitization

Next we tested whether cetuximab sensitizes cancer cells to radiation through inhibiting radiation-induced HIF-1α upregulation. Compared to the effect with radiation treatment alone, addition of cetuximab after radiation treatment substantially enhanced radiation-induced inhibition of clonogenic survival in HN5 and FaDu cells (Figure 9A), which is consistent with literature. Figure 9B and 9C showed that addition of cetuximab after radiation downregulated the expression level and inhibited the activity of radiation-induced HIF-1α.

To determine whether downregulation of HIF-1α is required for cetuximab-mediated radiosensitization, we established HN5 and FaDu cells stably expressing HIF-1α-ΔODD. Overexpression of HIF-1α-ΔODD conferred substantial resistance to cetuximab treatment alone in both HN5 and FaDu cells (Figure 9D). Figure 9E showed that in both HN5 and FaDu cells, overexpression of HIF-1α-ΔODD strongly abolished cetuximab-mediated radiosensitization that was observed in the parental cells (see Figure 9A). There were no significant differences in the clonogenic survivals between groups with or without addition of cetuximab after radiation in HN5-HIF-1α-ΔODD and FaDu-HIF-1α-ΔODD cells. These data suggested that cetuximab-induced inhibition of HIF-1α is critical in cetuximab-mediated radiosensitization of HNSCC cells.

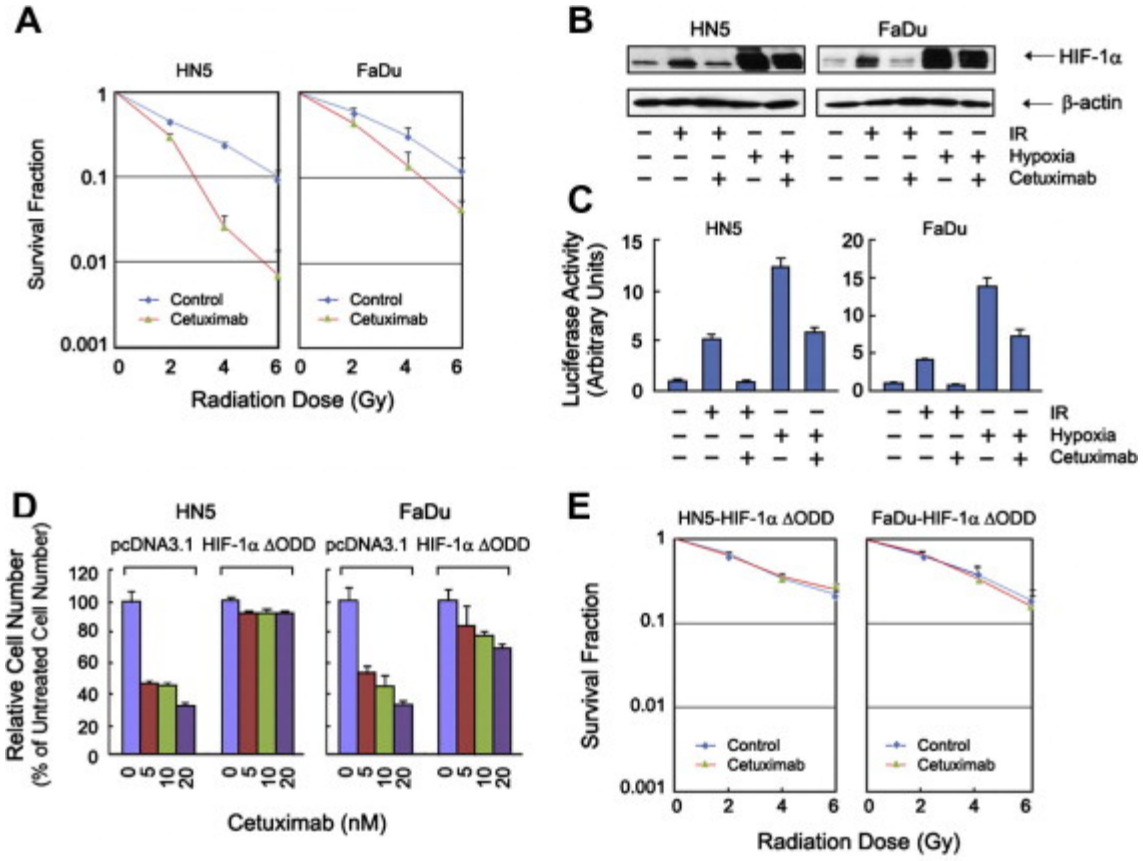

Figure 9. Cetuximab sensitizes HNSCC cells to radiation through downregulating HIF-1α. (A) HN5 and FaDu cells were irradiated with the indicated doses of ionizing radiation and then subjected to clonogenic survival assays in the presence or absence of 2 nM cetuximab (HN5) or 5 nM cetuximab (FaDu) as described in materials and methods. (B) and (C) HN5 and FaDu cells were transfected with pBI-GL-V6L vector 24 h prior to irradiation. After exposure to 3 Gy, the cells were cultured in the presence or absence of 10 nM cetuximab for 8 h. Unirradiated HN5 and FaDu cells cultured in hypoxia with and without 10 nM cetuximab for the same time period were used to compare HIF-1α upregulation. The cells were harvested for detection of the level of HIF-1α by Western blot analysis (B) and for detection of HIF-1 transcriptional activity on HRE-luciferase reporter by a luciferase assay as described in materials and methods (C). (D) and (E) HN5 and FaDu cells were transiently transfected with HIF-1α-ΔODD construct or control vector (pcDNA3.1) for 48 h. The cells were then assayed for responses to cetuximab treatment for 5 days by MTT assays (D) and for responses to treatment with ionizing radiation in the presence and absence of cetuximab (2 nM for HN5 cells and 5 nM for FaDu cells) in the post-radiation period for 14 days by clonogenic survival assays (E).

3.2.4 Silencing of HIF-1α improves radiosensitization by cetuximab and overcomes oncogenic H-Ras-mediated radiation resistance

To explore whether silencing HIF-1α may sensitize HNSCC cells to radiation, we employed both cetuximab-sensitive cell lines HN5 and FaDu, in which HIF-1α was strongly downregulated by cetuximab, and cetuximab-resistant cell lines UMSCC1 and OSC19. Although UMSCC1 and OSC19 contain EGFR levels similar to FaDu cells, they were resistant to HIF-1α downregulation by cetuximab (Figure 10). Cetuximab failed to downregulate HIF-1α protein levels either in HN5 and FaDu cells transfected with a constitutively active H-Ras mutant (H-Ras G12V) (Figure 10). Figure 11A shows that pre-treatment with HIF-1α siRNA strongly increased responses to cetuximab in UMSCC1 and OSC19 cells. The inhibition rate to cetuximab increased from ~20% (UMSCC1) and ~10% (OSC19) in control siRNA groups to ~50% (UMSCC1) and ~40% (OSC19) in HIF-1α siRNA groups. Similar results were observed in the HN5 and FaDu cells that were transfected for stable expression of H-Ras G12V (Figure 11C). Experimental expression of H-Ras G12V in HN5 and FaDu cells not only caused the failure of cetuximab in downregulating HIF-1α protein levels, but also conferred considerable resistance to cetuximab-induced growth inhibition in control siRNA-treated HN5-RasG12V cells (<10% inhibition) and FaDu-RasG12V cells (only 10–20% inhibition). Pre-treatment with HIF-1α siRNA resensitized responses to cetuximab in HN5-RasG12V and FaDu-RasG12V cells by increasing inhibition rate to 50-60% and 40-50%, respectively.

HIF-1α silencing not only increased response to cetuximab in cetuximab-resistant cells, but more importantly, also restored the role of cetuximab in radiosensitization. As

measured by clonogenic survival assay, cetuximab failed to sensitize UMSCC1 or OSC19 cells to radiation; however, cetuximab substantially sensitized HIF-1α-silenced UMSCC1 and OSC19 cells to radiation (Figure 11B). Similar results were observed in HN5-RasG12V and FaDu-RasG12V cells. Cetuximab substantially sensitized HIF-1α-silenced, but not control siRNA-transfected, HN5-RasG12V and FaDu-RasG12V cells to radiation (Figure 11D). These results indicated a critical role of cetuximab-induced downregulation of HIF-1α in both the response of cells to cetuximab-induced proliferation inhibition and radiosensitization.

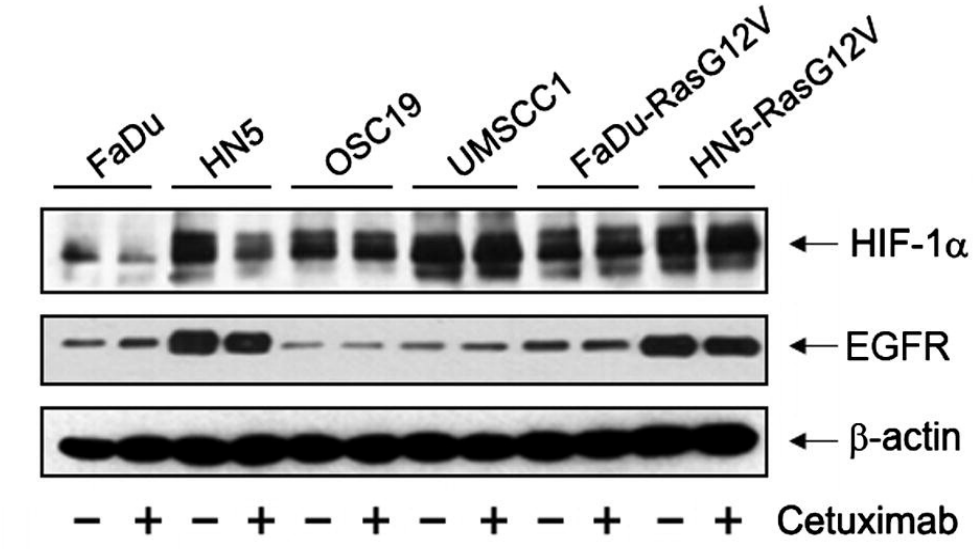

Figure 10. Cetuximab downregulates HIF-1α protein levels in sensitive, but not in resistant HNSCC cell lines. The indicated HNSCC cell lines (FaDu, HN5, OSC19, UMSCC1, and FaDu and HN5 cells transfected with H-Ras G12V) were cultured in the presence or absence of 20 nM cetuximab for 16 h, and then the cells were collected for detection of the levels of HIF-1α and EGFR protein by Western blot analysis. The level of β-actin was used as an internal control of equal protein loading in each lane.

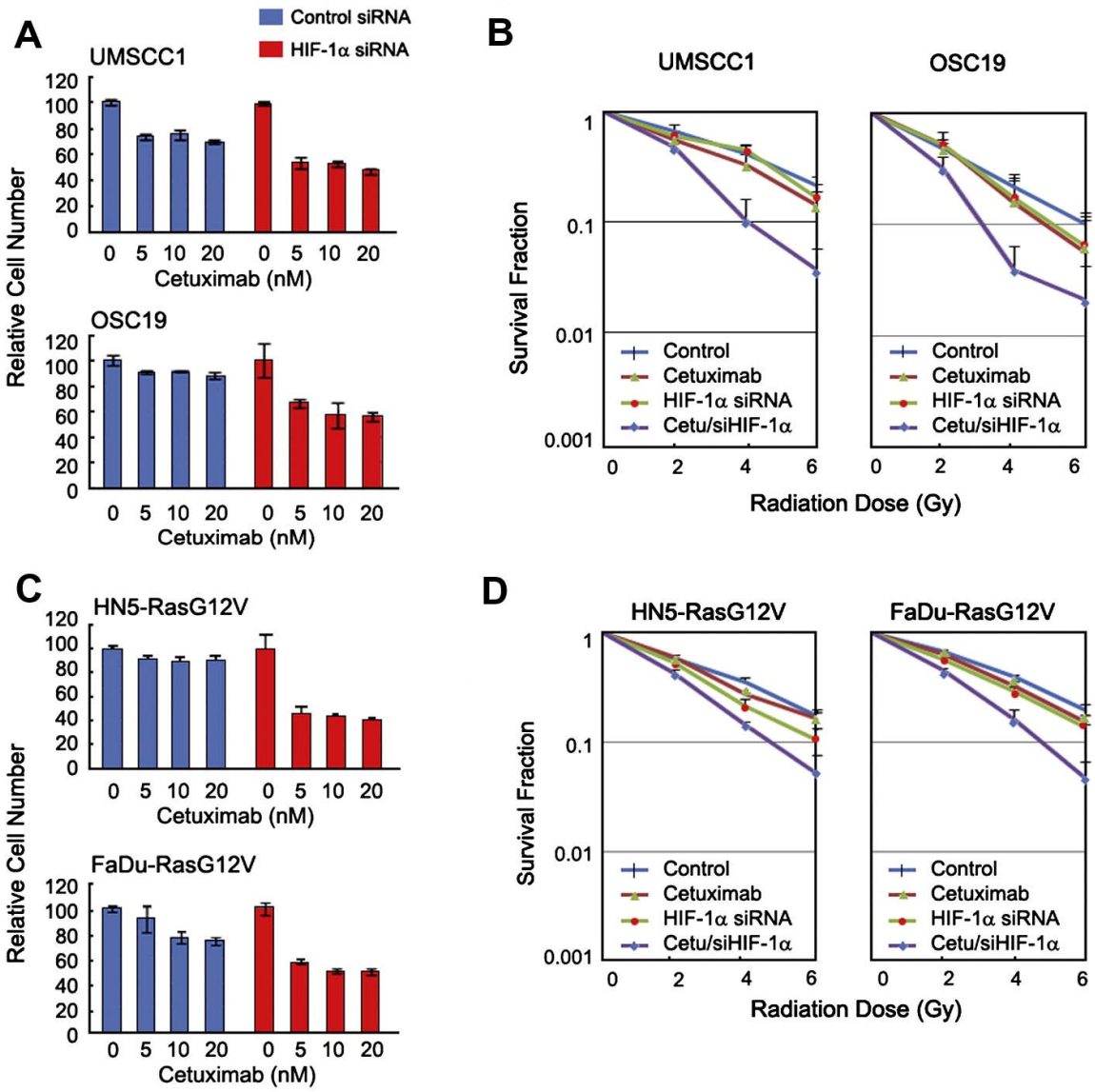

Figure 11. Silencing HIF-1α enhances responses of cetuximab-resistant HNSCC cells to cetuximab-induced growth inhibition and radiosensitization. (A) and (B) UMSCC1 and OSC19 cells were transiently transfected with HIF-1α-specific siRNA or control siRNA for 48 h. The cells were then assayed for responses to cetuximab treatment for 5 days by MTT assays (A) and for responses to treatment with ionizing radiation in the presence and absence of 10 nM cetuximab for 14 days by clonogenic survival assays (B). (C) and (D) HN5-RasG12V and FaDu-RasG12V cells were similarly transfected with HIF-1α siRNA or control siRNA for 48 h and subjected to MTT assays (C) and clonogenic survival assays (D) for response to treatment with cetuximab and ionizing radiation as described in (A) and (B). Cetu, cetuximab; siHIF-1α, HIF-1α siRNA.

3.2.5 The combination of cetuximab and 1-methyl 1, 9 PA sensitizes HNSCC cells to radiation

Our previous work showed that 1-methyl 1, 9 PA, a small molecule compound that is a derivative of anthrapyrazolone, downregulates HIF-1α protein levels and is a potential HIF-1 inhibitor [90]. We thus evaluated whether addition of 1-methyl 1, 9 PA can sensitize UMSCC1 and OSC19 cells to cetuximab and cetuximab plus radiation treatment. It has been reported that 1-methyl 1, 9 PA alone at a dose of 10 μM can strongly downregulate HIF-1α in various types of cancer cells. Figure 12A shows that addition of 10 μM 1-methyl 1, 9 PA significantly increased responses to cetuximab in cetuximab-resistant UMSCC1 and OSC19 cells ($p < 0.01$). Figure 12B shows that the combination of cetuximab and 1-methyl 1, 9 PA increased the sensitivity of UMSCC1 and OSC19 cells to radiation, while either agent alone did not enhance the responses to radiation. These results from this pilot study provide a novel concept that inhibition of HIF-1α with a small molecule compound may improve response of cetuximab-resistant HNSCC cells to treatment with the combination of radiation and cetuximab.

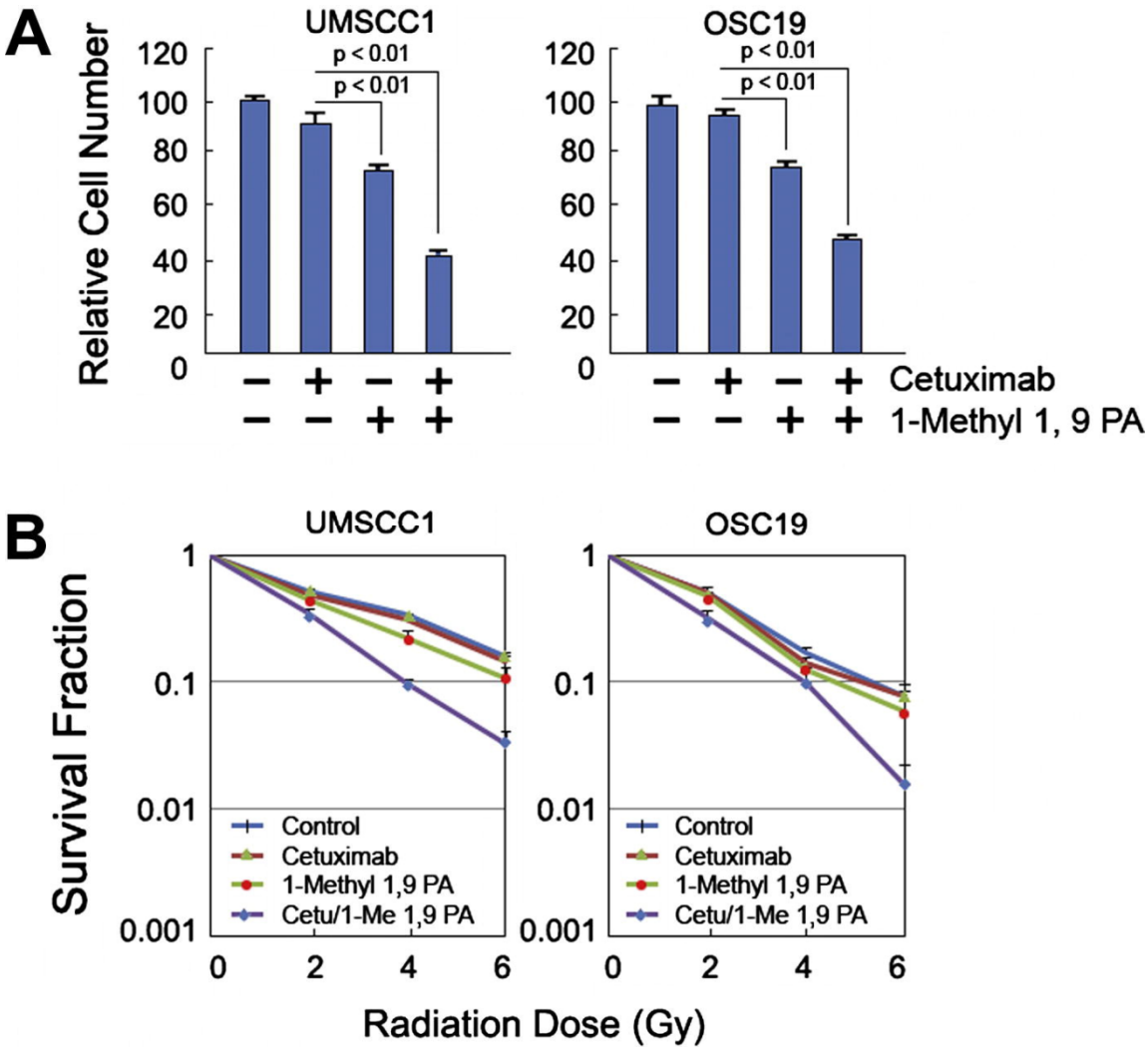

Figure 12. The small molecule compound 1-methyl-1, 9 PA sensitizes HNSCC cells to treatment with cetuximab and ionizing radiation. (A) UMSCC1 and OSC19 cells were treated with 20 nM cetuximab, 10 μM 1-methyl-1, 9 PA or the combination of these two agents for 5 days, and then MTT assays were performed for determination of the responses of the cells to the treatment. Results of statistical analysis are shown. (B) UMSCC1 and OSC19 cells were irradiated with the indicated doses of ionizing radiation and subjected to clonogenic survival assays in the presence or absence of 5 nM cetuximab, 2.5 μM 1-methyl-1, 9 PA, or the combination of these two agents in the postradiation period for 14 days. Cetu, cetuximab; 1-Me 1, 9 PA, 1-methyl 1, 9 PA.

3.3 Discussion

In this part, our major findings are: (1) Ionizing radiation upregulates HIF-1α through *de novo* protein synthesis in HNSCC cells; (2) Cetuximab inhibits radiation-induced HIF-1α upregulation; (3) Inhibition of HIF-1α by siRNA or small molecular compound increases responses to cetuximab and cetuximab plus radiation. Consistent with the findings reported in the literature for other types of cancers [91-93], our data confirm that ionizing radiation can upregulate HIF-1α in HNSCC cells irrespective to hypoxia. These findings suggest a novel strategy by targeting HIF-1α to enhance the response of HNSCC cells to treatment with the combination of radiation and cetuximab.

Radiation is a major treatment modality for patients with locally advanced and inoperable head and neck cancer. However, about 50% of patients treated with definitive radiotherapy with or without chemotherapy go onto experience local recurrence or even remote metastasis [2, 78]. Cetuximab is approved by FDA for enhancing the response of HNSCC to radiation. Although in clinical trials, combination of cetuximab and radiotherapy showed prolonged survival, there are multiple mechanisms in HNSCC that can render cancer cells resistant to cetuximab as a monotherapy or in combination with radiation. Common resistance mechanisms to cetuximab include constitutive activation of EGFR downstream signals, such as oncogenic activation of H-Ras mutant (in contrast to K-Ras mutation in colorectal cancers), mutational inactivation of tumor suppressors, such as PTEN, or cross-activation of EGFR downstream signaling pathways by other growth factor receptors in the same family (e.g., HER2, HER3) or different families (e.g., IGF-1R) or through tumor-stromal interactions [94-96]. Previous work in our lab showed that HIF-1α is one of the most important effector molecules downstream of

EGFR pathway and downregulation of HIF-1α by cetuximab is required for cetuximab's anti-tumor effect [88-90, 97]. Our work in this part expanded the serial studies in our lab demonstrating the role of downregulating HIF-1α in mediating cetuximab-induced antitumor activities and suggesting a novel approach of co-targeting HIF-1α to overcome resistance of cancer cells to cetuximab monotherapy or in combination with radiation.

HIF-1 has been suggested to play an important role in tumor radioresistance. However, the mechanisms through which irradiation regulates HIF-1α expression remain unclear. One of the mechanisms reported in the literature by which HIF-1α is upregulated by irradiation is radiation-induced tumor reoxygenation [91]. However, in this study, we found that HIF-1α can be upregulated independent of tumor reoxygenation, as the cells were cultured *in vitro* in normoxia. Our observation that upregulation of HIF-1α by radiation involves *de novo* protein synthesis in head and neck cancer cell models is consistent with a recent study in lung cancer cell models. Kim *et al.* reported that radiation induced HIF-1α protein expression mainly through two distinct pathways, including activation of PI3K/Akt/mTOR, which leads to stimulation of de novo synthesis of HIF-1α, and stimulation of Hsp90 function, which leads to stabilization of HIF-1α protein [92]. Our finding indicates that there are multiple mechanisms by which HIF-1α is upregulated after radiation.

Although overexpression of HIF-1α caused by tumor hypoxia or aberrant signaling in cancer cells have been reported to be associated with a poor response to radiation [91, 92, 98-102], the impact of radiation-induced HIF-1α upregulation on tumor response to radiation is not clear. The impact of radiation-induced upregulation of HIF-1α on overall tumor radiosensitivity is pleiotropic: by promoting ATP metabolism, cell proliferation

and p53 activation, HIF-1 has a radiosensitizing effect on tumors; however, through stimulating endothelial cell survival, HIF-1 promotes tumor radioresistance [103]. Our findings derived from clonogenic survival assays performed in cell culture, support a conclusion that at least in HNSCC cells, HIF-1 has a net role of promoting radioresistance. Upregulation of HIF-1α conferred radioresistance whereas silencing of HIF-1α sensitized cancer cells to radiation. Our data also expand understanding of antitumor effect of cetuximab that downregulation of HIF-1α by cetuximab plays an important role in cetuximab-mediated radiosensitization. However, *in vivo* experiments are needed to further confirm the exact role of inhibition of radiation-induced HIF-1α upregulation in cetuximab-mediated radiosensitization. Results from *in vivo* experiments may provide further guidance for designing novel therapeutic strategies by targeting HIF-1 to enhance clinical responses to combination treatment of cetuximab and radiation in head and neck cancer.

In summary, our results in this part show that downregulation of HIF-1α contributes to cetuximab-mediated radiosensitization in HNSCC cells and indicate that targeting HIF-1α is a promising strategy for sensitizing cetuximab-resistant HNSCC cells to combination of cetuximab and radiation.

Chapter 4 Cetuximab inhibits aerobic glycolysis and reverses Warburg effect in HNSCC via inhibition of HIF-1-regulated LDHA

4.1 Introduction

Glucose is considered to be the most important energy and carbon source for both nontransformed and transformed cells. It has been observed for many years that cancer cells have different glucose metabolic pattern with normal cells. normal cells metabolize glucose mainly via a low rate of glycolysis followed by oxidative phosphorylation in the mitochondria through the tricarboxylic acid cycle, while cancer cells prefer to metabolize glucose by a high rate of glycolysis followed by lactate production in the cytosol even when oxygen is abundant, a phenomenon known as aerobic glycolysis or the "Warburg effect" [54, 104]. Because of the low efficiency of glycolysis in generating ATP, the reliance of tumor cells on glycolysis cause them to consume more glucose [105]. Aerobic glycolysis is important for cancer cell proliferation not only because this process provides the energy needed by cells to survive and perform various functions but more importantly because this process generates building blocks and reducing power, both of which are needed for cellular biosynthesis fueling cell growth and proliferation [106, 107]. Although the molecular mechanisms underlying the Warburg effect has not been fully understood yet, the altered glucose metabolism has been reported to be correlated directly with aberrant cell signaling caused by overexpression of growth factor receptors, activation of oncogenes, and/or inactivation of tumor suppressor genes to permit unlimited cancer cell proliferation [105-109].

The transcription factor HIF-1 plays a key role in reprogramming cancer cell metabolism from oxidative phosphorylation towards aerobic glycolysis through regulating expression of the genes coding for proteins involved in various steps of cancer metabolism including glucose transporters, glycolytic enzymes, and lactate transporters. Most importantly, HIF-1 activates lactate dehydrogenase A (LDH-A), the enzyme that catalyzes conversion from pyruvate to lactate [62]; and activates pyruvate dehydrogenase kinase 1 (PDK1), which phosphorylates and negatively regulates pyruvate dehydrogenase (PDH), the gatekeeper of tricarboxlic acid cycle [64]. Thus, activation of HIF-1 contributes to Warburg effect and mediates a glucose metabolic transition from oxidative phosphorylation towards glycolysis. HIF-1 has been reported to be overexpressed in many types of cancers, including colon, breast, gastric, lung, skin, ovarian, pancreatic, prostate, and renal carcinomas [110-112]. The high level of HIF-1α in cancer cells is caused not only by decreased ubiquitination and degradation of HIF-1α protein via a posttranslational mechanism associated with tumor hypoxia [44, 45] but also by increased expression of HIF-1α protein via a translational mechanism as a result of aberrant cell signaling [48-50, 113, 114].

Our work in Chapter 3 as well as previous work in our lab showed that cetuximab inhibits expression and function of HIF-1 through inhibition of the PI3K/Akt and MEK/Erk pathways, and this downregulation of HIF-1 by cetuximab is required, although may not be sufficient, for its anti-tumor effect [97, 115, 116]. Our work in Chapter 3 also showed that inhibition of HIF-1α by siRNA or small molecular inhibitor overcame resistance of cancer cells to cetuximab treatment as a monotherapy or in combination with radiation. Although the importance of HIF-1α downregulation in

mediating cetuximab-induced antitumor effects is well established, however, no studies so far have carefully examined the mechanism underlying growth inhibition after downregulation of HIF-1α by cetuximab. In this chapter, we hypothesized that cetuximab inhibits cancer cell proliferation through inhibition of glycolysis by downregulating HIF-1α, thereby reversing the Warburg effect that is critically important for cancer cell survival and proliferation. To test this hypothesis, we analyzed the impact of cetuximab treatment on changes in the two major energy-producing pathways of cells, glycolysis and mitochondrial respiration using the Seahorse XF96 extracellular flux analyzer in cetuximab sensitive and genetic matched acquired resistant HNSCC cell lines. We measured the effect of cetuximab on the expression and enzymatic activity of LDH-A, which regulates the conversion of pyruvate to lactate, and on the levels of glucose consumption, lactate production, and intracellular ATP in cetuximab-sensitive and cetuximab-resistant cells. Findings in this chapter provide novel insights into the mechanisms underlying cetuximab-induced antiproliferative and apoptotic effects in cancer cells and suggest a novel therapeutic strategy for improving the response of cancer patients to cetuximab treatment.

4.2 Results

4.2.1 Acquired resistance to cetuximab is not linked to the failure of cetuximab to inhibit EGFR downstream cell signaling

To study different responses to cetuximab between parental and cetuximab-acquired resistant HNSCC cells, we first generated two pairs of isogenic cetuximab-sensitive and cetuximab-resistant HNSCC cell lines by subjecting cetuximab-sensitive HN5 and FaDu cells to cetuximab-containing media in continuous culture for more than 1 year with stepwise increases in concentration up to 20 nM, which is approximately 10 times the Kd of cetuximab for binding to EGFR [26]. Figure 13A showed that the resultant sublines, termed HN5-R and FaDu-R respectively, were more resistant to cetuximab compared with parental HN5 and FaDu cells. HN5 cells have higher protein levels of EGFR and HIF-1α than FaDu cells. In both HN5 and FaDu cells, the protein levels of HIF-1α were decreased by cetuximab (Figure 13B). In contrast, HN5-R and FaDu-R cells exhibited higher levels of HIF-1α than their respective parental cells, and the effect of cetuximab in decreasing levels of HIF-1α in HN5-R and FaDu-R cells were minimal. Levels of LDH-A were decreased by cetuximab only in parental HN5 and FaDu cells but not in HN5-R and FaDu-R cells. Interestingly, HN5-R and FaDu-R cells remained sensitive or partially sensitive to cetuximab-induced inhibition of cell signaling, shown by inhibition of EGFR autophosphorylation and reduced phosphorylation of Akt-S473 and Erk T202/Y204, two important signaling molecules downstream of EGFR (Figure 13B). These novel findings suggested that acquired resistance to cetuximab may not be linked to the failure of cetuximab in inhibiting EGFR downstream signals.

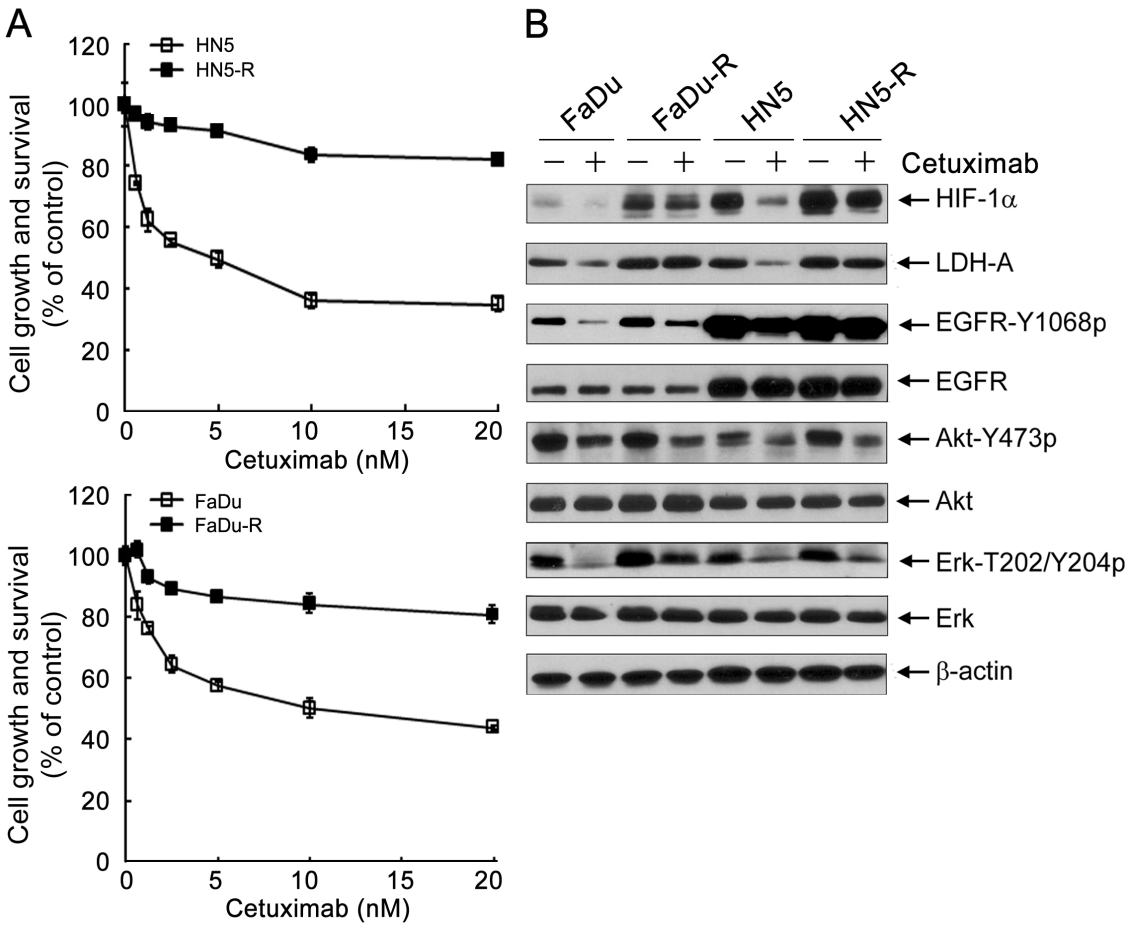

Figure 13. Acquired resistance to cetuximab is not linked to the failure of cetuximab to inhibit EGFR downstream cell signaling. (A) HN5 and FaDu cells and their cetuximab-resistant sublines (HN5-R and FaDu-R) selected after long-term exposure to cetuximab were treated with cetuximab at the indicated doses for 5 days in 0.5% FBS medium. Cell growth responses to cetuximab were measured by an MTT assay. (B) The indicated cells were left untreated or treated with 20 nM cetuximab for 24 hours. Cell lysates were prepared, and equal amounts of cell lysates were subjected to Western blot analysis with the indicated antibodies.

4.2.2 Cetuximab inhibits aerobic glycolysis, and resistance to cetuximab is linked to increased glycolytic flux

To further analyze the metabolic changes after cetuximab treatment, we employed the Seahorse XF96 extracellular flux analyzer to record metabolic profiles with and without cetuximab treatment in cetuximab-sensitive and cetuximab-resistant cell lines. Compared to the parental HN5 and FaDu cells, the cetuximab-resistant HN5-R and FaDu-R cells had higher levels of aerobic glycolysis, indicated by higher extracellular acidification rates (ECAR, black lines versus red lines in Figure 14). Furthermore, cetuximab decreased ECAR and increased oxygen consumption rate (OCR, blue lines versus red lines) in parental HN5 and FaDu cells, but not in HN5-R and FaDu-R cells (black lines versus green lines). It is noteworthy that after challenge of the cells with oligomycin, an ATP synthase inhibitor, the oxygen consumption rate in both the parental and cetuximab-resistant cell lines, particularly the resistant sublines, did not decrease significantly, indicating that the metabolic pattern of these cells are highly glycolytic. After challenge of the cells with FCCP, an uncoupler of oxidative phosphorylation and ATP synthesis, the resistant cell lines had higher capacity to increase ECAR than the parental cells. This finding is consistent with the higher HIF-1α and LDH-A levels in the resistant sublines than in the parental cells.

Taken together with 4.2.1, these novel findings indicate that LDH-A was downregulated and Warburg effect was reversed by cetuximab in cetuximab-sensitive HNSCC cells but not in the resistant sublines. The resistant sublines exhibited increased levels of HIF-1α as well as increased glycolytic potential.

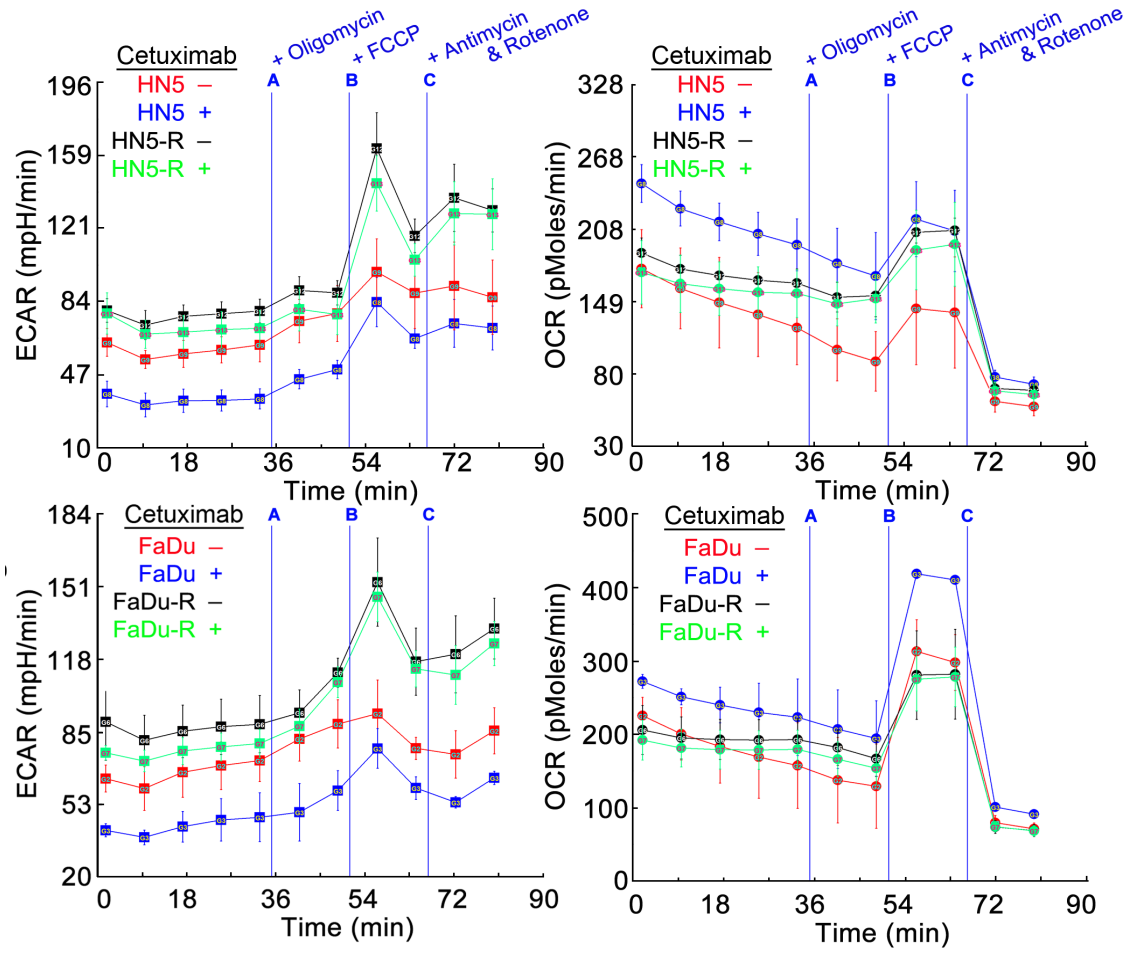

Figure 14. Cetuximab inhibits glycolytic flux in cetuximab-sensitive, but not acquired-resistant HNSCC cells. HN5, HN5-R, FaDu, and FaDu-R cells were left untreated or treated with 20 nM cetuximab for 10 hours, and metabolic flux analysis was performed to measure changes in extracellular acidification rate (ECAR) and oxygen consumption rate (OCR).

4.2.3 High level of HIF-1α are directly related with increased glycolysis in cetuximab acquired resistant cells

To further confirm a direct role of high level of HIF-1α in promoting aerobic glycolysis in HN5-R and FaDu-R cells, we knocked down HIF-1α in the cells and found that level of LDH-A was markedly decreased in both parental and the cetuximab-resistant sublines (Figure 15A). Knockdown of HIF-1α also induced significant decreases of ECAR and increases of OCR in HN5-R and FaDu-R cell lines (Figure 15B).

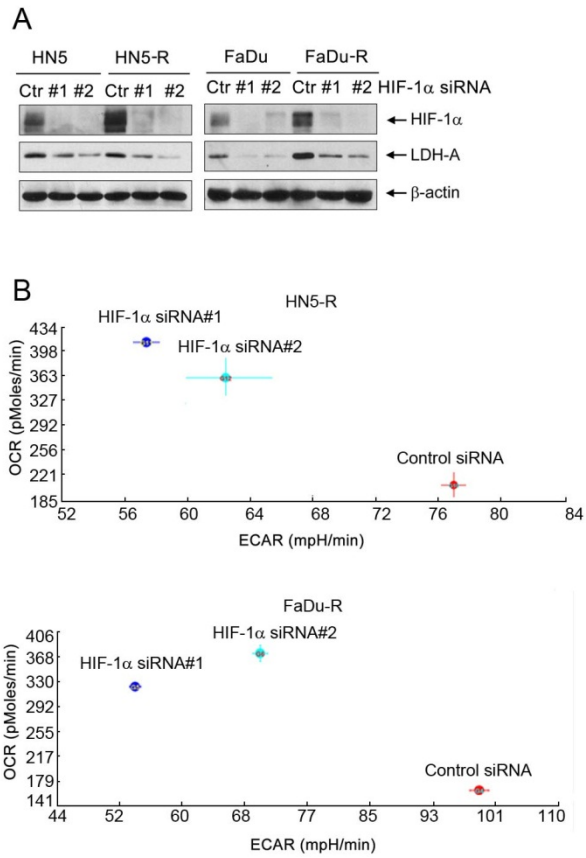

Figure 15. Knockdown of HIF-1 downregulates LDH-A and reverse Warburg effect. (A) HN5, HN5-R, FaDu, and FaDu-R cells were subjected to knockdown of HIF-1α by siRNA, followed by Western blotting with indicated antibodies. (B) HN5-R and FaDu-R cells were treated with each of 2 pairs of HIF-1 siRNA or control siRNA for 48 hours and metabolic flux analysis was performed to measure changes in ECAR and OCR.

4.2.4 Cetuximab reduces glucose consumption, lactate production and intracellular ATP level in a HIF-1α downregulation-dependent manner

To further confirm the inhibition of aerobic glycolysis by cetuximab we found in 4.2.2, we directly measured consumption of glucose and production of lactate after cetuximab treatment in HN5 and FaDu cells, and found that cetuximab inhibited glucose consumption and lactate production in a time-dependent manner (Figure 16A and B). To elucidate the mechanism through which cetuximab inhibits glycolysis, we transfected HN5 and FaDu cells with HIF-1α-ΔODD. As described in 3.2.2, this mutant retains the majority of the transcriptional activity of full-length HIF-1α and can be stably overexpressed in normoxic culture. Consistent with the knowledge that HIF-1 promotes aerobic glycolysis, overexpression of HIF-1α-ΔODD in HN5 and FaDu cells (HN5-HIF-1α-ΔODD and FaDu- HIF-1α-ΔODD cells) significantly increased the levels of glucose consumption and lactate production and conferred resistance to cetuximab mediated inhibition of glucose consumption and lactate production.

We also measured the changes of intracellular ATP levels after cetuximab treatment for a short time (4 hours) in HN5 and FaDu cells transfected with control vectors or with HIF-1α-ΔODD (Figure 16C). No changes in cell numbers were detected at 4 hours after treatment between cells treated and not treated with cetuximab. In HN5 and FaDu cells, cetuximab substantially decreased intracellular ATP levels (39% and 31%, respectively). In contrast, in HN5-HIF-1α-ΔODD and FaDu-HIF-1α-ΔODD cells, only modest decreases in the ATP levels (15% and 11%, respectively) were observed between after cetuximab treatment. Taken together, these findings showed that cetuximab inhibits glycolysis in a HIF-1α inhibition dependent manner.

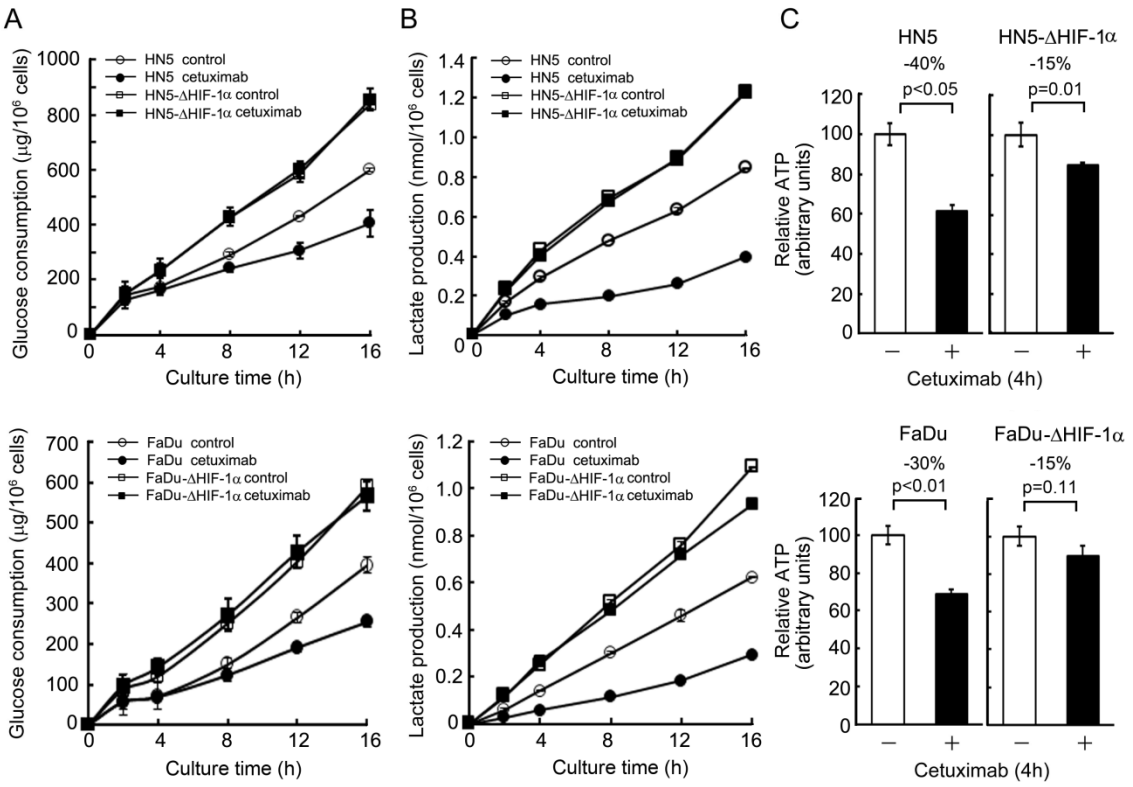

Figure 16. Cetuximab inhibits glucose consumption, lactate production, and intracellular ATP levels in a HIF-1α inhibition-dependent manner. (A) HN5, HN5-HIF-1α-ΔODD, FaDu, and FaDu-HIF-1α-ΔODD cells were seeded into 6-well plates with 3 mL of low glucose (1 g/L) medium supplemented with 0.5% FBS. The cells were treated with 20 nM cetuximab or not as indicated. At each time point after treatment, the level of glucose remaining in the conditioned medium was determined with an assay described in materials and methods. (B) The indicated cells were seeded and treated similarly as described in (A). At each time point after treatment, the level of lactate produced in the conditioned medium was determined with an assay described in materials and methods. (C) The indicated cells were left untreated or treated with 20 nM cetuximab in low-glucose (1 g/L) medium supplemented with 0.5% FBS for 4 hours. Cell pellets were harvested, and the intracellular level of ATP was measured with a luciferase based ATP determination assay as described in Materials and Methods. The relative values of ATP in treated groups were expressed as a percentage of the value of ATP in corresponding untreated groups.

4.2.5 Cetuximab inhibits LDH-A expression and enzymatic activity through downregulation of HIF-1α

To further elucidate the biochemical mechanisms through which cetuximab inhibits glycolysis via downregulation of HIF-1α, we studied the changes of LDH-A, a direct target of HIF-1 transcription factor, after cetuximab treatment in different time points. We compared the effect of cetuximab on downregulation of LDH-A and on EGFR downstream signaling pathways between HN5 and HN5-HIF-1α-ΔODD cells and between FaDu and FaDu-HIF-1α-ΔODD cells. We found that cetuximab treatment downregulated the protein levels of LDH-A in both HN5 and FaDu cells but not in HN5-HIF-1α-ΔODD and FaDu-HIF-1α-ΔODD cells (Figure 17A). Interestingly, the phosphorylation levels of Akt and Erk were still sensitive to cetuximab in HN5-HIF-1α-ΔODD and FaDu-HIF-1α-ΔODD cells. This is consistent with phosphorylation levels of these molecules after cetuximab treatment in HN5-R and FaDu-R cells, as described in 4.2.1.

Consistent with the decrease in LDH-A protein levels in HN5 and FaDu cells induced by cetuximab, the activity of LDH-A in catalyzing the production of lactate was also decreased in these cells, as early as 4 hours after cetuximab treatment (Figure 17B). Overexpression of HIF-1α-ΔODD significantly increased the enzymatic activity of LDH-A, and abolished the effect of cetuximab in inhibiting LDH-A activity. Taken together, these findings showed that cetuximab downregulates LDH-A expression and inhibits LDH-A activity via downregulation of HIF-1α, leading to inhibition of glycolysis.

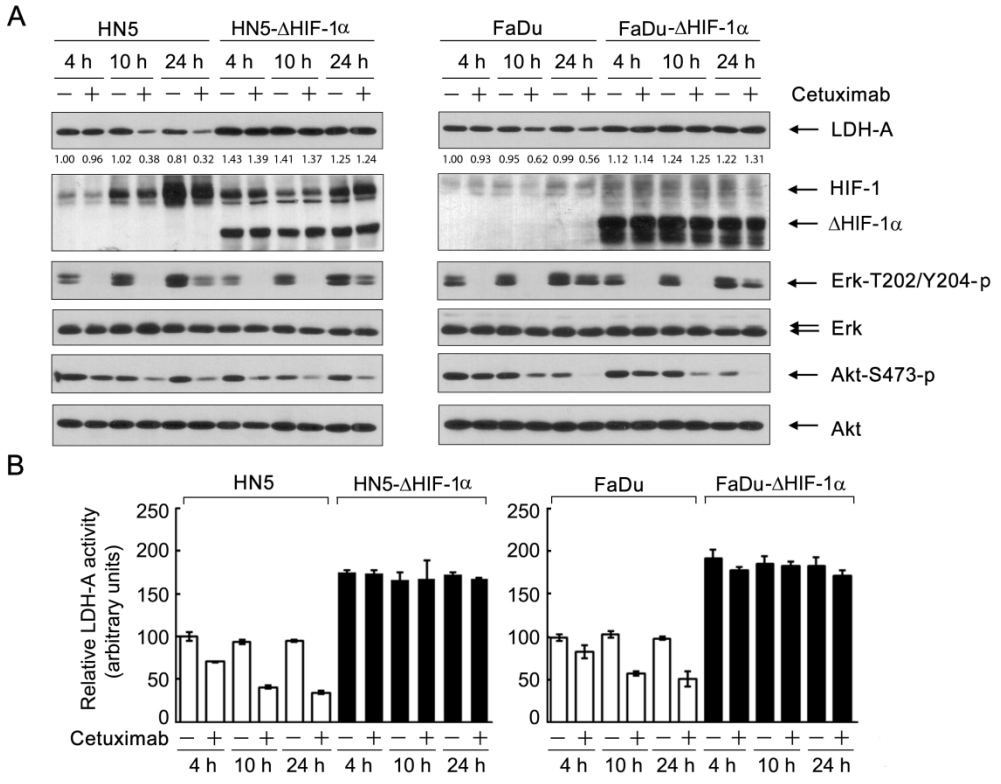

Figure 17. Cetuximab downregulates LDH-A expression and reduces LDH-A activity in a HIF-1α inhibition-dependent manner. HN5 and FaDu cells expressing control vector or HIF- 1α-ΔODD were left untreated or treated with 20 nM cetuximab for the indicated time periods. (A) Cell lysates were prepared, and equal amounts of cell lysates were subjected to Western blot analysis with the indicated antibodies. (B) Cells were harvested and homogenized, and samples containing equal amounts of proteins were subjected to an LDH-A activity assay as described in materials and methods.

4.2.6 Knockdown of LDH-A overcomes resistance to cetuximab-induced G1 arrest

Aerobic glycolysis has been suggested to be a means of fueling cancer cells with energy and biomass needed for proliferation [117]. To find the correlation between cetuximab-induced inhibition of glycolysis through downregulating HIF-1α and LDH-A and the effect of cetuximab in inhibiting cancer cell proliferation, we performed cell cycle analysis after treatment with cetuximab and LDH-A siRNA, alone and in combination. To avoid off-target effect of LDH-A, three different LDH-A-specific siRNA were tested in our experiments, all of which successfully knocked down the level of LDH-A in all four cell lines (Figure 18A, C, and E). LDH-A siRNA #1 and #2 were used for knockdown of LDH-A in the cells for cell cycle analysis.

Treatment of HN5 and FaDu cells with cetuximab increased the percentage of cells in G1 phase from 67.9% to 85% in HN5 cells and from 64.9% to 83.2% in FaDu cells (Figure 18B). Knockdown of LDH-A expression alone by siRNA #1 modestly increased the percentage of G1 phase cells from 67.9% to 73% in HN5 cells and 64.9% of 70.2% in FaDu cells. The combination of cetuximab and LDH-A knockdown had an additive effect on G1 arrest, increasing the percentage of G1 phase cells to 90.3% in HN5 cells and 87.1% in FaDu cells. Similar results were confirmed by using LDH-A siRNA #2 (Figure 19).

Compared with HN5 and FaDu cells, both the acquired resistant sublines and the HIF-1α-ΔODD-overexpressing cell lines showed increases in the percentage of proliferating cells. The percentage of cells in G2/M phase increased from 24% in HN5 cells to 33.9% and 39.4% in HN5-R and HN5-HIF-1α-ΔODD cells respectively and from 22.3% in FaDu cells to 28.1% and 27.7% in FaDu-R and FaDu-HIF-1α-ΔODD

cells respectively (Figure 18B, D, and F). These cells were also resistant to cetuximab-induced G1 arrest. Cetuximab failed to increase the percentage of G1 phase cells in either acquired resistant sublines or HIF-1α-ΔODD-overexpressing cell lines. Since both HN5-R and FaDu-R have much higher HIF-1α levels compared with their parental counterpart, this finding is consistent with the role of HIF-1α in counteracting cetuximab-induced inhibition of glycolysis and downregulation of LDH-A. Knockdown of LDH-A by siRNA #1 largely restored the activity of cetuximab in inducing G1 cell cycle arrest in these cells: compared to cetuximab alone, the combination of cetuximab and LDH-A knockdown increased the percentage of G1 phase cells from 54.0% to 72.3% in HN5-R cells, from 52.5% to 84.7% in HN5-HIF-1α-ΔODD cells, from 60.7% to 76.5% in FaDu-R cells, and from 67.9% to 83.0% in FaDu-HIF1α-ΔODD cells. Similar results were confirmed by using LDH-A siRNA #2 (Figure 19). These findings confirm the role of HIF-1α in cetuximab-induced cell cycle arrest and suggest LDH-A as a good target to improve cancer cell response to cetuximab treatment.

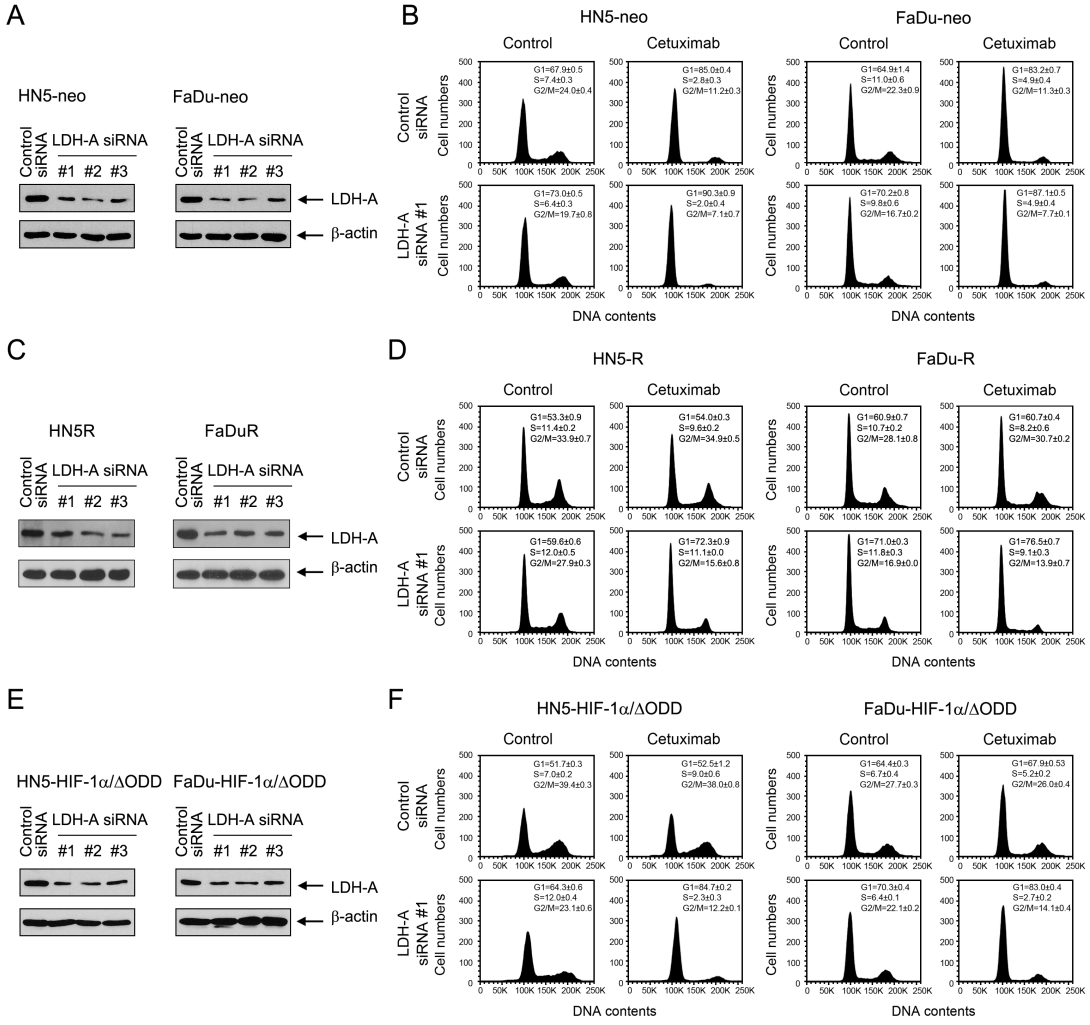

Figure 18. Knockdown of LDH-A overcomes resistance to cetuximab-induced G1 arrest. (A), (C) and (E) The indicated cells were subjected to knockdown of LDH-A with three different LDH-A-specific siRNA or control siRNA in low-glucose (1 g/L) and low-serum (0.5% FBS) medium for 48 hours. Cell lysates were prepared, and equal amounts of cell lysates were subjected to Western blot analysis with the indicated antibodies. (B), (D) and (F) The indicated cells were treated with LDH-A siRNA #1 or control siRNA as described in (A), (C) and (E). The cells were then left untreated or treated with 20 nM cetuximab for 24 hours, followed by fixation and propidium iodide staining for cell cycle distribution analysis by flow cytometry. The data presented are mean ± SD.

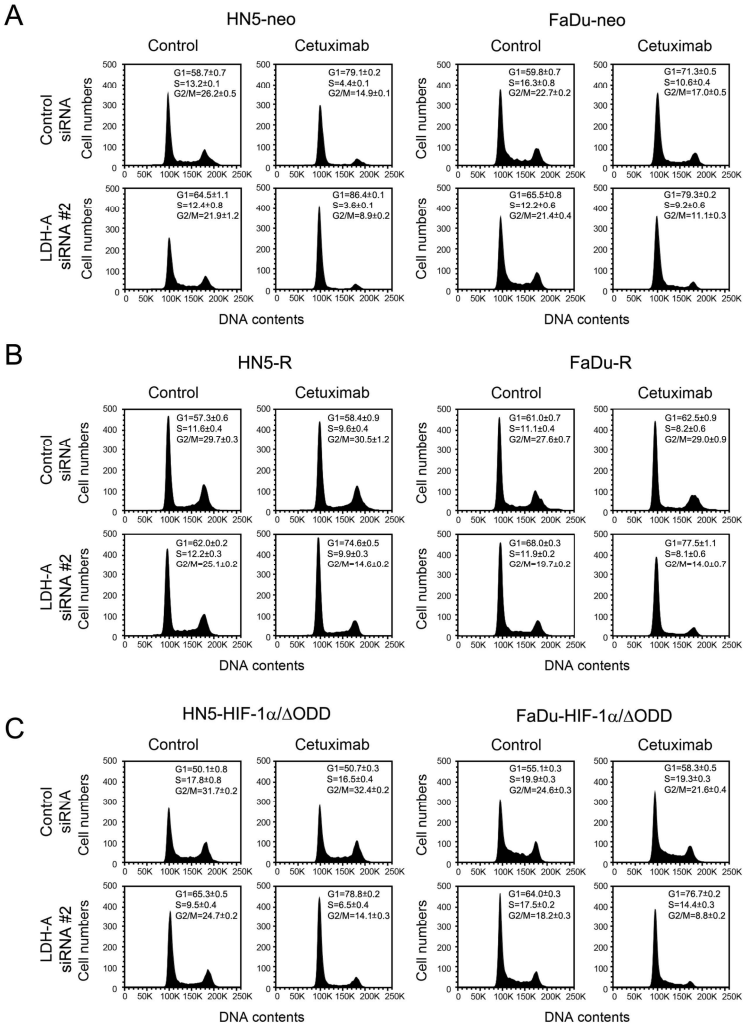

Figure 19. Knockdown of LDH-A overcomes resistance to cetuximab-induced G1 arrest. The indicated cells were treated with LDH-A siRNA #2 or control siRNA for 48hours, and then left untreated or treated with 20 nM cetuximab for 24 hours, followed by fixation and propidium iodide staining for cell cycle distribution analysis by flow cytometry. The data presented are mean ± SD.

4.2.7 Knockdown of LDH-A potentiates cetuximab to induce apoptosis but fails to overcome cetuximab resistance through inducing apoptosis

To determine whether knockdown of LDH-A can potentiate induction of apoptosis in addition to G1 cell cycle arrest by cetuximab, we examined induction of apoptosis using two independent apoptosis assays (PARP cleavage and DNA fragmentation) in the HN5 series (parental HN5, HN5-R, and HN5-HIF-1α-ΔODD cells) and FaDu series (parental FaDu, FaDu-R, and FaDu-HIF-1α-ΔODD cells) after treatment with cetuximab and knockdown of LDH-A, alone and in combination. The combination treatment resulted in an additive effect on decreasing the levels of LDH-A in parental HN5 and FaDu cells, but not in HN5-R and FaDu-R cells or in HN5-HIF-1α-ΔODD and FaDu-HIF-1α-ΔODD cells (Figure 20A). Compared with either single treatment alone, the combination treatment induced apoptosis in HN5 and FaDu cells but only had minimal such effect in the acquired resistant sublines and the HIF-1α-ΔODD-overexpressing cells (Figure 20A and B). These findings indicate that while knockdown of LDH-A can potentiate cetuximab to induce apoptosis, it alone may not be sufficient to induce apoptosis or to overcome cetuximab resistance to induce apoptosis when used in combination with cetuximab.

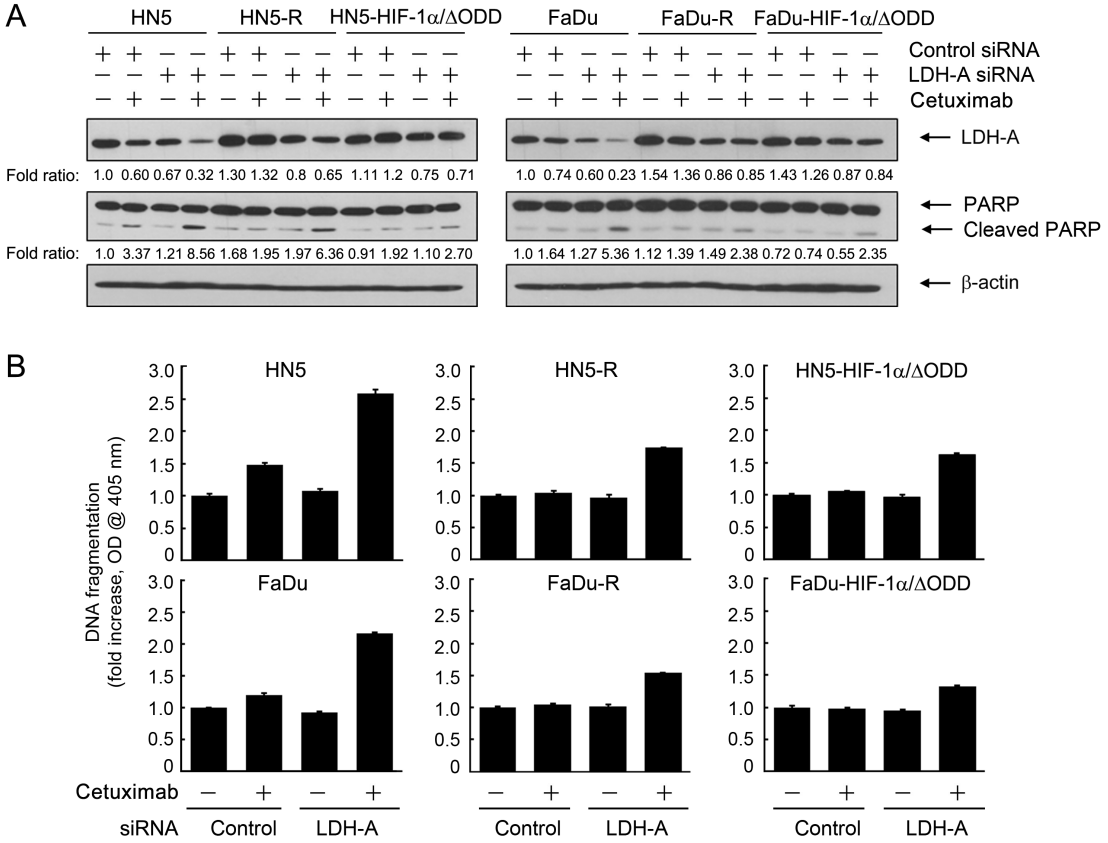

Figure 20. Knockdown of LDH-A minimally potentiates induction of apoptosis by cetuximab. The indicated cells were subjected to knockdown of LDH-A with specific siRNA or control siRNA for 48 hours and then treated with 20 nM cetuximab or not as indicated for 24 hours in low glucose (1 g/L) and low serum (0.5% FBS) medium. (A) After treatment, cell lysates were prepared, and equal amounts of cell lysates were subjected to Western blot analysis with the indicated antibodies. Quantification of the LDH-A and cleaved PARP bands was performed with ImageJ software and the data were expressed as fold increases in reference to the leftmost lane of the blots, the value of which was arbitrarily set as 1. (B) The same cell lysates as in (A) were analyzed for the level of DNA fragmentation with an apoptosis ELISA kit as described in materials and methods. The data in the treated groups were expressed as fold increases in the optical density value compared to the value in corresponding untreated cells.

4.2.8 Combination of cetuximab and LDH-A inhibitor oxamate effectively inhibit cell proliferation in cetuximab resistant cancer cells

To further confirm LDH-A as a target to increase cetuximab response and to overcome cetuximab resistance, we examined the effects of a small molecule inhibitor of LDH-A, oxamate [118], alone and in combination with cetuximab on growth and survival of HNSCC cells after 5-day extended culture (Figure 21). MTT assays, which collectively measure the effects of cell cycle arrest and induction of apoptosis, showed that combination treatment with cetuximab and oxamate significantly enhanced inhibition of cell growth and survival compared with either single treatment alone, particularly in the cetuximab-resistant sublines. We found similar results by the combination treatment in other HNSCC cell lines, UMSCC1, OSC19, Sqcc/Y1, and TU167, which are naturally resistant to cetuximab-induced growth inhibition (Figure 22). Together, these data support a novel strategy of co-targeting LDH-A to improve the therapeutic effect of cetuximab in cancer cells.

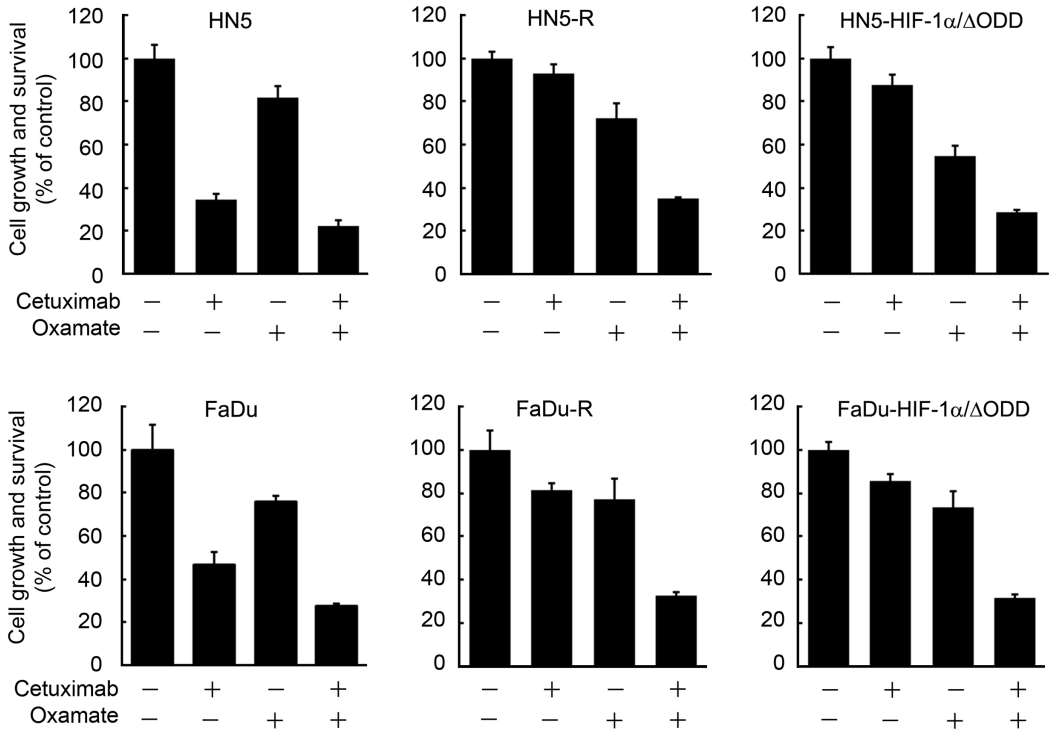

Figure 21. Combination of cetuximab and oxamate effectively inhibit cell proliferation in HNSCC cells. The indicated cells were left untreated or treated with 20 nM cetuximab, 5 mM oxamate, or both for 5 days. Cell growth responses to cetuximab were measured by an MTT assay. The cell growth and survival in treated groups were expressed as a percentage of the optical density value in the corresponding untreated cells.

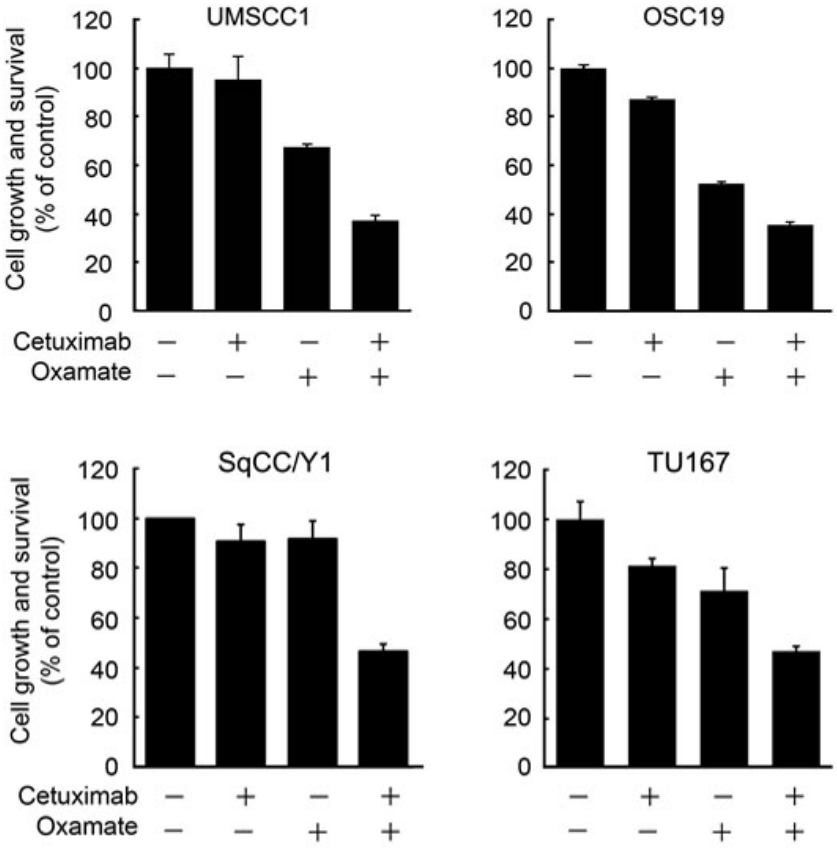

Figure 22. Combination of cetuximab and oxamate effectively inhibit cell proliferation in cetuximab-resistant HNSCC cells. The indicated cells were left untreated or treated with 20 nM cetuximab, 5 mM oxamate, or both for 5 days. Cell growth responses to cetuximab were measured by an MTT assay. The cell growth and survival in treated groups were expressed as a percentage of the optical density value in the corresponding untreated cells.

4.2.9 Cetuximab has no significant effect on inhibiting glycolysis in nontransformed cells in normoxia

Most nontransformed cells consume much less glucose compared with cancer cells because normal cells use a more energy-efficient pathway, oxidative phosphorylation, for energy production. To determine whether the effect of cetuximab in inhibiting glycolysis is cancer cell selective, we examined the changes in cell proliferation, glucose consumption, lactate production, LDH-A activity and ATP level in NOM9-TK cells, an immortalized human head and neck epithelial cell line, with and without cetuximab treatment in normoxic culture. Proliferation of NOM9-TK cells in the absence of EGF was slow and was barely inhibited by cetuximab (Figure 23A). NOM9-TK cells express a very low level of HIF-1α in culture under normoxia compared to hypoxia. Cetuximab treatment did not decrease LDH-A protein level in NOM9-TK cells (Figure 23B) and did not significantly inhibit glucose consumption (Figure 23C), lactate production (Figure 23D), LDH-A activity (Figure 23E), or intracellular ATP level (Figure 23F) in the cells in normoxic culture. The absolute amount of lactate production was markedly less in NOM9-TK cells (Figure 23D) than in HN5 and FaDu cells for the same period (Figure 16B). These findings indicate that cetuximab may inhibit aerobic glycolysis selectively in cancer cells through downregulation of LDH-A, which causes cancer cells that rely heavily on aerobic glycolysis for biosynthetic metabolism and energy production, to arrest at G1 phase.

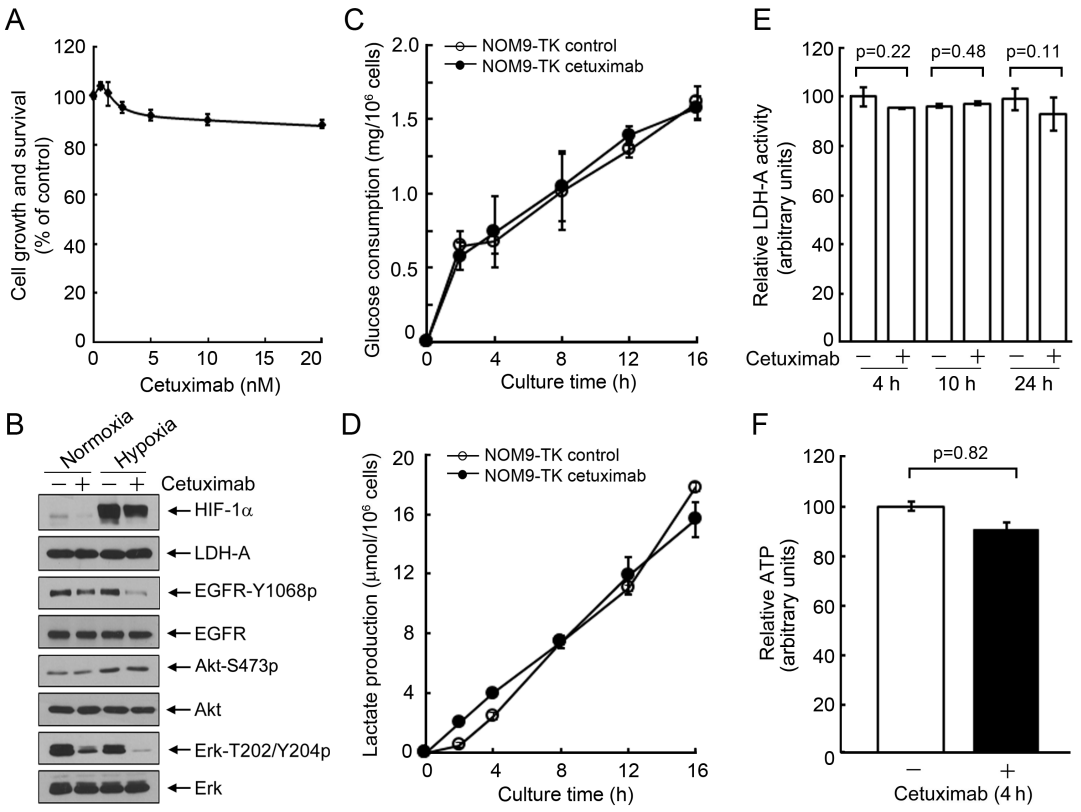

Figure 23. Cetuximab does not affect glycolysis in normal cells. (A) NOM9-TK cells were left untreated or treated with 20 nM cetuximab for 5 days in chemically-defined KGM medium supplemented with components provided in the SingleQuots kit except EGF. Cell growth response to cetuximab was measured by an MTT assay. (B) NOM9-TK cells were left untreated or treated with 20 nM cetuximab for 24 hours under normoxia. Cells treated the same way under hypoxia served as controls. Cell lysates were subjected to Western blot analysis with the indicated antibodies. (C) and (D) NOM9-TK cells were seeded into 6-well plates with 3 mL of low-glucose (1 g/L) cell culture medium and treated with or without 20 nM cetuximab for the indicated times. At each time point after treatment, the level of glucose remaining in the conditioned medium (C) and the level of lactate produced in the conditioned medium (D) were determined with assays described in materials and methods. (E) NOM9-TK cells were left untreated or treated with 20 nM cetuximab for the indicated time periods. Cells were harvested and homogenized, and samples containing equal amounts of proteins were subjected to an LDH-A activity assay as described in materials and methods. (F) NOM9-TK cells were left untreated or treated with 20 nM cetuximab in serum-free keratinocyte growth medium for 4 hours. Cell pellets were harvested, and the intracellular level of ATP was measured with a luciferase-based ATP determination assay as described in materials and methods. The data presented are mean ± SD.

4.3 Discussion

Previously our lab has reported that cetuximab downregulates HIF-1, one of the key players in regulating tumor metabolism. Thus far, how cetuximab affects cancer cells in the perspective of metabolism is not clear. Here we reported that (1) Cetuximab inhibits glycolysis in cancer cells, but not in normal cells; (2) Overexpression of HIF-1 could abolish the role of cetuximab in mediating glycolysis inhibition in cancer cells; (3) Cetuximab mediated glycolysis inhibition is associated with the role of cetuximab in cell cycle arrest; (4) Combination of cetuximab and glycolysis inhibitor resensitizes responses to cetuximab in cetuximab-resistant cell lines. Our study, for the first time in literature, expands understanding of cetuximab-mediated EGFR targeted therapy to the field of cancer metabolism.

Cancer cells rely on an uninterrupted supply of energy and building blocks for fueling unlimited cell proliferation. An adequate supply of energy and biomass depends in large part on elevated glycolytic flux in cancer cells. On the other hand, the high reliance of cancer cells on glycolysis for energy and building blocks also made glycolysis, the “sweet tooth” of cancer, an appealing target for cancer therapeutics. Inhibition of glycolysis in cancer cells by cetuximab decreases the supply of energy and biomass needed for proliferation, and the cells are therefore arrested at G1 phase. Depending on the extent to which glucose-derived pyruvate is redirected to the tricarboxylic acid cycle for oxidative phosphorylation induced by glycolysis inhibition, inhibition of LDH-A may also induce apoptosis in addition to cell cycle arrest. This is because excess oxidative phosphorylation of pyruvate may cause overproduction of reactive oxygen species that are cytotoxic to cells, leading to apoptosis. Indeed, we

found evidence of apoptosis when cells were treated with cetuximab in combination with LDH-A knockdown by siRNA.

The most important characteristics of a cancer therapeutic drug is the highly selectivity to cancer cells and low cytotoxicity to normal cells. Here we reported that cetuximab selectively inhibits glycolysis only in tumor cells, but not in normal NOM9-TK cells. This selectivity is based on the different glucose metabolic pattern of cancer cells and normal cells. Cancer cells and normal cells share the biochemical process of glycolysis from glucose to pyruvate. However, in the presence of oxygen, normal cells prefer to use pyruvate in mitochondria for tricarboxlic acid cycle and following oxidative phosphorylation to produce large amount of ATP; while cancer cells prefer to use pyruvate for aerobic glycolysis to produce intermediate metabolites as building blocks for anabolism, with an end-product of lactate. We found that cetuximab selectively inhibits the expression level and activity of LDHA, but not the other key glycolytic enzymes which catalyze conversion from glucose to pyruvate. In addition, we also found that cetuximab has only mild effects on the function of mitochondria. Both of them prove that in the perspective of metabolism, the effect of cetuximab is highly selective to cancer cells.

Another interesting finding of the current work is that HNSCC cells with resistance to cetuximab acquired through long-term adaptation or through experimental overexpression of HIF-1α-ΔODD remained at least partially sensitive to cetuximab-induced inhibition of major cell signaling pathways downstream of EGFR, in contrast to resistance to cetuximab-induced decrease in the level of LDH-A. This finding indicates LDH-A as a potential better biomarker than the downstream signaling molecules for

predicting cancer cell responsiveness to cetuximab treatment. It is noteworthy that despite the elevation of HIF-1α or HIF-1α-ΔODD in the cetuximab-resistant sublines of HN5 (HN5-R and HN5-HIF-1α/ΔODD) and FaDu (FaDu-R and FaDu-HIF-1α/ΔODD), the basal level of LDH-A was only modestly elevated in these cells. This is most likely because the basal level of LDH-A was sufficient to drive the direction of glycolysis towards lactate production in these cells. It was when the cells were treated with cetuximab, the elevated HIF-1α or HIF-1α-ΔODD protected against downregulation of LDH-A by cetuximab.

The phenomenon that cetuximab could still inhibit EGFR-downstream signaling pathway activities in cetuximab-resistant cell lines also provides a novel strategy in overcoming cetuximab-resistance by targeting both EGFR-signaling pathways and tumor glycolysis in cetuximab-resistant cancer cells. Although targeting EGFR broadly inhibits its downstream signaling networks activated by the receptor tyrosine kinase, some of its downstream signaling pathways can be bypassed due to alternative and/or constitutive activation of these pathways at various levels, which causes the failure of EGFR-targeted therapy. Glycolysis is important for cancer progression by providing bioenergy and building blocks for cell growth. Here our data showed that combination of cetuximab and glycolysis inhibitor oxamate has synergetic effect in inhibiting cell growth in cetuximab-resistant cell lines.

An important caveat is that glycolysis inhibition by cetuximab may not be mediated only through inhibition of LDH-A. Inhibition of other glycolytic enzymes, which are subjected to regulation by HIF-1, might also be important for cetuximab to successfully inhibit cancer cell proliferation. Therefore, in contrast to overexpression of HIF-1α,

overexpression of LDH-A alone may not be sufficient to confer resistance to cetuximab.

In summary, we demonstrated that cetuximab inhibits cancer cell proliferation via inhibiting glycolysis. Our findings suggest that LDH-A may be a novel predictor of cetuximab response and also a target for sensitizing cetuximab-resistant cells to cetuximab treatment. Our work fills in a major gap in knowledge regarding the link between EGFR-targeted therapy and cancer cell metabolism, which could lead to a major advance in our understanding of how cetuximab inhibits the proliferation of cancer cells and development of new strategies for enhancing cetuximab-mediated anti-EGFR therapy.

Chapter 5 Cetuximab downregulates EGFR-associated ASCT2 and decreases antioxidant capacity of HNSCC

5.1 Introduction

The majority of HNSCCs express a high level of EGFR, however, only a small fraction of head and neck cancer patients respond to EGFR antibody cetuximab [119, 120]. A consensus is emerging that many tumors are resistant to cetuximab because of frequent constitutive activation of oncogenes and/or mutational inactivation of tumor suppressor genes in EGFR downstream signaling pathways or redundant activation of EGFR downstream pathways by receptor tyrosine kinase other than EGFR [94, 121]. *In vitro* studies showed that even in cetuximab-sensitive cancer cell lines, cetuximab majorly induces cytostatic, rather than cytotoxic effect, through arresting cell cycle in G1 phase, accompanied by a decrease in cyclin-dependent kinase 2 activity, and an increase in the expression of cyclin-dependent kinase inhibitor p27KIP1 [122, 123]. Our novel findings in Chapter 4 elucidated that cetuximab-mediated glycolysis inhibition is the underlying mechanism of antitumor effect of cetuximab in the perspective of metabolism, further supporting that the effect of cetuximab is mainly through cell growth inhibition.

Different from normal cells, cancer cells prefer to convert glucose-generated pyruvate into lactate, even in the presence of oxygen, a phenomenon called “Warburg effect”. One of the major advantages for cancer cell to adopt the low-efficient energy yielding glycolytic pathway is the reduction of reactive oxygen species (ROS) production [124]. Mitochondria are the principle source of metabolically produced ROS

[125]. The flux of electrons carried by NADH and $FADH_2$ through electron transport chain (ETC) leads to the formation of ROS in complex I, II, and III, where electrons can be prematurely reduce oxygen [126, 127]. Low levels of mitochondrial ROS production are required for cellular processes such as proliferation and differentiation; however, overproduction of ROS will lead to the initiation of senescence and apoptosis, or even non-signaling, irreversible damage to cellular components [69].

Evidence from recent studies showed that cancer cells, compared with normal cells, exhibit increased intrinsic ROS stress, because of oncogenic stimulation, increased metabolic activity, and mitochondrial malfunction [128-131]. Although increased amounts of ROS in cancer cells might stimulate cellular proliferation, promote mutations and genetic instabilities, and cause drug resistance, it can also be toxic to cancer cells, since cancer cells with increased oxidative stress are more vulnerable to damage by further ROS insults [132]. Therefore, it is rational to induce ROS overproduction by redox modulation to selectively kill cancer cells without causing significant toxicity to normal cells [133].

The fate of glucose metabolism, which either ends with glycolysis in cytoplasm or continues with tricarboxylic acid cycle (TCA cycle) for fully oxidation, is controlled by gate-keeping mitochondrial enzyme pyruvate dehydrogenase (PDH). PDH converts pyruvate to acetyl-CoA, which is fed to the TCA cycle, leading to the production of the electron donors NADH and $FADH_2$ for further oxidative phosphorylation. PDH is phosphorylated and negatively regulated by PDH kinase (PDK). Targeting PDK in cancer cells may redirect the glycolysis product pyruvate to mitochondria for oxidative phosphorylation, which may lead to overproduction of ROS. However, our preliminary

studies showed that targeting PDK alone, either by siRNA or small molecule inhibitor dicholoroacetate, could not induce overproduction of ROS and apoptosis, because cancer cells, through unknown mechanisms, maintain a homeostatic balance between the formation of ROS and their removal by endogenous antioxidant defense mechanism in response to PDK inhibition. In this chapter, we hypothesized that cetuximab decreases intracellular GSH level, causing inadequate antioxidant defensive capacity in cancer cells. We tested the cytotoxic effect induced by combination of cetuximab and PDK1 targeting in a couple of cetuximab-sensitive and cetuximab-resistant HNSCC models, *in vitro* and *in vivo*. We elucidated the contribution of cetuximab in the novel combination strategy by finding an EGFR associated membrane protein ASCT2, which regulates glutamine uptake and following GSH synthesis. Findings in this chapter discover a novel mechanism of cetuximab in regulating anti-oxidant capacity in cancer cells, and provide a novel and efficient therapeutic strategy for improving the response of cancer patients to cetuximab, which is synergetic and synthetic lethal and is independent of EGFR kinase inhibition.

5.2 Results

5.2.1 Combination of cetuximab and silencing PDK1, but not either treatment alone, induces apoptosis.

Inhibition of PDK1, through activation of PDH, redirects the glucose-derived pyruvate for oxidative phosphorylation through the tricarboxylic acid cycle, and generates ROS as a by-product. We firstly hypothesized that inhibition of PDK1 may result in apoptosis through overproduction of ROS in cancer cells. However, we found that in HN5 and FaDu cells, silencing PDK1 with any 3 of different siRNAs for 72 hours only resulted in a slight inhibition of cell proliferation through MTT assay (Figure 24A). The growth inhibition induced by PDK1 siRNA is similar to that induced by cetuximab treatment for 24 hours. Silencing PDK1 failed to increase cleavage of PARP and Caspase 3, indicators of apoptosis, and to decrease clonogenic capacity in HN5 and FaDu cells (Figure 24B and C), indicating that the inhibitory effect induced by PDK1 siRNA is mainly cytostatic rather than cytotoxic effect. Consistent with our result in 4.2.7, cetuximab treatment alone for 24 hours did not readily induce apoptosis or decrease clonogenic capacity in HN5 and FaDu cells either. Interestingly, we found that combination of cetuximab and PDK1 siRNA significantly lowered cell viability compared with the viability with either treatment alone (Figure 24A), induced cleavage of PARP and Caspase 3 (Figure 24B), and markedly reduced the number of surviving clones (Figure 24C). These data showed that different from either treatment alone, combination of cetuximab and PDK1 siRNA are toxic to HNSCC cells.

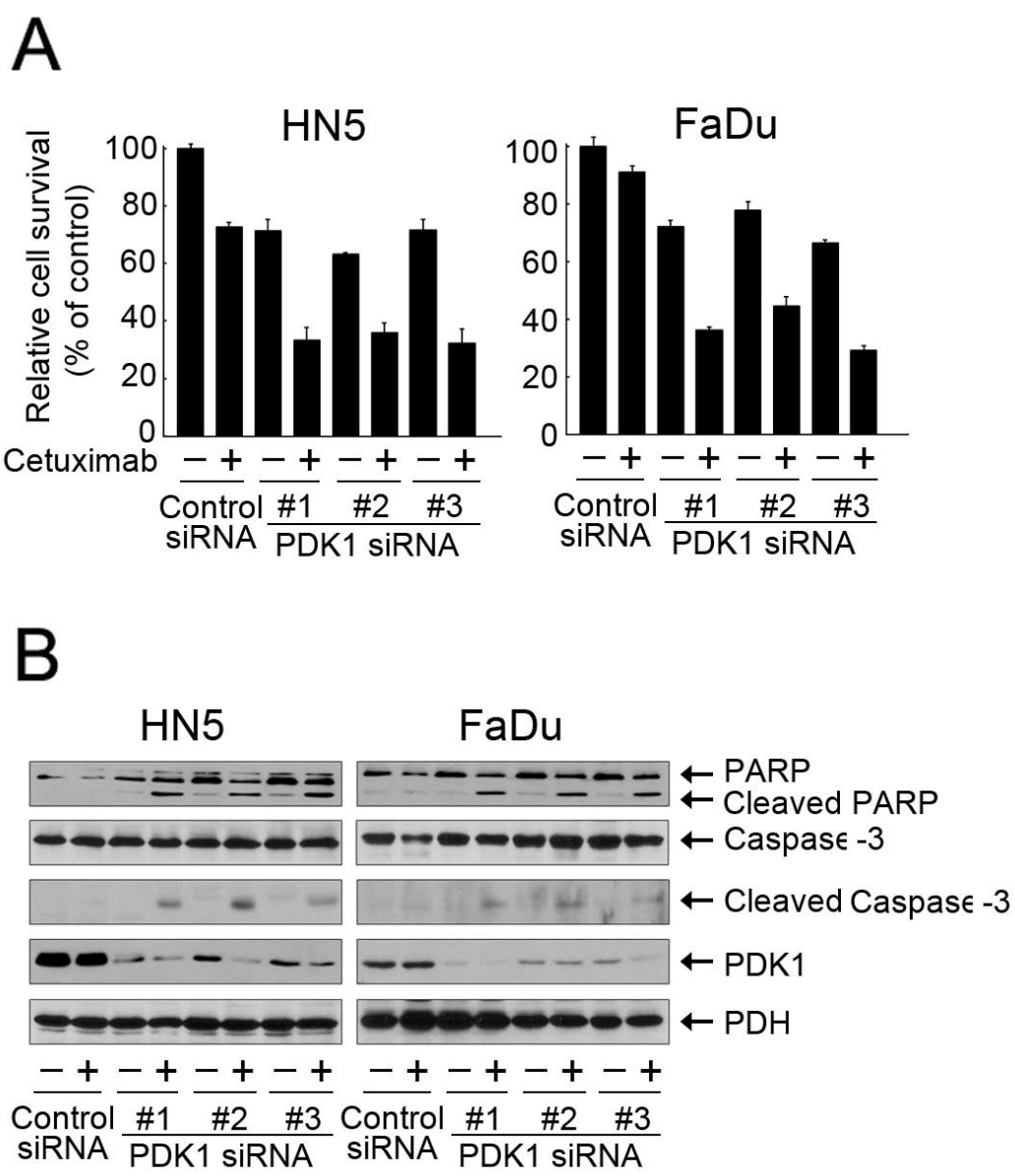
A
HN5
FaDu
Relative cell survival
(% of control)
100
80
60
40
20
0
Cetuximab
− + − + − + − +
Control siRNA
#1 #2 #3
PDK1 siRNA
B
HN5
FaDu
← PARP
← Cleaved PARP
← Caspase -3
← Cleaved Caspase -3
← PDK1
← PDH
− + − + − + − +
Control siRNA
#1 #2 #3
PDK1 siRNA

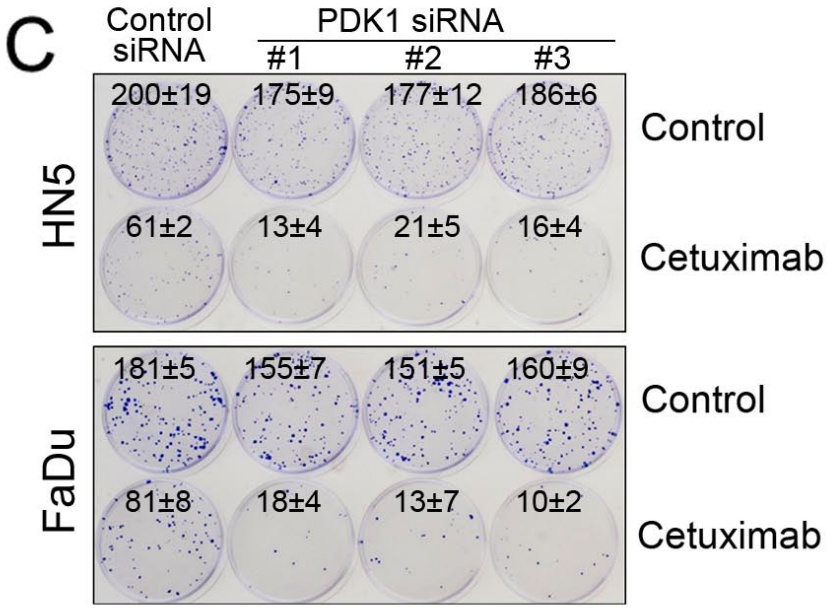

Figure 24. Impact of cetuximab and PDK1 silencing, alone or in combination, on cell proliferation, apoptosis, and clonogenic capacity. (A) HN5 and FaDu cells were subjected to PDK1 silencing with each of 3 different PDK1 siRNAs or control siRNA for 72 hours. During the last 24 hours, cells were then treated with or without 20 nM cetuximab, and then MTT assays were performed for determination of the responses of the cells to the treatment. (B) HN5 and FaDu cells treated as in (A) were harvested. Cell lysates were prepared, and equal amounts of cell lysates were subjected to Western blot analysis with the indicated antibodies. (C) HN5 and FaDu cells treated as in (A) were seeded at low density and subjected to a clonogenic survival assay as described in materials and methods.

5.2.2 Combination of cetuximab and silencing PDK1 induces overproduction of ROS and loss of mitochondrial membrane potential

Both cetuximab and PDK1 inhibition could reverse Warburg effect and redirect glucose metabolism from aerobic glycolysis to oxidative phosphorylation, which will generate ROS. To elucidate the mechanism through which combination of cetuximab and PDK1 siRNA are toxic to cancer cell, we examined the effect of cetuximab and PDK1 siRNA, alone or in combination, in inducing ROS production. Figure 25A showed that either cetuximab or PDK1 silencing alone did not result in detectable ROS, while combination of them led to overproduction of ROS in both HN5 and FaDu cells. Similar phenomenon was confirmed in an independent ROS detection assay with flow cytometry (Figure 25B).

Mitochondrial membrane potential, $\Delta\psi m$, is an important parameter of mitochondrial function used as an indicator of cell health [134]. Overproduction of ROS will cause dysfunction of complex I of electron transport chain, limit the efflux of H^+, and lead to the decrease of $\Delta\psi m$. Upon sustained and significant decrease in $\Delta\psi m$, the voltage-sensitive mitochondrial transition pore opens, allowing the efflux of many proapoptotic factors and the initiation of apoptosis. To directly link the ROS overproduction and apoptosis induced by combination of cetuximab and PDK1 siRNA, we measured $\Delta\psi m$ in HN5 and FaDu cells with treatment of cetuximab and PDK1 siRNA, alone or in combination by the staining of $\Delta\psi m$-dependent fluorescent dye tetramethyl rhodamine methyl ester (TMRM). Consistence with the finding in ROS production, either treatment alone did not induce loss of $\Delta\psi m$, while combination treatment caused a significant decrease of $\Delta\psi m$ (Figure 25C and D).

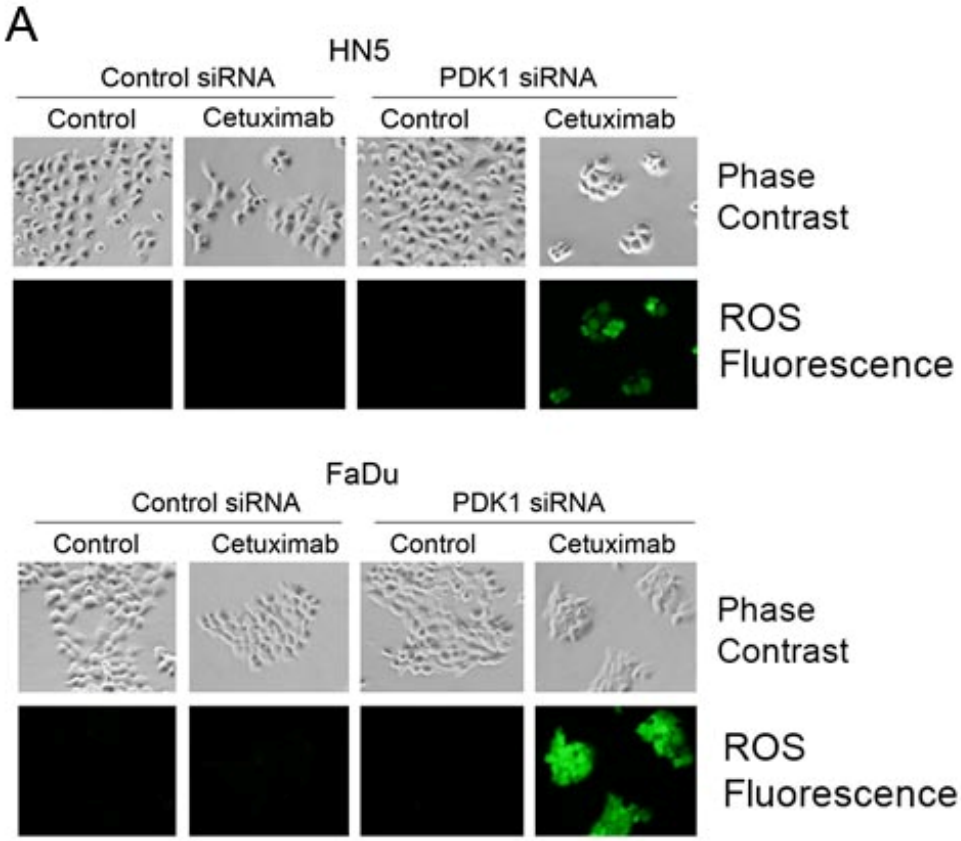
A
HN5
Control siRNA
PDK1 siRNA
Control
Cetuximab
Control
Cetuximab
Phase Contrast
ROS Fluorescence
FaDu
Control siRNA
PDK1 siRNA
Control
Cetuximab
Control
Cetuximab
Phase Contrast
ROS Fluorescence

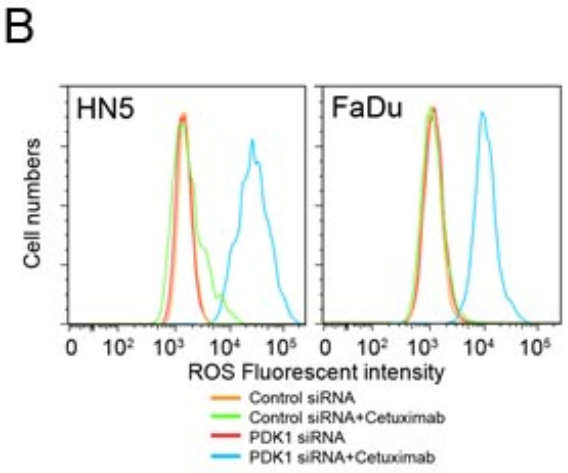
B
HN5
FaDu
Cell numbers
0
10²
10³
10⁴
10⁵
ROS Fluorescent intensity
Control siRNA
Control siRNA+Cetuximab
PDK1 siRNA
PDK1 siRNA+Cetuximab

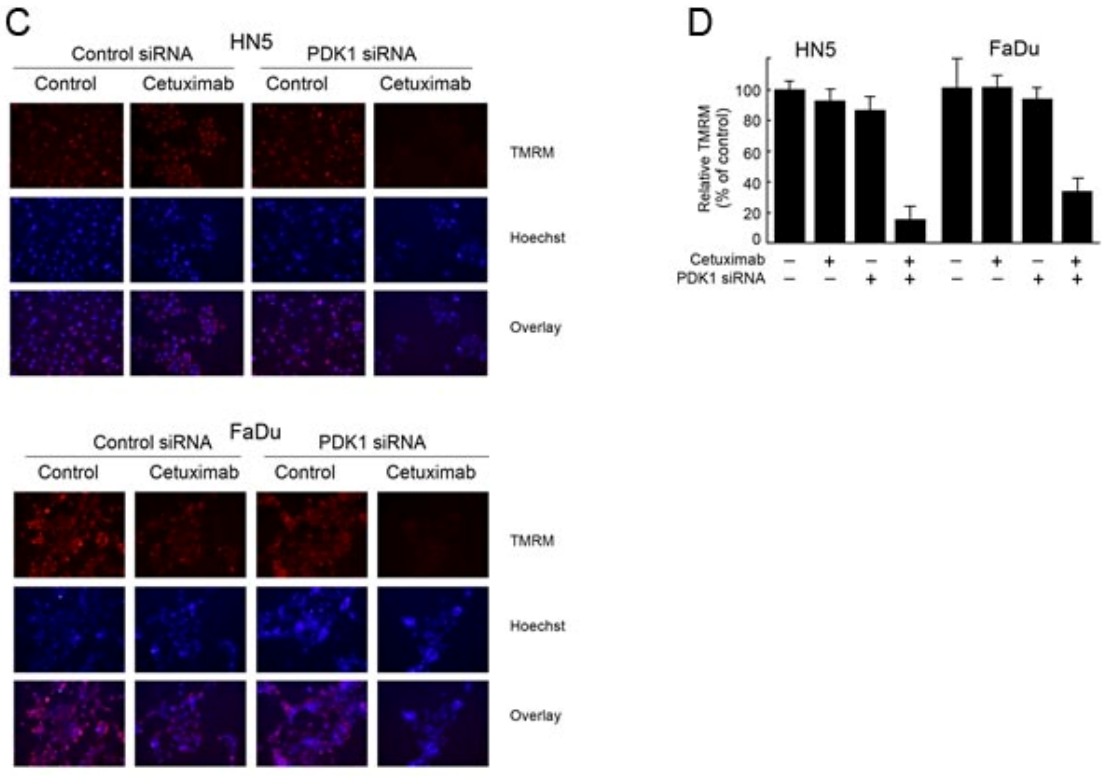

Figure 25. Combination of cetuximab and PDK1 siRNA induces ROS overproduction and loss of Δψm. (A) and (B) HN5 and FaDu cells treated as indicated for 24 hours were stained with ROS-sensitive fluorescent dye provided in Enzo's ROS detection kit for 1 hour. In (A), cells were screened under fluorescent microscope and representative area of ROS-stained cells and their phase contrast pictures are shown. In (B), cells were subjected to flow cytometry analysis. (C) and (D) HN5 and FaDu cells treated as indicated for 24 hours were stained with Δψm-sensitive fluorescent dye TMRM and counterstained with Hoechst for nuclei. In (C), cells were screened under fluorescent microscope and representative areas of TMRM- and Hoechst-stained cells and their overlay are shown. In (D), relative TMRM was determined by ratio of the reading at 590 nm (TMRM) over 460 nm (Hoechst) wavelength with a fluorescence plate reader and expressed as a percentage of the value of control group.

5.2.3 Combination of cetuximab and PDK1 inhibitor DCA induces overproduction of ROS, loss of Δψm, and apoptosis, all of which could be rescued by addition of antioxidant N-acetyl-cysteine

To confirm the effect of PDK1 targeting, we employed a PDK1 specific inhibitor, dicholoroacetate (DCA), to mimic PDK1 siRNA. HN5 and FaDu cells were treated with cetuximab and 10 mM DCA for 24 hours, alone or in combination, and cellular ROS, mitochondrial membrane potential, and apoptosis were detected. Similar to PDK1 siRNA, DCA alone did not induce detectable ROS production (Figure 26A and B) or loss of Δψm (Figure 26C and D). DCA also failed to induce apoptosis (Figure 26E and F). Cetuximab plus DCA significantly caused overproduction of ROS and loss of Δψm, and led to apoptosis, as indicated by PARP and Caspase 3 cleavage, and an independent DNA fragmentation assay.

Addition of N-acetyl-cysteine (NAC), a precursor of antioxidant GSH, almost totally depleted overproduction of ROS (Figure 26A and B) and rescued loss of Δψm (Figure 26C and D) induced by combination of cetuximab and DCA. In HN5 cells, addition of NAC or membrane permeable GSH in cell culture medium largely rescued the cytotoxic effect induced by cetuximab plus DCA (Figure 26G and H). All of these data above indicated that the cytotoxic effect induced by cetuximab and PDK1 targeting is through ROS overproduction.

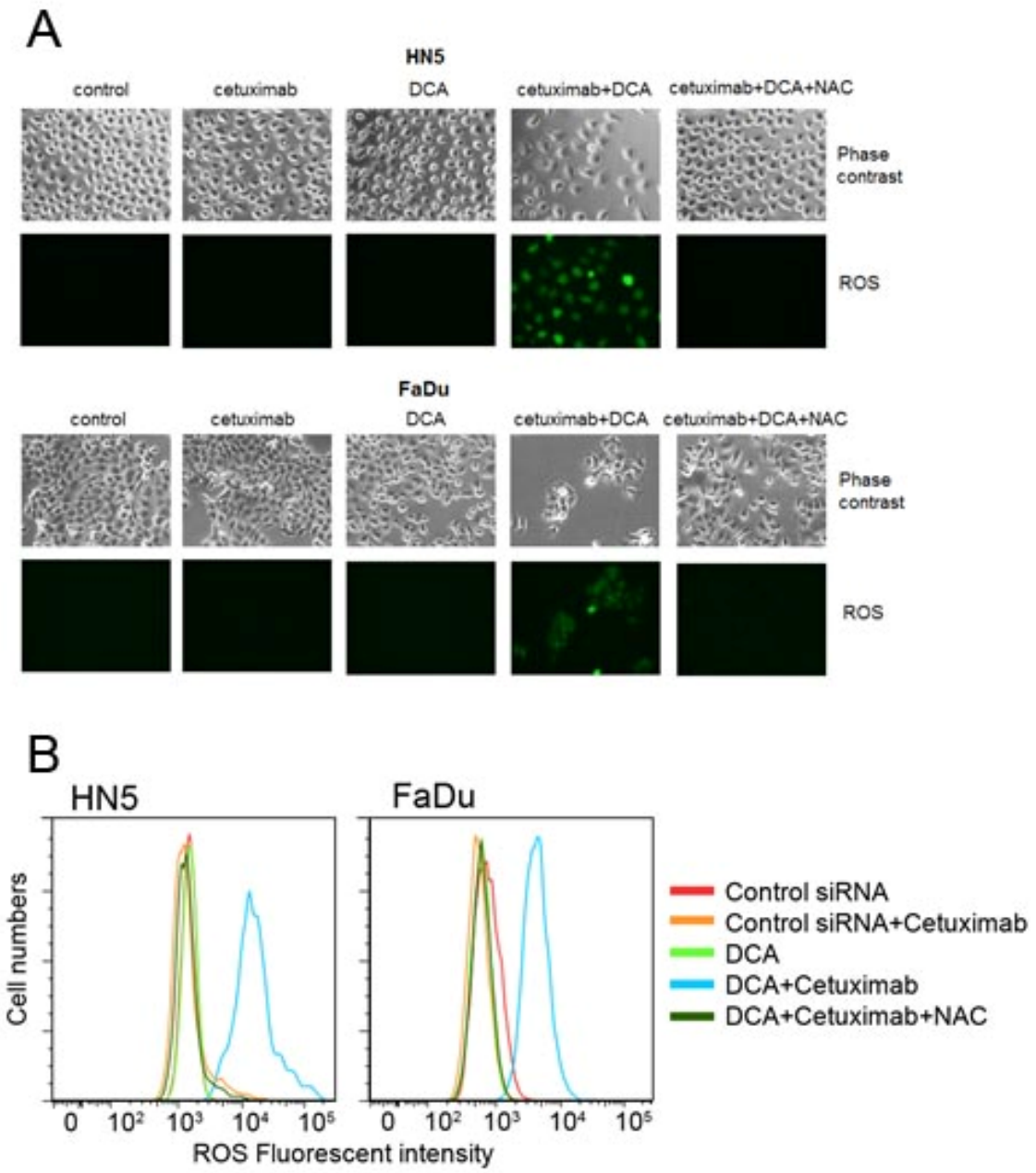
A
HN5
control
cetuximab
DCA
cetuximab+DCA
cetuximab+DCA+NAC
Phase contrast
ROS
FaDu
control
cetuximab
DCA
cetuximab+DCA
cetuximab+DCA+NAC
Phase contrast
ROS
B
HN5
FaDu
Cell numbers
0
10²
10³
10⁴
10⁵
ROS Fluorescent intensity
Control siRNA
Control siRNA+Cetuximab
DCA
DCA+Cetuximab
DCA+Cetuximab+NAC

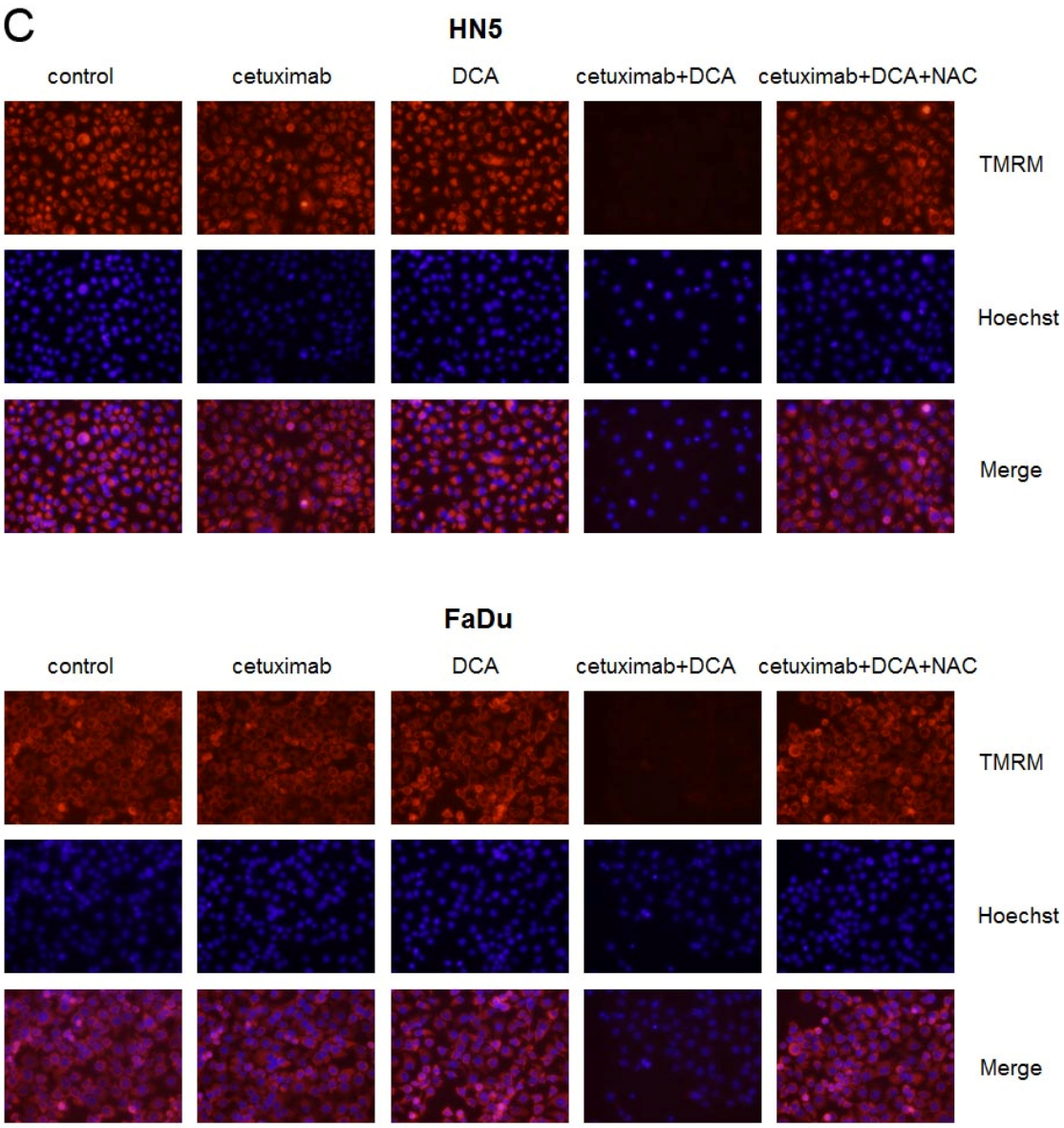
C
HN5
control
cetuximab
DCA
cetuximab+DCA
cetuximab+DCA+NAC
TMRM
Hoechst
Merge
FaDu
control
cetuximab
DCA
cetuximab+DCA
cetuximab+DCA+NAC
TMRM
Hoechst
Merge

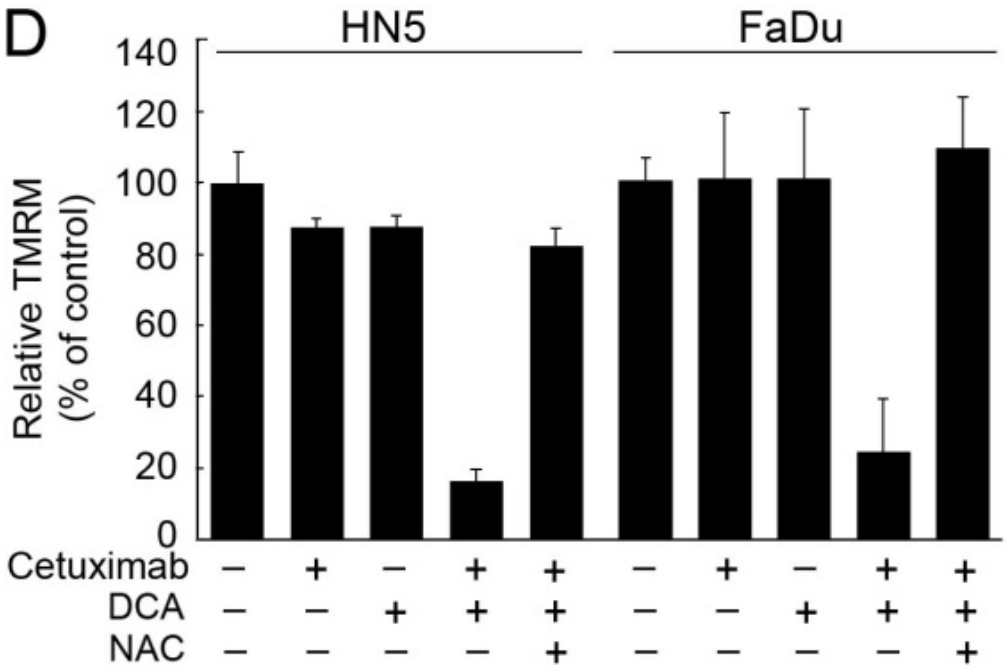
D
HN5
FaDu
Relative TMRM
(% of control)
140
120
100
80
60
40
20
0
Cetuximab – + – + + – + – + +
DCA – – + + + – – + + +
NAC – – – – + – – – – +

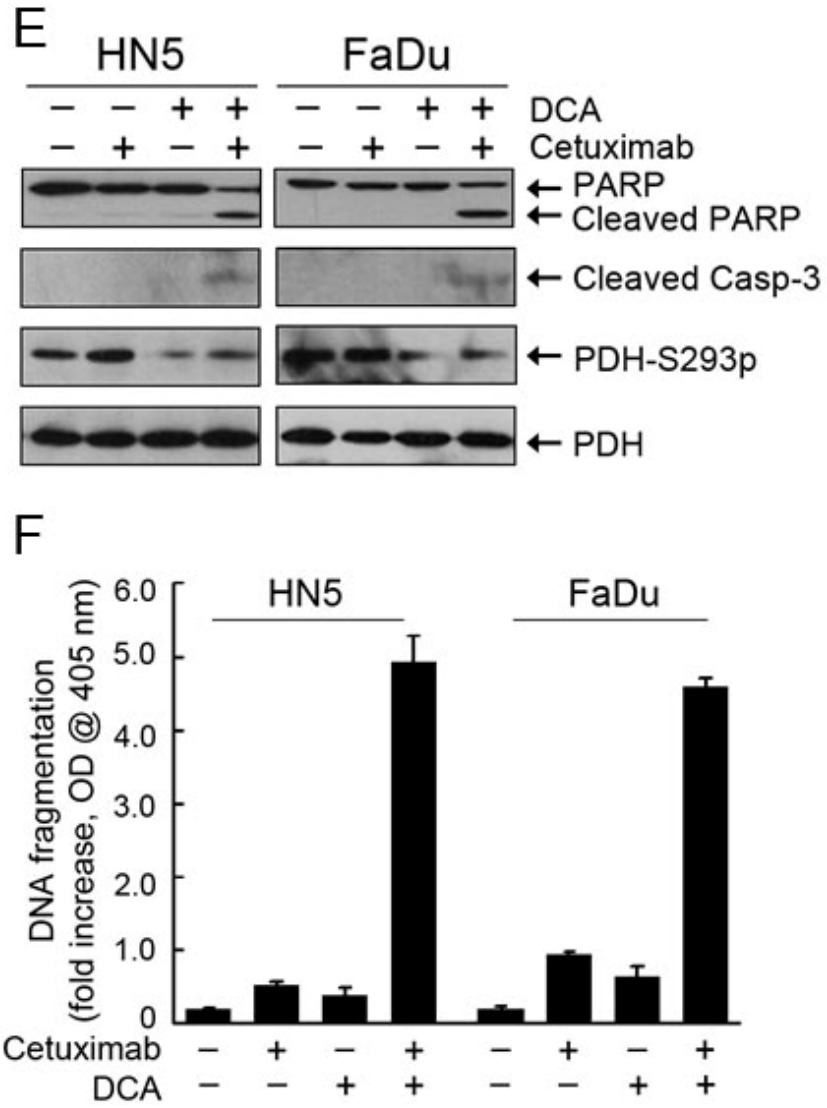
E
HN5
FaDu
DCA
Cetuximab
PARP
Cleaved PARP
Cleaved Casp-3
PDH-S293p
PDH
F
HN5
FaDu
DNA fragmentation
(fold increase, OD @ 405 nm)
6.0
5.0
4.0
3.0
2.0
1.0
0
Cetuximab
DCA

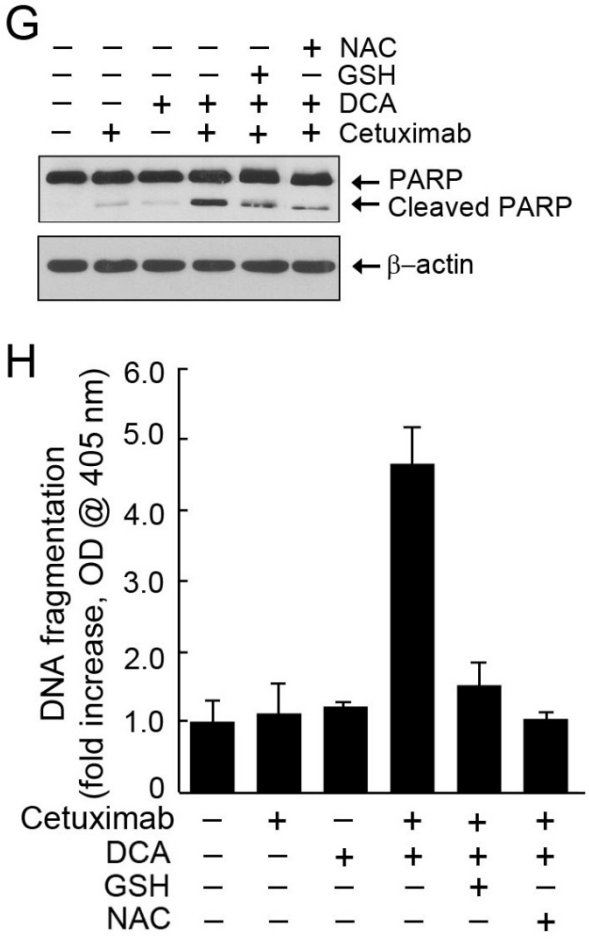
G
– – – – – + NAC
– – – – + – GSH
– – + + + + DCA
– + – + + + Cetuximab
← PARP
← Cleaved PARP
← β–actin
H
DNA fragmentation (fold increase, OD @ 405 nm)
6.0
5.0
4.0
3.0
2.0
1.0
0
Cetuximab – + – + + +
DCA – – + + + +
GSH – – – – + –
NAC – – – – – +

Figure 26. Combination of cetuximab and DCA induces overproduction of ROS, loss of Δψm, and apoptosis. (A) and (B) HN5 and FaDu cells treated as indicated for 24 hours were stained with ROS-sensitive fluorescent dye provided in Enzo's ROS detection kit for 1 hour. In (A), cells were screened under fluorescent microscope and representative area of ROS-stained cells and their phase contrast pictures are shown. In (B), cells were subjected to flow cytometry analysis. (C) and (D) HN5 and FaDu cells treated as indicated for 24 hours were stained with Δψm-sensitive fluorescent dye TMRM and counterstained with Hoechst for nuclei. In (C), cells were screened under fluorescent microscope and representative areas of TMRM- and Hoechst-stained cells and their overlay are shown. In (D), relative TMRM was determined by ratio of the reading at 590 nm (TMRM) over 460 nm (Hoechst) wavelength with a fluorescence plate reader and expressed as a parentage of the value of control group. (E) and (F) HN5 and FaDu cells were treated with cetuximab (20 nM) and DCA (10 mM), alone or in combination for 24 hours. Cell lysates were prepared for Western blot with indicated antibodies in (E) and for detection of apoptosis by ELISA using a kit from Roche in (F). (G) and (H) HN5 cells were treated with cetuximab (20 nM) and DCA (10 mM) for 24 hours, alone or in combination in the presence or absence of GSH-ester (2 mM) or NAC (4 mM). Cell lysates were prepared for Western blot with indicated antibodies in (G) and for detection of apoptosis by ELISA in (H).

5.2.4 Combination of cetuximab and PDK1 targeting induces apoptosis in cetuximab-resistant cells

Most patients treated with cetuximab develop acquired resistance, even they respond to cetuximab treatment in the beginning. To examine whether co-targeting PDK1 re-sensitizes responses of cancer cells to cetuximab treatment in cetuximab resistant cells, we used cetuximab-acquired resistant sublines HN5-R and FaDu-R, generated from HN5 and FaDu by subjecting to cetuximab with stepwise increases in concentration as described in 4.2.1. HN5-R and FaDu-R were treated with each of 3 pairs of PDK1 siRNAs and cetuximab, alone or in combination. We found that cetuximab could still induce apoptosis (Figure 27A and B) and decrease clonogenic capacity (Figure 27C) in HN5-R and FaDu-R cells. These results indicated that the contribution of cetuximab in this novel combination might be different from its role in EGFR-downstream cell signaling inhibition, failure of which is the major mechanism underlying cetuximab resistance. In addition, silencing PDK1 alone showed cytotoxic effect to some extent in HN5-R and FaDu-R cells, which is a different phenomenon in HN5 and FaDu cells. This is because the resistant sublines are more relied on glycolysis compared to their counterparts (Figure 14), and redirection of glucose metabolism away from glycolysis induced by PDK1 silencing will be more toxic to the resistant sublines.

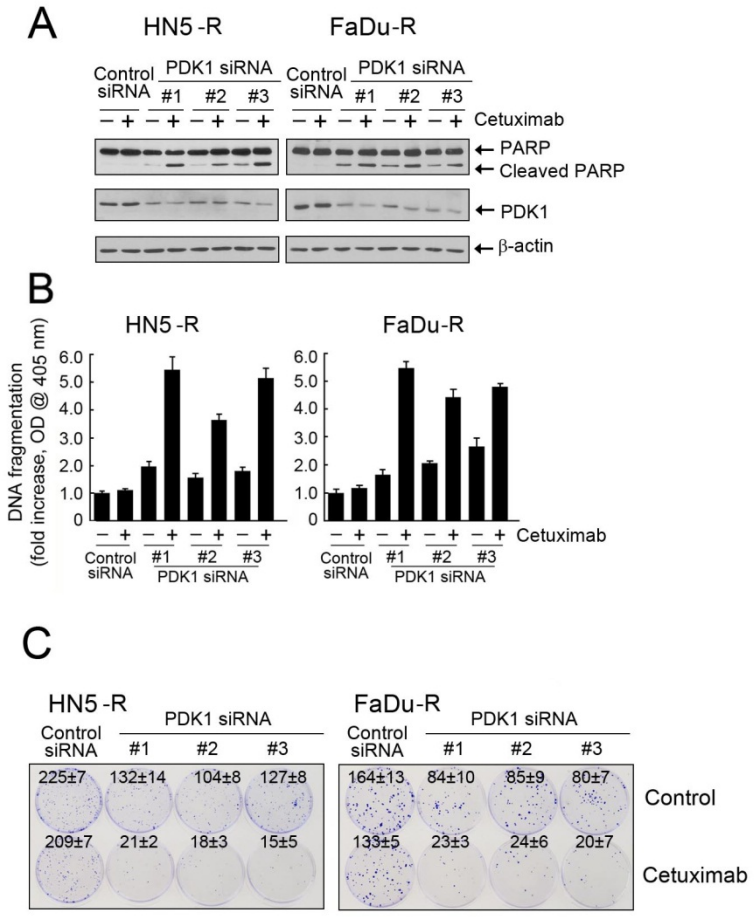

Figure 27. Combination of cetuximab and PDK1 siRNA are cytotoxic in cetuximab-resistant cancer cells. (A) and (B) HN5-R and FaDu-R cells were subjected to PDK1 silencing with each of 3 different PDK1 siRNAs or control siRNA for 72 hours. During the last 24 hours, cells were then treated with or without 20 nM cetuximab. Cells were harvested and cell lysates were prepared for Western blot with indicated antibodies in (A) and for detection of apoptosis by ELISA using a kit from Roche in (B). (C) HN5-R and FaDu-R cells were seeded at low density, treated as in (A) and (B) and subjected to a clonogenic survival assay as described in materials and methods.

5.2.5 Combination of cetuximab and DCA inhibits growth of HNSCC xenografts

To determine whether combination of cetuximab and PDK1 targeting would have better therapeutic effect compared with either drug alone *in vivo*, we used bioluminescent sublines of paired FaDu and FaDu-R that not only can grow in nude mice but also can be tracked using an *in vivo* imaging system (IVIS) to monitor tumor growth. A bioluminescent subline of natural occurred cetuximab-resistant cell line UMSCC1 and paired HN5 and HN5-R cell lines, all of which can form tumors in nude mice, were also employed in the *in vivo* experiments. Different cells were inoculated subcutaneously on the right flanks of nude mice. When tumors were well established at the volume of 150-250 mm^3, the nude mice that had developed tumors were divided into six groups (6-7 mice in each group) with similar average tumor volume, and treated with vehicle, cetuximab (0.25 mg/mouse, bi-weekly), DCA (50 mg/kg/day or 250 mg/kg/day, daily), or combination of cetuximab and DCA for 21 days. Tumor volume was measured twice a week with a digital caliper. For bioluminescent sublines, tumors were also screened under IVIS system at day 21 from treatment start date. After the end of treatment, measurement of tumor volume was continued in each group until the group had less than 4 mice.

Xenograft of FaDu cells showed some responses to the treatment of cetuximab or DCA alone during treatment time, and much better response to the combination (Figure 28A and B). Interestingly, when the treatment was stopped, in the groups treated with either cetuximab or DCA alone, FaDu xenograft tumors grew back very quickly; while in the groups treated with cetuximab plus DCA, the xenograft tumors were examined for 5 months and did not grow back. Xenograft of FaDu-R cells exhibited considerable

resistance to cetuximab treatment alone. Combination of cetuximab and DCA produced substantially better therapeutic effects than either treatment alone, and xenograft tumors treated with combination did not grow back in 5 months. Since xenograft of HN5 cells has a very good response to cetuximab mono-treatment (Figure 28C), we did not combine the treatment with DCA. In xenograft of HN5-R cells, we also observed that combination of cetuximab and DCA had a significant better effect in inhibiting tumor growth; and compare with either treatment alone, combination treatment totally abolished the capacity of xenograft tumors to grow, even the treatment was stopped, suggesting that tumor cells were killed rather than static. Similar therapeutic effect was also confirmed in the xenograft of natural occurred cetuximab-resistant cell line UMSCC1 (Figure 28D and E). All these data indicated that cetuximab or DCA treatment alone may have cytostatic effect *in vivo*, depending on different xenograft of cells; however, they have little or no cytotoxic effect. Xenograft tumors treated with either drug alone grew back as soon as the treatments were stopped. Combination of cetuximab and DCA efficiently inhibited xenograft tumors, not only in cetuximab-sensitive models, but also in cetuximab-resistant models. More importantly, xenograft tumors with combination treatment did not recur after treatment stopped, indicating that tumor cells were killed.

A

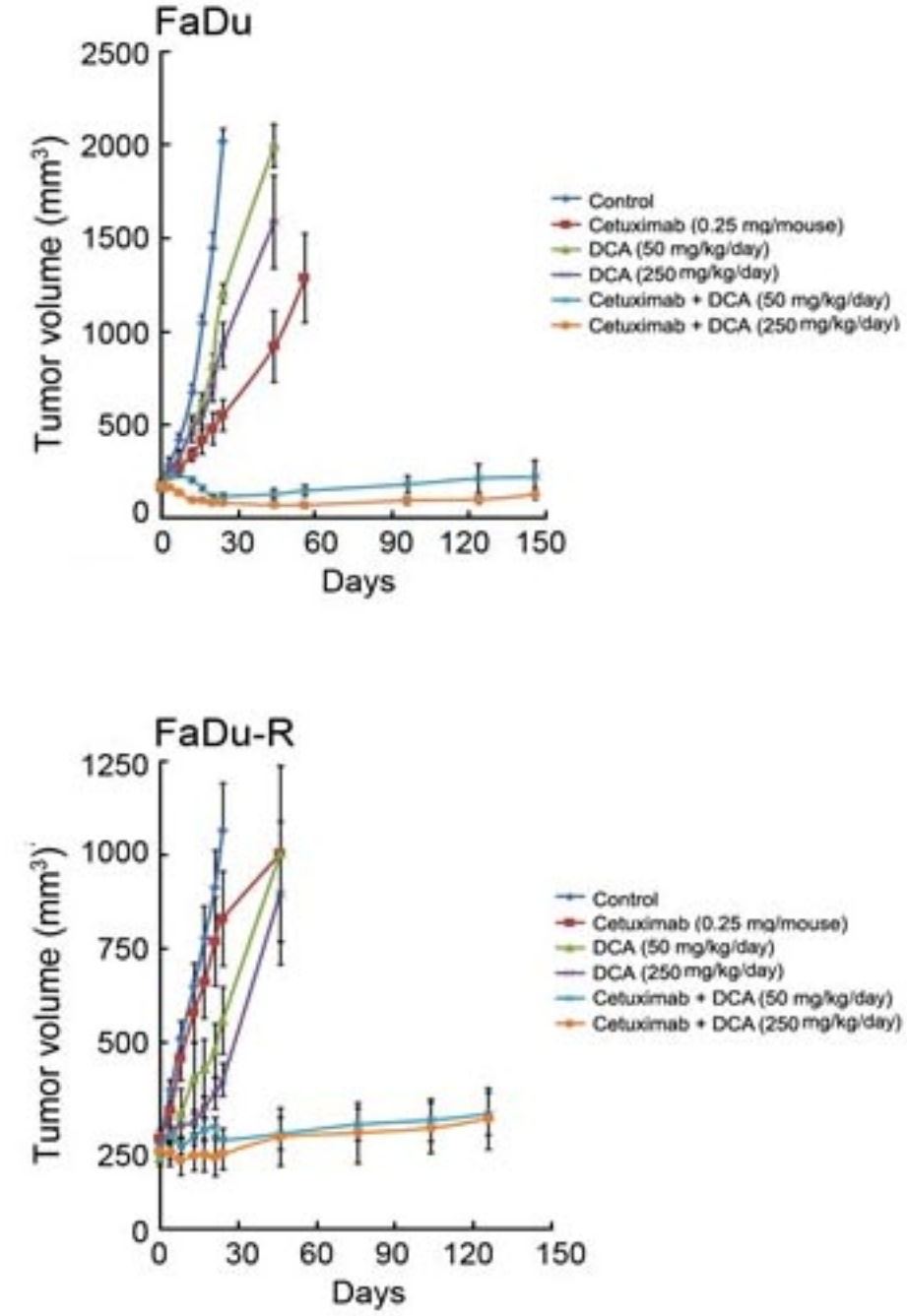
FaDu
Tumor volume (mm3)
2500
2000
1500
1000
500
0
0
30
60
90
120
150
Days
Control
Cetuximab (0.25 mg/mouse)
DCA (50 mg/kg/day)
DCA (250 mg/kg/day)
Cetuximab + DCA (50 mg/kg/day)
Cetuximab + DCA (250 mg/kg/day)
FaDu-R
Tumor volume (mm3)
1250
1000
750
500
250
0
0
30
60
90
120
150
Days
Control
Cetuximab (0.25 mg/mouse)
DCA (50 mg/kg/day)
DCA (250 mg/kg/day)
Cetuximab + DCA (50 mg/kg/day)
Cetuximab + DCA (250 mg/kg/day)

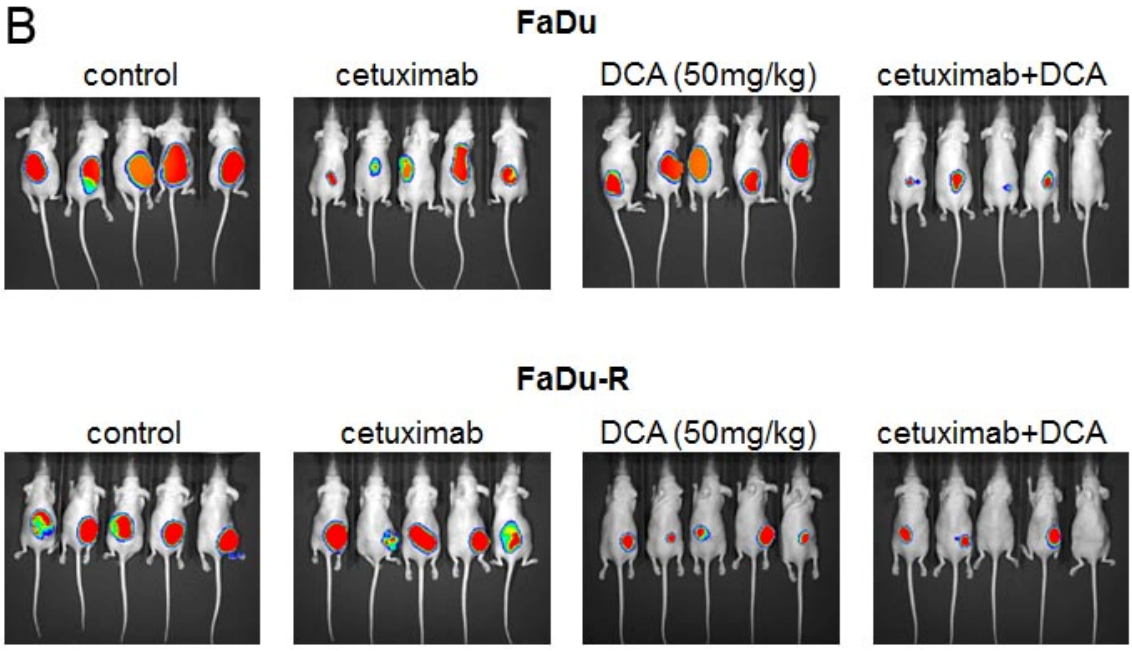
B
FaDu
control
cetuximab
DCA (50mg/kg)
cetuximab+DCA
FaDu-R
control
cetuximab
DCA (50mg/kg)
cetuximab+DCA

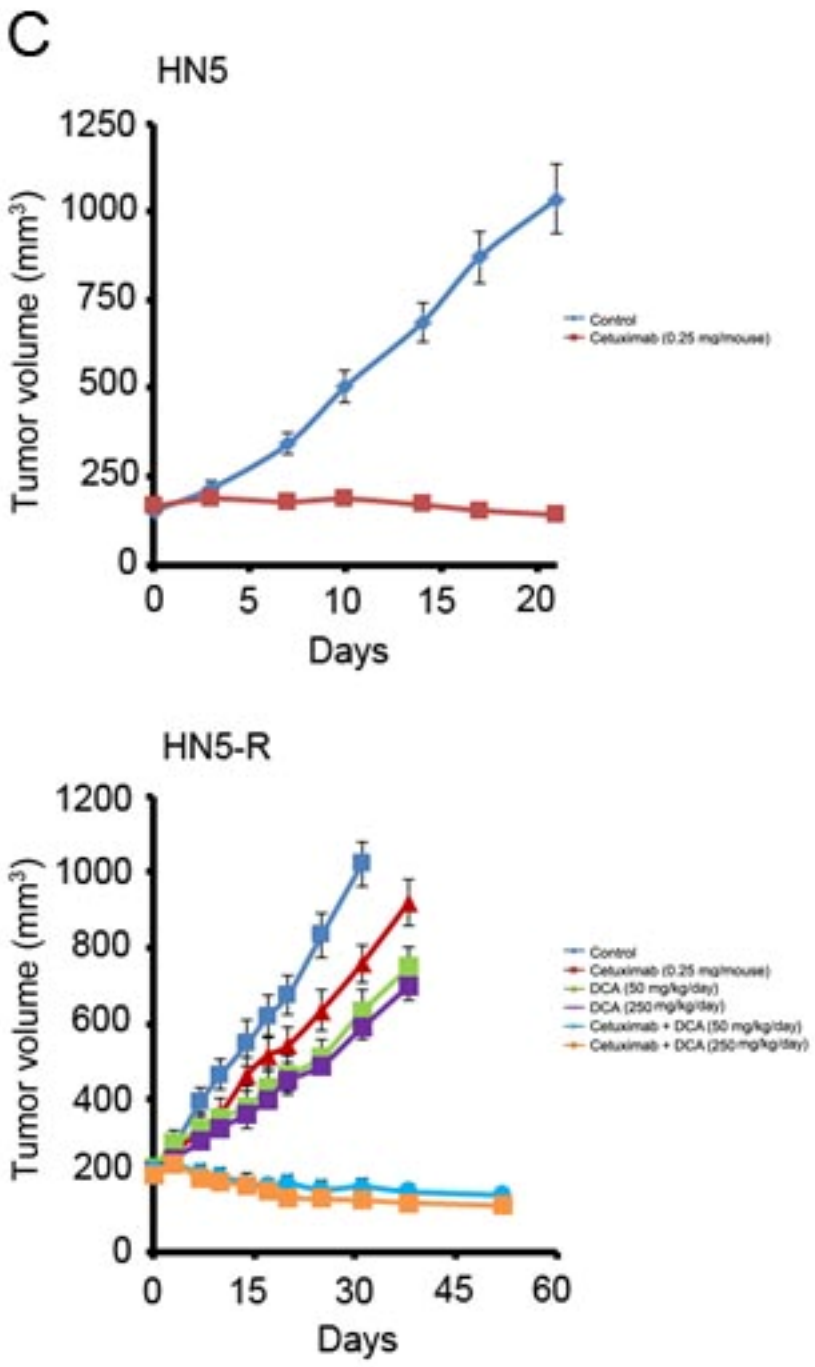
C
HN5
1250
1000
750
500
250
0
Tumor volume (mm3)
0
5
10
15
20
Days
Control
Cetuximab (0.25 mg/mouse)
HN5-R
1200
1000
800
600
400
200
0
Tumor volume (mm3)
0
15
30
45
60
Days
Control
Cetuximab (0.25 mg/mouse)
DCA (50 mg/kg/day)
DCA (250 mg/kg/day)
Cetuximab + DCA (50 mg/kg/day)
Cetuximab + DCA (250 mg/kg/day)

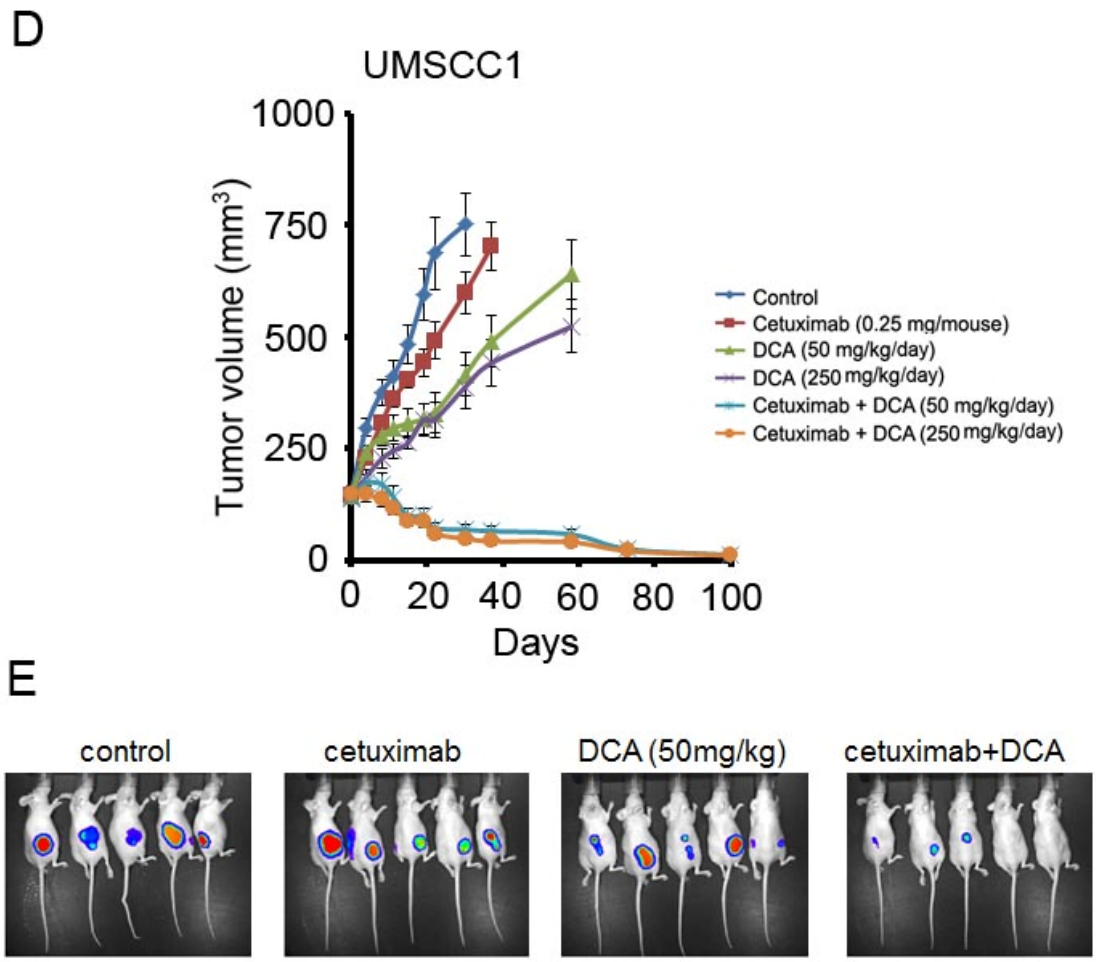

Figure 28. Combination of cetuximab and DCA inhibits tumor growth *in vivo*. Bioluminescent sublines of FaDu and FaDu-R, parental HN5 and HN5-R, and bioluminescent sublines of UMSCC1 were inoculated subcutaneously into the right flanks of nude mice. When tumors were well established at the volume of 150-250 mm^3, the nude mice of each kind of xenograft tumors that had developed were divided into six groups (6-7 mice in each group) with similar average tumor volume, and treated with vehicle, cetuximab (0.25 mg/mouse, bi-weekly), DCA (50 mg/kg/day or 250 mg/kg/day, daily), or combination of cetuximab and DCA for 21 days. In (A), (C) and (D), tumor volume was measured twice a week with calipers and was plotted as a function of the days. After the end of treatment, measurement of tumor volume was continued. Mice in any groups were sacrificed when the tumor burdens were too big or when the mice became morbid or moribund. When the remaining numbers of mice in any groups became less than 4, the entire group was terminated. In (B) and (E), xenograft tumor of bioluminescent sublines of FaDu, FaDu-R and UMSCC1 were screened under IVIS system at day 21 from treatment start date.

5.2.6 Induction of apoptosis by cetuximab plus PDK1 silencing or DCA is not dependent on inhibition of EGFR kinase activity by cetuximab

The major cetuximab-resistant mechanism is the constitutively activation of EGFR-downstream cell signals induced by activation of oncogenes or loss-of-function mutation of tumor suppressor genes. Since combination of cetuximab and PDK1 targeting by siRNA or DCA induced apoptosis *in vitro* and *in vivo*, even in cetuximab-resistant cell lines, we hypothesized that the contribution of cetuximab in this novel combination treatment is independent on its function in inhibiting EGFR kinase activity. To test this hypothesis, we determined whether treatment with the small molecule EGFR kinase inhibitor gefitinib plus PDK1 silencing or DCA would result in similar effects to those achieved with cetuximab plus PDK1 silencing or DCA with respect to apoptosis. Unlike cetuximab, gefitinib, which successfully inhibited EGFR kinase activity as shown by reduced autophosphorylation of EGFR on Y1068, did not have the synergetic effect on inducing cleavage of PARP and Caspase 3, and apoptosis (Figure 29A). Combination of gefitinib and DCA did not have synergetic effect on inducing apoptosis either, despite of strong EGFR kinase activity inhibition by gefitinib (Figure 29B).

To further confirm the combination effect of cetuximab and PDK1 targeting is independent of the role of cetuximab in EGFR kinase activity inhibition, we transfected HN5 with a constitutively active H-Ras mutant (H-Ras G12V), as described in 3.2.4. H-Ras mutation is one of the major cetuximab-resistant mechanisms in HNSCC. Constitutively activation of Ras abolishes the anti-proliferation effect of cetuximab through activating EGFR-downstream signals. Interestingly, although overexpression of RasG12V conferred resistance to cetuximab-induced inhibition of EGFR-downstream

signaling, as shown by the unchanged level of phosphorylation of Akt at S473 and phosphorylation of p70S6k at S371 after cetuximab treatment, it did not protect cells from induction of apoptosis by the combination of cetuximab and PDK1 siRNA (Figure 29C). Together, these data not only support that cetuximab plus PDK1 targeting induces apoptosis independently of inhibition of EGFR kinase activity by cetuximab, but also provide a potential novel therapeutic strategy to bypass most current known cetuximab resistant mechanism.

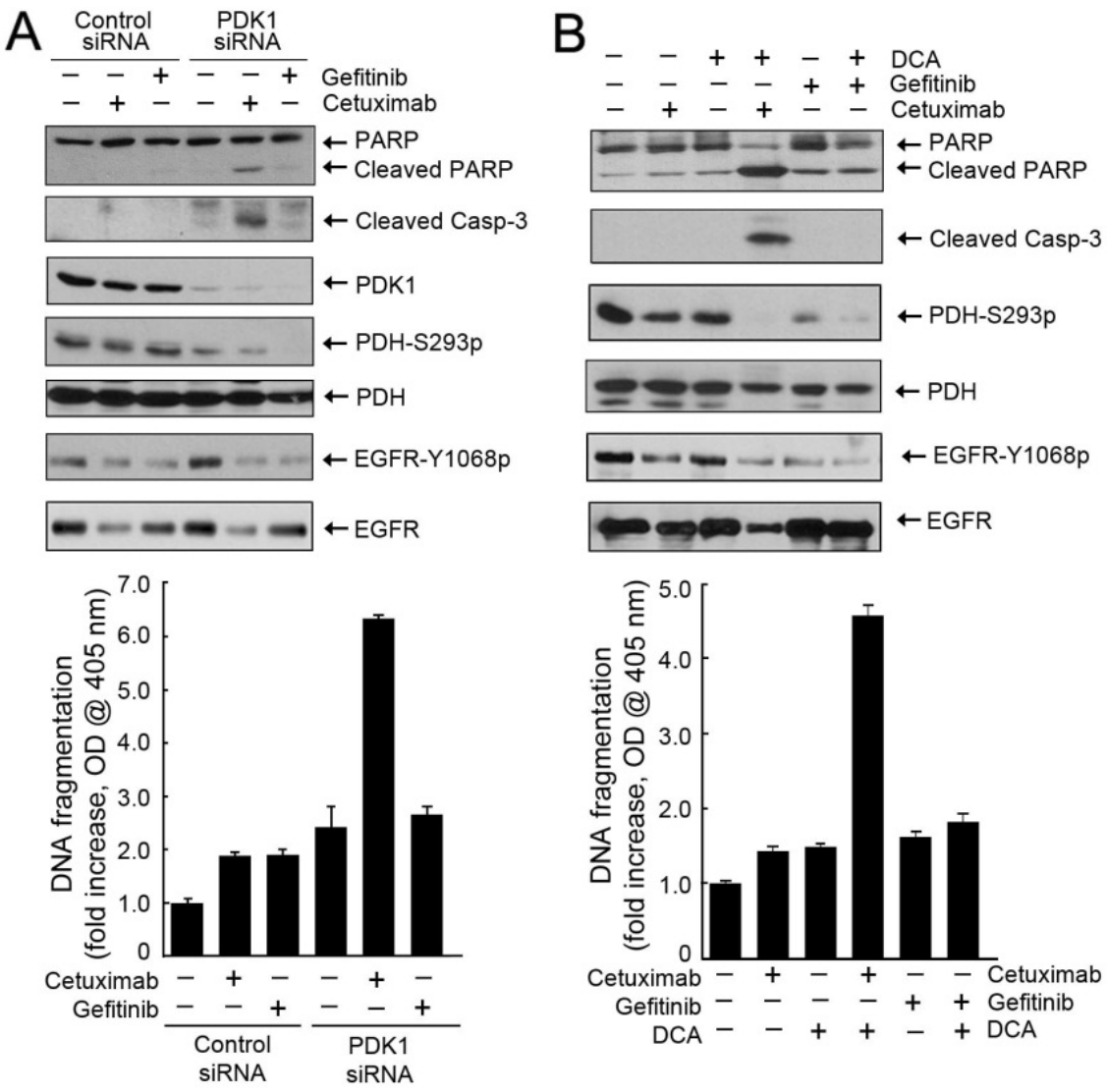
A
Control siRNA
PDK1 siRNA
Gefitinib
Cetuximab
PARP
Cleaved PARP
Cleaved Casp-3
PDK1
PDH-S293p
PDH
EGFR-Y1068p
EGFR
DNA fragmentation (fold increase, OD @ 405 nm)
Cetuximab
Gefitinib
Control siRNA
PDK1 siRNA
B
DCA
Gefitinib
Cetuximab
PARP
Cleaved PARP
Cleaved Casp-3
PDH-S293p
PDH
EGFR-Y1068p
EGFR
DNA fragmentation (fold increase, OD @ 405 nm)
Cetuximab
Gefitinib
DCA

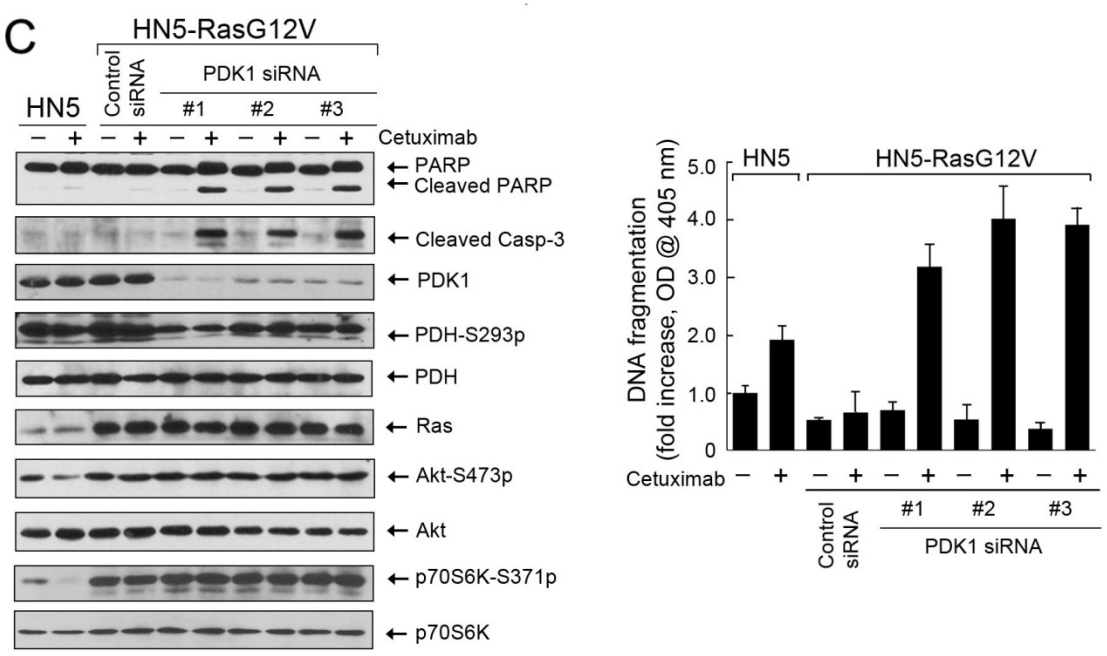

Figure 29. Induction of apoptosis by combination of cetuximab and PDK1 targeting is independent of EGFR kinase inhibition by cetuximab. (A) HN5 cells were subjected to PDK1 siRNA or control siRNA for 72 hours. During the last 24 hours, cells were then treated with cetuximab (20 nM), gefitinib (0.2 μM), or neither as indicated. (B) HN5 cells were treated with cetuximab (20 nM) or gefitinib (0.2 μM) alone or in combination with DCA (10 mM) for 24 hours. (C) HN5 cells transfected with RasG12V were subjected to knockdown of PDK1 with each of different PDK1 siRNAs or control siRNA for 72 hours. During the last 24 hours, these cells and parental HN5 cells were treated with cetuximab or not. In (A), (B), and (C), cells were harvested after treatment. Cell lysates were prepared for Western blot analysis with antibodies shown and for detection of apoptosis by ELISA.

5.2.7 Induction of cetuximab plus DCA requires both expression of EGFR on the cell surface and effective internalization of EGFR by cetuximab

To elucidate the role of EGFR in induction of apoptosis by combination of cetuximab and DCA, we next tested whether EGFR silencing plus DCA produced effects similar to those of cetuximab plus DCA and whether expression of EGFR on the cell surface is still required for the combination treatment-induced apoptosis. Figure 30A showed that compared with cetuximab plus DCA which induced PARP cleavage, knockdown of EGFR by each of 3 different EGFR siRNAs plus DCA did not induce PARP cleavage in FaDu cells. This finding was further confirmed in HN5 cells (Figure 30B). Moreover, knockdown of EGFR decreased the level of apoptosis induced by the combination of cetuximab and DCA, indicating that EGFR expression was required for induction of apoptosis by this combination treatment.

The anti-proliferation effect of cetuximab is not only through inhibition of EGFR kinase activity, but also through induction of EGFR internalization and degradation by its bivalent binding to EGFR. We thus hypothesized that cetuximab contributes to the combination of cetuximab and PDK1 targeting in perspective of EGFR internalization and degradation. We tested whether silencing selected members of the Rab G proteins, which are involved in EGFR endocytosis, had any effect on induction of apoptosis by the combination treatment. Figure 30C showed that knockdown of Rab5, which involved in early endosomes, inhibited cleavage of PARP induced by the combination treatment, whereas knockdown of Rab11, which involved in recycling endosomes, did not have similar effect. Taken together, these observations indicated that cetuximab-induced

EGFR internalization, which is EGFR kinase inhibition independent, plays a critical role in induction of apoptosis by cetuximab plus PDK1 targeting.

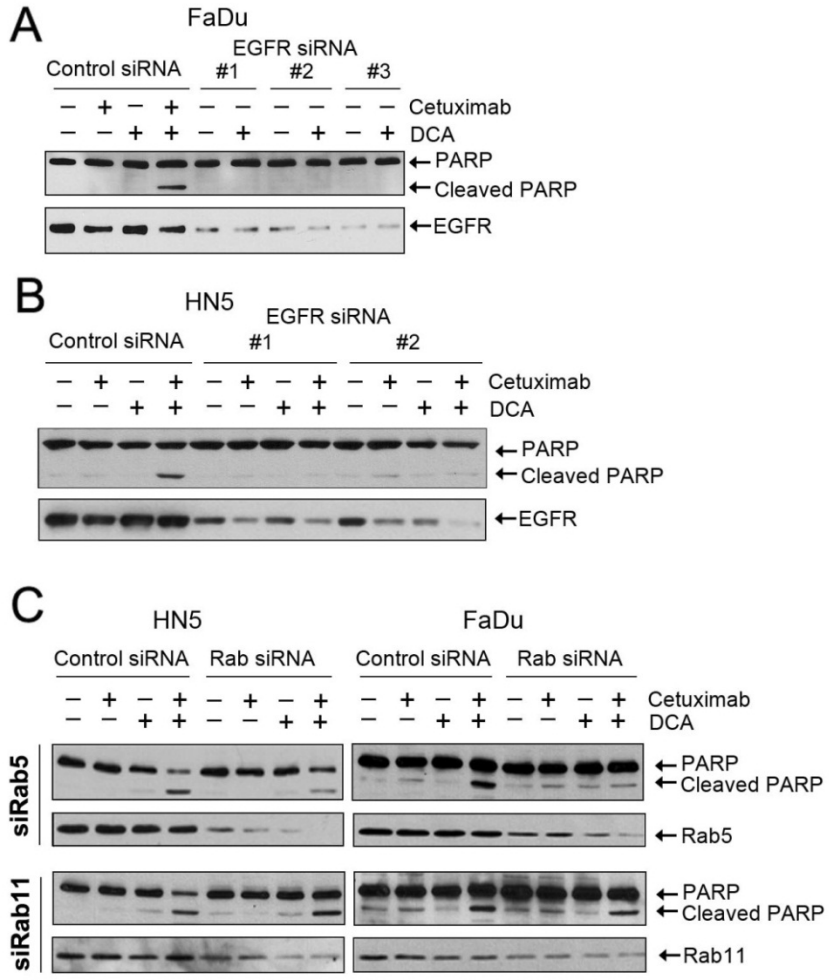

Figure 30. Induction of apoptosis by combination of cetuximab and DCA required both expression of EGFR on the cell surface and effective internalization of EGFR by cetuximab. (A) FaDu cells were subjected to knockdown of EGFR with each of 3 pairs of different EGFR siRNAs or control siRNA for 72 hours. During the last 24 hours, cells were treated with cetuximab (20 nM) or DCA (10 mM), alone or in combination in control siRNA-treated cells and with DCA only in EGFR-siRNA treated cells. (B) HN5 cells were exposed to control siRNA or each of 2 pairs of different EGFR siRNAs for 72 hours. During the last 24 hours, cells were treated with cetuximab (20 nM) or DCA (10 mM), alone or in combination in both control siRNA and EGFR siRNA treated cells. (C) HN5 and FaDu cells were exposed to Rab5 and Rab11 siRNA or control siRNA for 72 hours. Cells were then treated as in (B). After treatments, cell lysates were prepared for Western blot analysis with indicated antibodies.

5.2.8 DCA upregulates glutamine transporter ASCT2 and increase glutamine uptake, which leads to resistance to DCA treatment

To elucidate the mechanism of cetuximab in contributing to the apoptosis induction by combination treatment with PDK1 targeting, we first need to figure out why targeting PDK1, a theoretical approach to produce ROS, failed to induce detectable ROS and apoptosis, as described in 5.2.2. We found that in both HN5 and FaDu cells, DCA treatment upregulated the protein expression of ASCT2, one of the most major glutamine transporters (Figure 31A), as well as glutamine uptake (Figure 31B), both of which could be rescued by addition of NAC.

Catalyzed by mitochondrial enzyme glutaminase, glutamine is converted to glutamate, which is one of the precursors for GSH synthesis. We hypothesized that upregulation of ASCT2 induced by DCA would increase glutamine uptake and GSH synthesis, leading to the upregulation of intracellular GSH levels. In HN5 cells, knockdown of ASCT2 with siRNA decreased glutamine uptake, and overexpression of ASCT2 increased glutamine uptake (Figure 31C), indicating a direct link between levels of ASCT2 protein and intracellular GSH.

To confirm ASCT2 upregulation induced by DCA is a mechanism conferring resistance to DCA, we knockdown ASCT2 with siRNA and treated HN5 and FaDu cells with DCA. Knockdown of ASCT2 significantly increased responses to DCA in HN5 and FaDu cells, as shown by induction of PARP cleavage (Figure 31D). All these observations indicated that DCA upregulates ASCT2 and promote glutamine uptake in a ROS-dependent manner, and upregulation of ASCT2 is a cellular protection mechanism against oxidative stress and leads to resistance to DCA treatment.

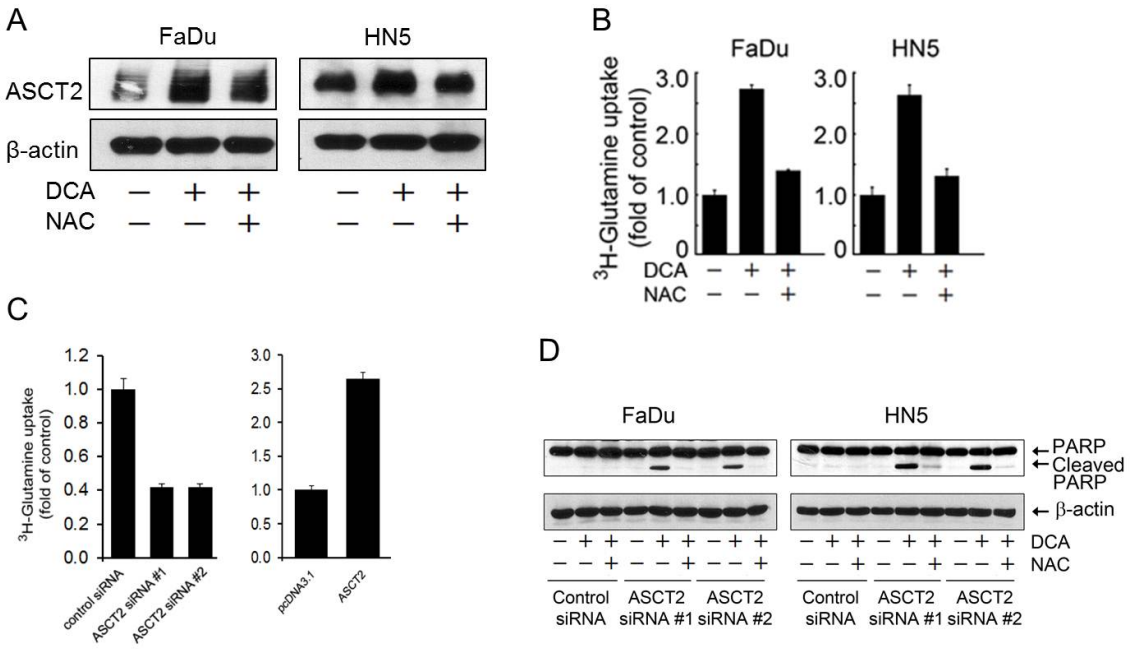

Figure 31. DCA upregulates ASCT2 and glutamine uptake, leading to resistance to DCA treatment. (A) FaDu and HN5 cells were treated with DCA for 24 hours with and without concurrent treatment of 10 mM NAC. After treatments, cell lysates were prepared for Western blot analysis with indicated antibodies. (B) FaDu and HN5 cells were treated as in (A), and ^{3}H-glutamine uptake was determined afterwards as described in materials and methods. (C) HN5 cells were exposed to control siRNA or each of 2 pairs of different ASCT2 siRNAs for 72 hours, or transfected with a vector containing ASCT2 or a control vector for 48 hours. ^{3}H-glutamine uptake was determined afterwards as described in materials and methods. (D) FaDu and HN5 cells were subjected to knockdown of ASCT2 with each of 2 individual ASCT2 siRNA or control siRNA for 72 hours. During the last 24 hours, cells were treated with 10 mM DCA with or without concurrent treatment of 10 mM NAC. Cell lysates were prepared for Western blot analysis with indicated antibodies.

5.2.9 ROS upregulates ASCT2, knockdown of which sensitizes responses to H_2O_2 and other ROS inducers

To further confirm the role of ASCT2 upregulation in protecting cells from oxidative stress, HN5 and FaDu cells were treated with H_2O_2, then glutamine uptake and intracellular GSH levels were measured. Similar to the effect induced by DCA, H_2O_2 upregulated glutamine uptake (Figure 32A) and intracellular GSH level (Figure 32B), both of which could be regulated by addition of NAC. Overexpression of ASCT2 largely rescued apoptosis induced by high dose of H_2O_2 (1 mM) (Figure 32C), and knockdown of ASCT2 by siRNA sensitized responses to low dose of H_2O_2 (0.1 mM) by inducing apoptosis (Figure 32D), showing the critical role of ASCT2 in protecting cells against oxidative stress.

Two other well-known ROS inducer, pyocyanin and phenethyl isothiocyanate (PEITC), were also used to test their effects on ASCT2 and PARP cleavage in HN5 and FaDu cells. Pyocyanin induces ROS through inactivating catalase by reducing its gene transcription and directly targeting the enzyme itself, and PEITC induces ROS through affecting complexes within the mitochondrial electron transport chain [135]. Similar to the upregulation of ASCT2 induced by H_2O_2 (Figure 32D), pyocyanin and PEITC also upregulated ASCT2 in both HN5 and FaDu cells (Figure 32E and F). Low doses of pyocyanin (10 μM) and PEITC (5 μM) did not induce apoptosis, while knockdown of ASCT2 plus pyocyanin and PEITC significantly induced apoptosis, as shown by PARP cleavage. Taken together, these observations showed that cancer cells response to ROS by upregulating ASCT2, and subsequent increases of glutamine uptake and GSH synthesis, leading to protection from oxidative stress and resistance to ROS inducers.

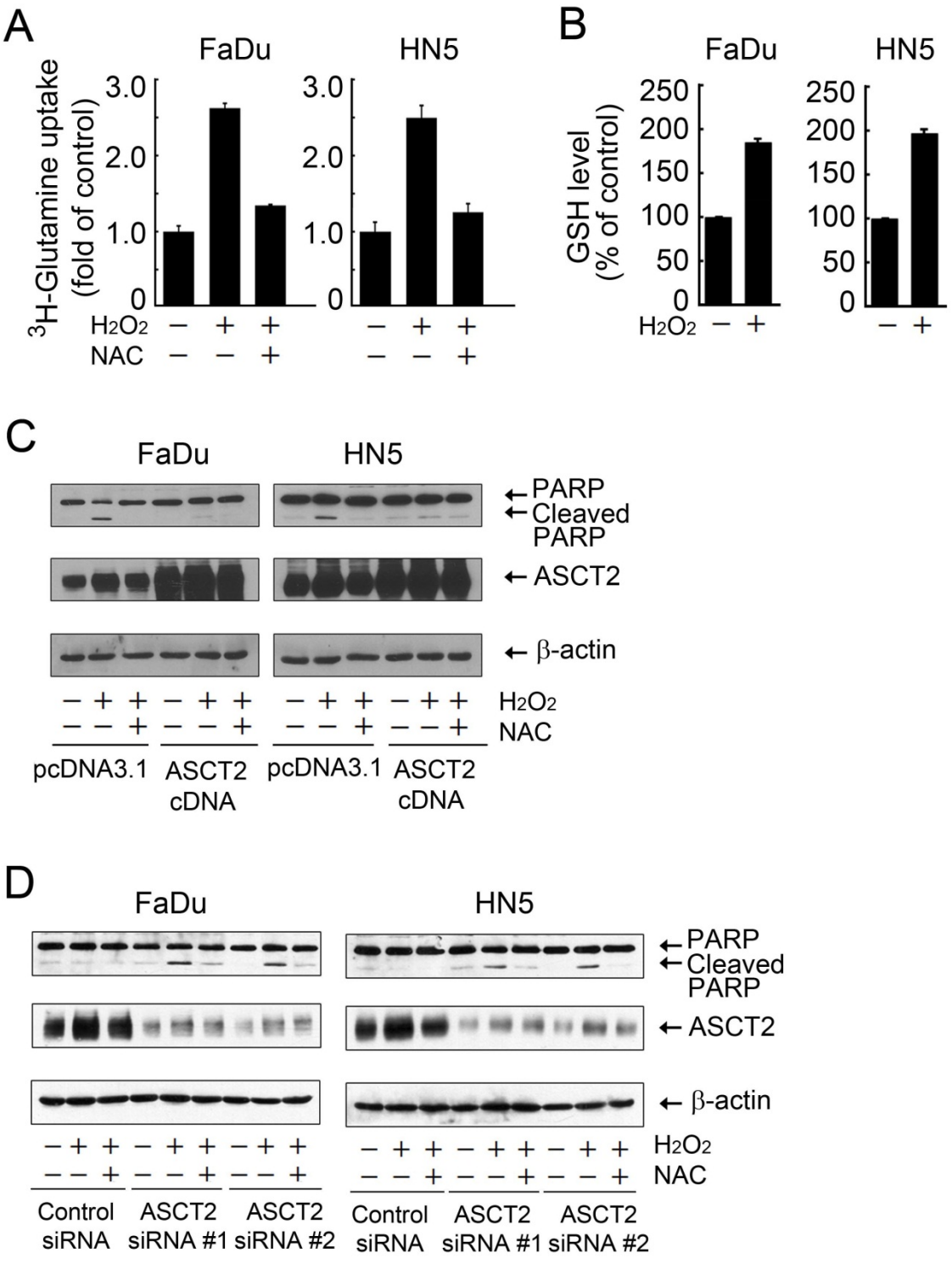
A
FaDu
HN5
^{3}H-Glutamine uptake (fold of control)
3.0
2.0
1.0
0
H2O2 − + + − + +
NAC − − + − − +
B
FaDu
HN5
GSH level (% of control)
250
200
150
100
50
0
H2O2 − + − +
C
FaDu
HN5
PARP
Cleaved PARP
ASCT2
β-actin
H2O2
NAC
pcDNA3.1
ASCT2 cDNA
pcDNA3.1
ASCT2 cDNA
D
FaDu
HN5
PARP
Cleaved PARP
ASCT2
β-actin
H2O2
NAC
Control siRNA
ASCT2 siRNA #1
ASCT2 siRNA #2
Control siRNA
ASCT2 siRNA #1
ASCT2 siRNA #2

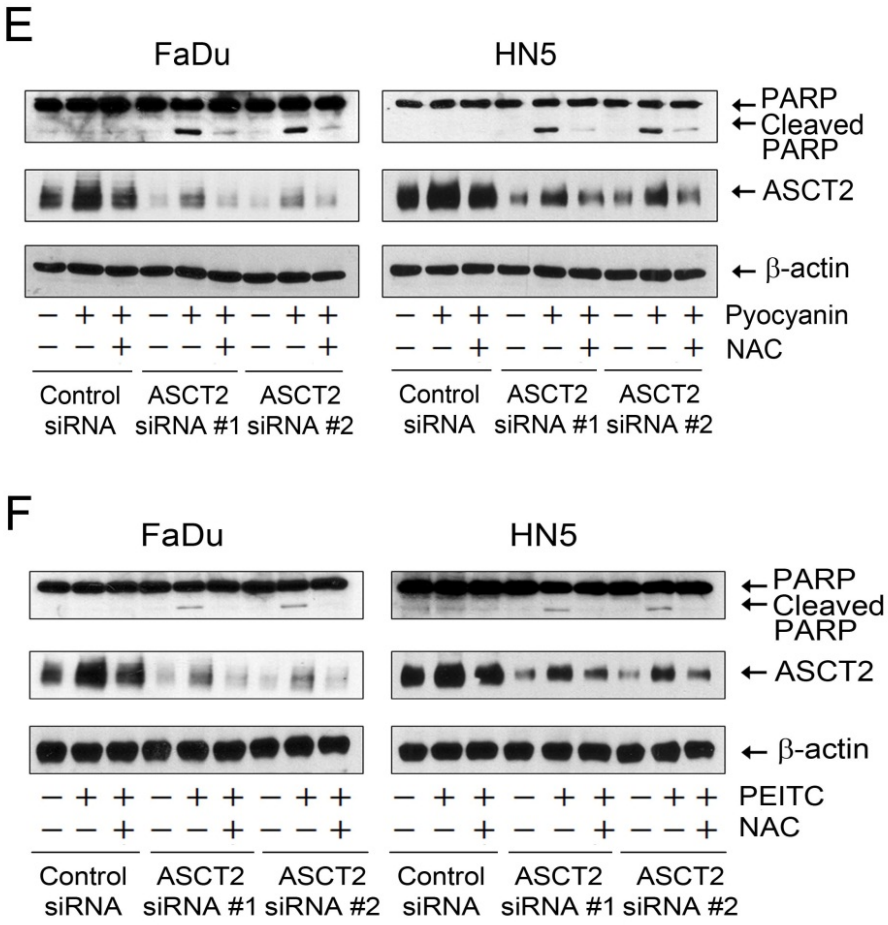

Figure 32. ROS upregulates ASCT2 and knockdown of ASCT2 sensitizes responses to H_2O_2 and other ROS inducers. (A) FaDu and HN5 cells were treated with 1 mM H_2O_2 for 24 hours with and without concurrent treatment of 10 mM NAC. ^{3}H-glutamine uptake was determined afterwards as described in materials and methods. (B) FaDu and HN5 cells were treated with 1 mM H_2O_2 for 24 hours. Intracellular GSH level was measured using the Cayman GSH kit as described in materials and methods. (C) FaDu and HN5 cells transfected with control vector or ASCT2 construct were exposed to 1 mM H_2O_2 for 24 hours with or without concurrent treatment of 10 mM NAC. Cell lysates were prepared for Western blot analysis with indicated antibodies. (D), (E), and (F) FaDu and HN5 cells were subjected to knockdown of ASCT2 with each of 2 individual ASCT2 siRNA or control siRNA for 72 hours. During the last 24 hours, cells were treated with 0.1 mM H_2O_2 (D), 10 μM pyocyanin (E), or 5 μM PEITC (F) with or without concurrent treatment of 10 mM NAC. Cell lysates were prepared for Western blot analysis with indicated antibodies.

5.2.10 Cetuximab downregulates ASCT2, decreases glutamine uptake and GSH levels, sensitizing cancer cells to DCA induced oxidative stress

Upregulation of ASCT2 and subsequent increase of GSH is a major mechanism underlying the resistance to DCA and other ROS inducers. In HN5 cells, treatment with cetuximab significantly downregulated protein level of ASCT2 (Figure 33A), and decreased glutamine uptake (Figure 33B) and intracellular GSH level (Figure 33C), suggesting that cetuximab contributes to the combination treatment with DCA to induce ROS by scavenging intracellular GSH.

Figure 33. Cetuximab downregulates ASCT2, decreases glutamine uptake and intracellular GSH levels. (A) HN5 cells were treated with cetuximab for 24, 48, or 72 hours. Cell lysates were prepared for Western blot analysis with indicated antibodies. (B) HN5 cells were treated as in (A). ^{3}H-glutamine uptake was determined afterwards as described in materials and methods. (C) HN5 cells were treated as in (A). Intracellular GSH level was measured using the Cayman GSH kit as described in materials and methods.

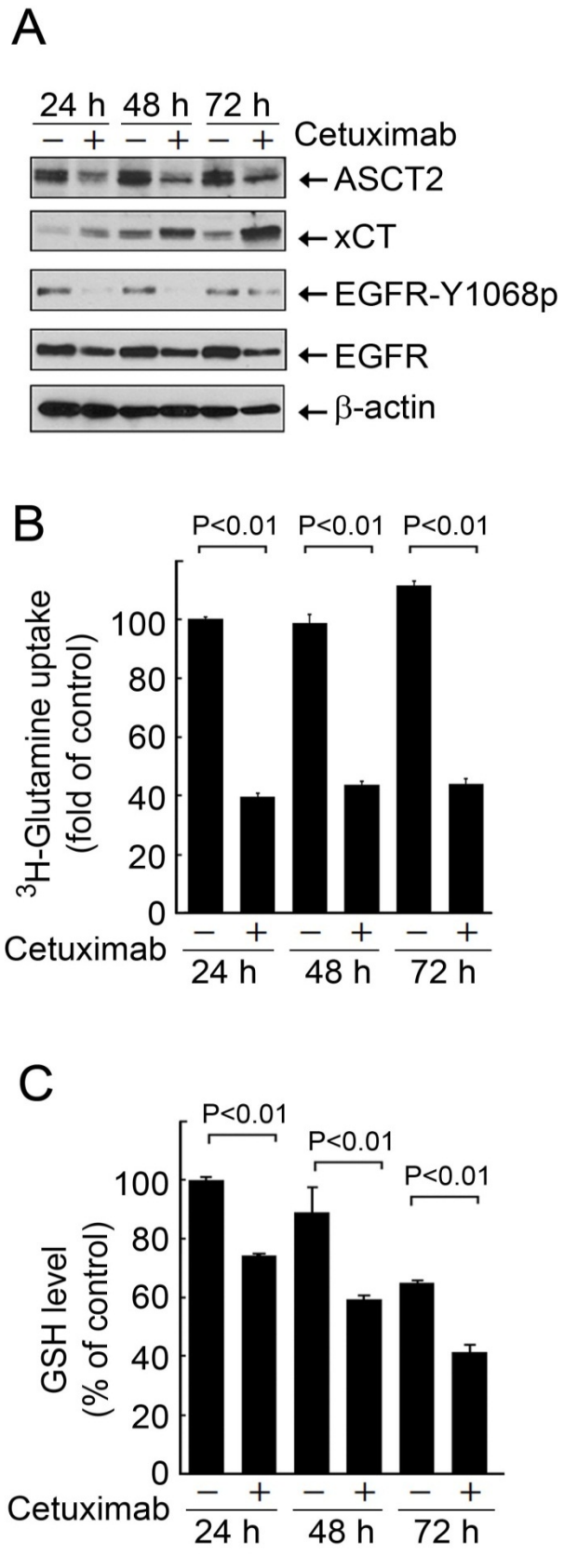
A
24 h
48 h
72 h
Cetuximab
ASCT2
xCT
EGFR-Y1068p
EGFR
β-actin
B
P<0.01
P<0.01
P<0.01
3H-Glutamine uptake
(fold of control)
100
80
60
40
20
0
Cetuximab
24 h
48 h
72 h
C
P<0.01
P<0.01
P<0.01
GSH level
(% of control)
100
80
60
40
20
0
Cetuximab
24 h
48 h
72 h

5.2.11 ASCT2 is associated with EGFR, both of which are co-internalized and degraded by induction of cetuximab

Cetuximab contributes to the combination treatment with targeting PDK1 to induce apoptosis mainly through downregulating ASCT2, and this role of cetuximab should be independent of EGFR kinase activity inhibition. So we hypothesized that cetuximab downregulates ASCT2 through EGFR-mediated internalization and degradation. Through immunoprecipitation, we found that in HN5 cells, ASCT2 and EGFR were associated with each other (Figure 34A). The association of ASCT2 and EGFR was confirmed by immunoprecipitation in multiple HNSCC cells, including FaDu, UMSCC1, UMSCC2, UMSCC22A, UMSCC22B, TU167, MDA1986, and HN30 (Figure 34B). In HN5 cells, treatment with cetuximab for 10 hours induced decreases in EGFR and ASCT2 protein levels in cell membranes, but significant increases in EGFR and ASCT2 protein levels in cytoplasm (Figure 34C), showing the internalization of associated EGFR and ASCT2 induced by cetuximab.

To prove that cetuximab-mediated ASCT2 downregulation is caused by ASCT2 internalization and degradation, HN5 cells were subjected to siRNA of Rab5, a critical factor for the formation of early endosome and membrane protein internalization (Figure 34D and E). Knockdown of Rab5 abolished the role of cetuximab in downregulating ASCT2 and EGFR, as well as decreasing intracellular GSH levels, indicating the critical role of ASCT2 internalization in cetuximab-mediated ASCT2 downregulation and GSH scavenging.

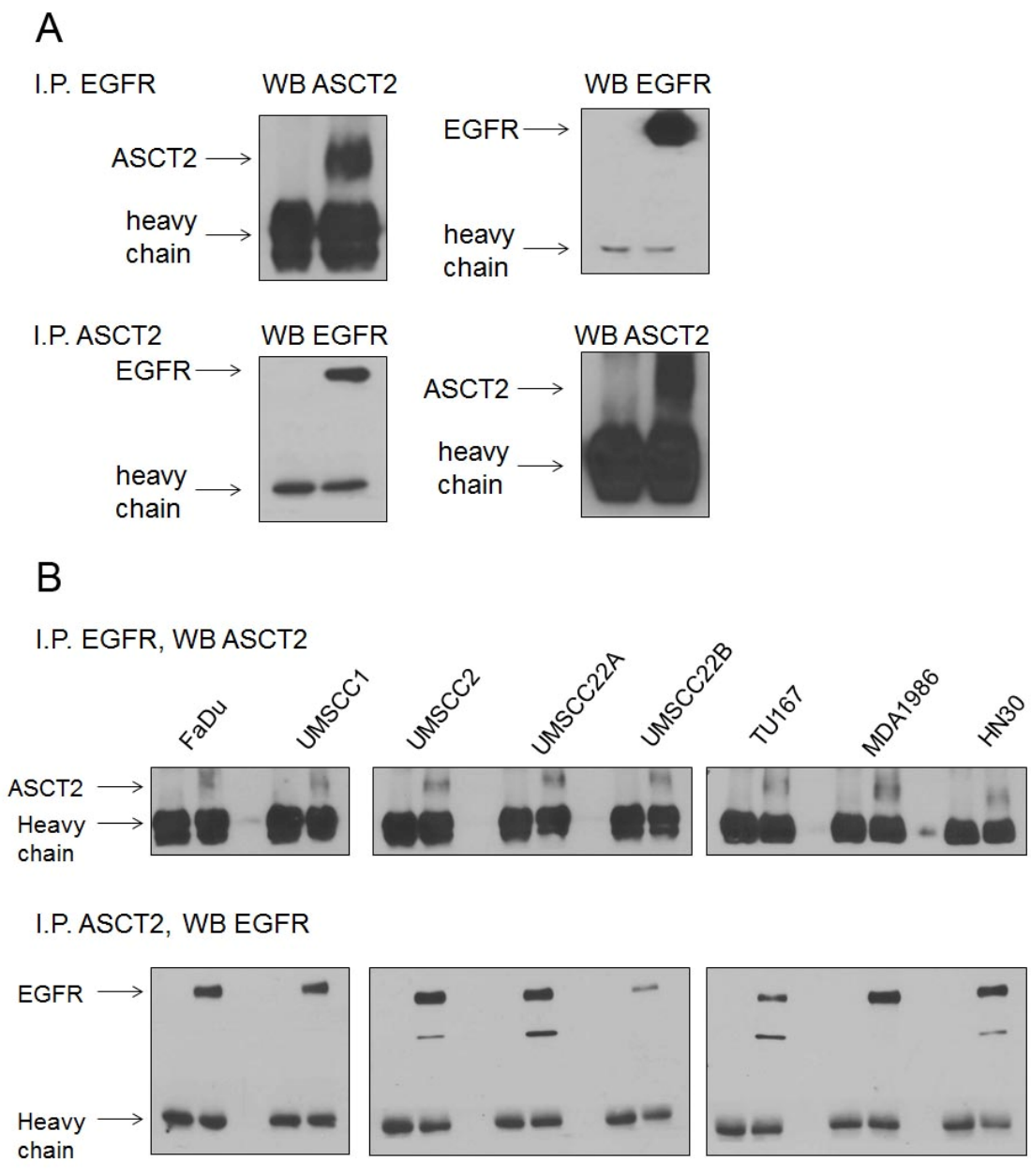
A
I.P. EGFR
WB ASCT2
ASCT2
heavy chain
WB EGFR
EGFR
heavy chain
I.P. ASCT2
WB EGFR
EGFR
heavy chain
WB ASCT2
ASCT2
heavy chain
B
I.P. EGFR, WB ASCT2
FaDu
UMSCC1
UMSCC2
UMSCC22A
UMSCC22B
TU167
MDA1986
HN30
ASCT2
Heavy chain
I.P. ASCT2, WB EGFR
EGFR
Heavy chain

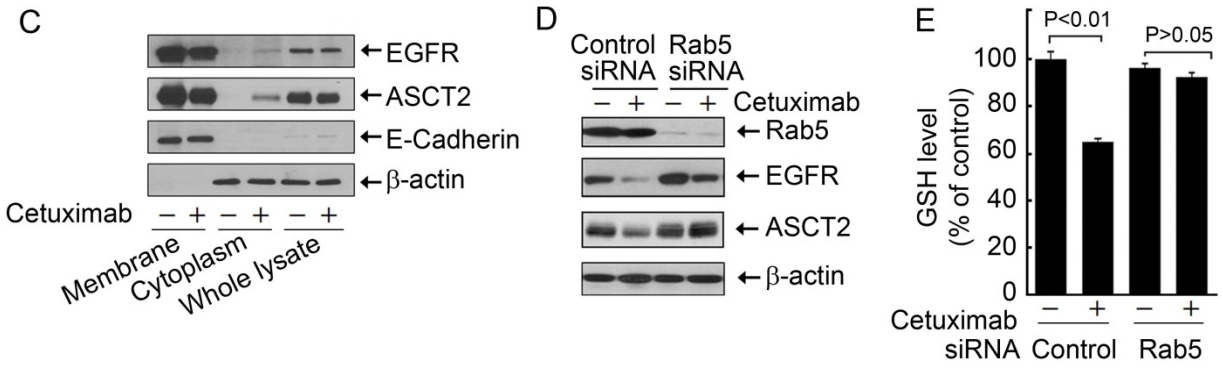

Figure 34. ASCT2 is associated with EGFR, and the complex can be internalized and degraded by cetuximab. (A) HN5 cells were lysed and the lysates were incubated with the anti-EGFR monoclonal antibody cetuximab (4 µg), rabbit anti-ASCT2 antibody (4 µg), or with nonspecific normal mouse immunoglobulin G (IgG) (4 µg), and then incubated with 20 µl protein A beads for 10 hours. The immunoprecipitates were analyzed by Western blot for indicated antibodies. (B) Indicated HNSCC cells were lysed and the lysates were analyzed for association of EGFR and ASCT2 by immunoprecipitation as described in (A). (C) HN5 cells were treated with 20 nM cetuximab for 10 hours. The cells were then subjected to cell membrane and cytoplasmic fractionations for Western blotting with the indicated antibodies. (D) HN5 cells were subjected to knockdown of Rab5 for 72 hours. During the last 24 hours, cells were treated with or without 20 nM cetuximab. Cell lysates were prepared for Western blot analysis with indicated antibodies. (E) HN5 cells were treated as in (D) and intracellular GSH level was measured using the Cayman GSH kit as described in materials and methods.

5.3 Discussion

The major findings in this part are: (1) The combination of cetuximab and PDK1 targeting induces overproduction of ROS and loss of mitochondrial membrane potential, leading to apoptosis; (2) The contribution of cetuximab in the above combination is independent of its function in EGFR kinase activity inhibition; (3) Cetuximab deceases intracellular GSH level through downregulating glutamine transporter ASCT2; (4) ASCT2 is associated with EGFR, and ASCT2-EGFR complex can be co-internalized and degraded mediated by cetuximab. These findings not only reveal a novel role of cetuximab in regulating cellular redox status, but also indicate an innovative therapeutic strategy to improve response to cetuximab, particularly in patients with EGFR-positive but cetuximab-resistant tumors.

A major mechanism underlying resistance to cetuximab is that cetuximab fails to inhibit EGFR downstream signaling cascade, because of oncogene gain-of-function mutation (such as H-Ras), tumor suppressor gene loss-of-function mutation (such as PTEN), and cross activation by activation of other growth factor receptors (such as IGF, c-MET). In this study, we reported that the novel combination effect by cetuximab and PDK1 targeting is independent of EGFR kinase activity inhibition induced by cetuximab. Thus, this novel combination strategy will reverse most currently known cetuximab resistance, if the tumors have expression of EGFR. In addition, since both cetuximab and PDK1 inhibitor DCA have been approved by FDA, findings in this part could be easily translated to clinical trials.

Most cancer cells depend on fast glucose consumption for their survival and continued growth, since the energy yielding efficiency is low for cancer cells which

adopt aerobic glycolysis as the major glucose metabolic pathway. Recently, it was reported that many cancer cells are also addicted to glutamine, although glutamine is considered to be a nonessential amino acid that can be synthesized within the cells [77, 136]. ASCT2 is the major transporter of glutamine in cancer cells. Information from Cancer Genome Anatomy Project (http://cgap.nci.nih.gov) indicates that expression of ASCT2 is elevated in a wide spectrum of primary human cancers compared with adjacent normal tissues. Many cancer cell lines have shown sensitivity to glutamine starvation [137], suggesting glutamine metabolism an appealing target for cancer therapeutics. However, although some glutamine metabolic inhibitors showed a significant cytotoxic effect against certain tumor types both in culture and in mouse xenograft models in preclinical tests, they were discontinued because of dose-limiting neurotoxicity, gastrointestinal toxicity and myelosuppression [138]. Since normal tissues also need uptake of glutamine, directly targeting ASCT2 was also considered to be highly toxic. Here we found that ASCT2 are associated with EGFR, which is overexpressed in many types of cancer. Our current study indicates that cetuximab-mediated EGFR internalization and degradation, which indirectly downregulates ASCT2, is an alternative and effective way to inhibit glutamine uptake and following GSH synthesis.

In addition, the high cancer cell selectivity of our new combination treatment is based on the major difference in metabolism between normal cells and cancer cells that lead them to respond differently to inhibition of PDK1. Normal cells use glucose more efficiently than cancer cells through oxidative phosphorylation in mitochondria. In normal cells, ROS are usually not overproduced. In contrast, cancer cells consume a lot

of glucose via aerobic glycolysis that is preferentially directed toward lactate production. Inhibition of PDK1 forcibly switches cancer metabolism from aerobic glycolysis to oxidative phosphorylation that will cause overproduction of ROS, leading to oxidative stress. Since cancer cells with increased oxidative stress are more vulnerable to damage by further ROS insults, induction of ROS overproduction will be more cytotoxic to cancer cells compared with normal cells.

It is rational to induce overproduction of ROS to selectively induce apoptosis in cancer cells, however, cancer cells respond to increased oxidative stress by increasing the anti-oxidant capacity. Here we found that ASCT2 is upregulated by oxidative stress, leading to the increase of glutamine uptake and intracellular GSH levels. The mechanism underlying the upregulation of ASCT2 by ROS is unknown. Whether upregulation of ASCT2 is a transcriptional or posttranslational effect need to be understood. Elucidation of the molecular players for upregulation of ASCT2 by ROS will provide another target to increase responses to therapeutic strategies by inducing oxidative stress.

An important caveat is that the synthesis of GSH might not only be regulated by uptake of glutamine. ASCT2 regulates the transport of glutamine, cysteine, and a few other neutral amino acids into cells. Because of the oxidizing environment in the extracellular space, most cysteine is oxidized into the dimeric cystine. Cells therefore mainly use the stable cystine as a precursor for GSH synthesis, and cystine is exclusively transported by the Xc(-) cystine/glutamate antiporter, which include xCT, the regulatory subunit of the system, and 4F2hc/CD98, the functional subunit of the system. Once inside the cell, cystine is rapidly reduced to cysteine because of the reducing intracellular milieu. Cysteine was considered to be the rate-limit part for GSH synthesis. Glutamate,

which is converted from glutamine, can either directly contribute to the synthesis of GSH as a precursor, or play a role as a driver to exchange for cysteine through xCT. To understand how ASCT2 upregulates GSH level, we need to determine whether ASCT2 increases GSH biosynthesis simply by directly increasing glutamine uptake and then converting glutamine to glutamate or also requires cooperation of the Xc(-) cystine/glutamate antiporter system. If xCT is also important in regulating GSH synthesis in ASCT2-inhibited cases, an xCT inhibitor, such as sulfasalazine, might be used to further increase the apoptotic effect induced by the combination of cetuximab and PDK1 targeting.

In conclusion, we demonstrated that combination of cetuximab and PDK1 targeting significantly induces apoptosis *in vitro* and *in vivo*, and the cytotoxic effect is independent of EGFR kinase activity inhibition induced by cetuximab. We discovered a novel role of cetuximab in regulating cellular redox status, by mediating internalization and degradation of EGFR-ASCT2 complex. Our findings will lead to a major advance in cetuximab-mediated EGFR targeted therapy by overcoming cetuximab resistance.

Chapter 6 Future direction

6.1 Role of cetuximab-induced downregulation of HIF-1α in sensitizing HNSCC to radiation *in vivo*

Our data in Chapter 3 showed that cetuximab sensitized HNSCC cells to radiation measured by clonogenic assay. Overexpression of HIF-1α-ΔODD conferred resistance to cetuximab-induced anti-tumor effects, and also abolished the role of cetuximab in radiosensitization. This study could be expanded *in vivo* to determine the extent to which overexpression of HIF-1α will confer resistance to cetuximab and radiation, alone and in combination, in mice. HNSCC cells with and without overexpressing the HIF-1α-ΔODD construct will be implanted into SCID mice as xenografts. Mice bearing the xenografts will be treated with cetuximab or equal volume of PBS, either alone or in combination with radiation.

Another finding need to be confirmed *in vivo* is the extent to which targeting HIF-1α through RNAi restores sensitivity of cetuximab-resistant HNSCC to cetuximab and radiation combination treatment. Although EGFR is highly expressed in most head and neck cancers, only a portion of EGFR-positive head and neck cancer respond to cetuximab treatment. Common resistant mechanisms include constitutive activation of important signaling molecules downstream of EGFR, such as oncogenic activation of Ras, or mutational inactivation of tumor suppressor, such as PTEN, or cross activation of EGFR downstream signaling pathways by other growth factor receptors, such as IGF-1R, or c-MET through tumor-stromal interactions, all of which may lead to partial or complete resistance to cetuximab treatment. To test our hypothesis *in vivo*, we will

establish a doxycycline-inducible HIF-1α-knockdown system and choose cetuximab-resistant HNSCC cells that are experimentally established (HN5-RasG12V and FaDu-RasG12V) and naturally occurring (OSC19 and UMSCC1) as our cell models. The cells expressing the inducible HIF-1α shRNA construct or control vector will be implanted into SCID mice as xenografts. Mice bearing xenograft will be fed with doxycycline-containing water before radiation, with or without concurrent treatment with cetuximab. Mice without receiving any treatment will be included as the control groups.

Whether radiation itself can upregulate HIF-1α in human head and neck cancer cells *in vivo*, and whether it can be blocked by cetuximab treatment also need to be determined. HN5 and FaDu cells stably expressing the HRE-luciferase reporter construct or control vector will be implanted into SCID mice and irradiated at different doses, with or without one single dose of cetuximab right after radiation. Intratumoral HIF-1α activity will be monitored by real time in vivo imaging of luciferase activity in tumor xenografts at different time intervals after intraperitoneal injection of luciferin. The xenografts in some mice will be surgically removed after irradiation and subjected to immunohistochemical staining with an anti-HIF-1α antibody.

6.2 Value of ^{18}FDG-PET for early prediction of response to cetuximab

^{18}FDG-PET is commonly used in the clinic to detect cancers because of the enhanced uptake of glucose by cancer cells as a result of increased glycolysis and glucose transport. Our data showed that HIF-1α is downregulated by cetuximab in sensitive but not resistant cells and that downregulation of HIF-1α is required for cetuximab's antiproliferative effects. HIF-1 plays a critical role in cancer cell growth and

survival by activating genes encoding for glycolysis. Thus, inhibition of glycolysis through targeting HIF-1α is an important mechanism underlying cetuximab's antiproliferative effects. This novel concept of the mechanism of cetuximab could be used as a biomarker for early predication of responses to cetuximab treatment. We expect that cetuximab-sensitive cells will show reduced ^{18}FDG uptake due to functional inhibition of glycolysis by cetuximab before tumor volumetric changes become apparent, whereas cetuximab-resistant cells will not show reduced ^{18}FDG uptake.

6.3 Role of AMPK-mediated energy homeostasis in mediating cancer cell resistance to cetuximab

Our findings in Chapter 4 established the impact of inhibition of bioenergetics and biosynthetic metabolism on cetuximab's antiproliferative effects in cetuximab-sensitive HNSCC cell lines. However, the resistant mechanism to cetuximab, in the perspective of metabolism, is not clear. Unpublished data in our lab suggested that the activity of AMPK may protect cells from cetuximab treatment: specifically, co-treatment of cetuximab-resistant HNSCC cells with compound C, a small molecule AMPK inhibitor, induced apoptosis, whereas either agent alone had no such effect. AMPK is typically activated in response to reduced cell bioenergetics metabolism in order to maintain energy homeostasis by stimulating fatty acid oxidation [139, 140] and glycolysis [141, 142], and suppressing cell biosynthesis through inhibition of the mTOR pathway and lipogenic pathways [143, 144]. AMPK can also be activated by Src activity through LKB1 independently of the AMP/ATP ratio in the cells [145-148]. Our lab previously reported that unsuppressed Src activity after cetuximab treatment is associated with

resistance to cetuximab [149]. We thus propose that unsuppressed Src activity confers resistance to cetuximab in part through regulating AMPK activity.

To confirm the role of AMPK in cancer cell response to cetuximab, we will compare the response to cetuximab of HNSCC cells with and without knockdown of AMPK expression by siRNA. If silencing AMPK enhances HNSCC cell response to cetuximab *in vitro*, we will expand the study to determine whether silencing of AMPK enhances response to cetuximab *in vivo*. We will establish a doxycycline-inducible AMPK-knockdown system and transfect the constructs containing doxycycline-inducible AMPK shRNA or control shRNA into luciferase positive, cetuximab resistant HNSCC cell lines and select stable expression pooled cells. Successfully characterized cells will be implanted as xenografts. Mice with established xenograft will be treated with cetuximab or equal amount of PBS with or without concurrent exposure to doxycycline added into the drinking water.

6.4 Role of ASCT2 in resistance to apoptosis induced by overproduction of ROS

In 5.2.7 and 5.2.8, we showed that DCA and other ROS inducer, including H_2O_2, pyocyanin, and PEITC, upregulate ASCT2. However, the underlying mechanism is unknown. To elucidate the mechanisms by which ROS leads to upregulation of ASCT2, we will perform ASCT2 real-time PCR, luciferase reporter assays and ^{35}S-metabolic pulse chase assays. Depending on whether these assays reveal a transcriptional or a posttranslational mechanism or both, we will pursue additional studies to identify molecular players and the mechanisms through which ROS upregulate ASCT2.

As discussed in 5.3, how glutamine, which is uptaken by ASCT2, contributes to GSH synthesis is not clear. Glutamine is converted to glutamate within the cells catalyzed by glutaminase. Glutamate can either directly contribute to GSH synthesis one of the precursors, or work as the driving force for the uptake of cystine, which is considered to be the rate-limit precursor for the synthesis of GSH, through Xc(-) cystine/glutamate antiporter system. We will address this question by assessing whether knockdown of xCT has any effect on ASCT2-stimulated GSH synthesis. To further determine whether ASCT2 is an independent determinant of GSH biosynthesis, we will add reducing agent β-mercaptoethanol into cell culture medium, which will chemically reduce cystine to cysteine and thus provide an unrestricted source of cysteine for GSH synthesis independent of xCT, and examine whether knockdown of ASCT2 affects GSH biosynthesis.

The role of ASCT2 in protecting cells from ROS-induced apoptosis could be confirmed *in vivo*. We will establish a doxycycline-inducible ASCT2-knockdown system. The HNSCC cells expressing the inducible ASCT2 shRNA construct or control vector will be implanted into nude mice as xenografts. Mice bearing xenograft will be fed with or without doxycycline-containing water, and with or without treatment of DCA.

6.5 Mechanism of interaction between EGFR and ASCT2

In 5.2.10, we showed that ASCT2 is associated with EGFR. Next, we will investigate how EGFR and ASCT2 form a complex. We will co-transfect HEK293 cells with ASCT2 and one of each of the following EGFR constructs: wild-type EGFR, kinase-dead EGFR, extracellular-domain EGFR, intracellular-domain EGFR, and the

juxtamembrane region plus the kinase domain. We will determine which part on the EGFR molecule is required for pull-down with ASCT2 by co-immunoprecipitation using ASCT2 antibody.

6.6 Effect of inhibiting xCT on improving the therapeutic outcome of combination treatment with cetuximab plus DCA *in vitro* and *in vivo*

In Figure 33A, we found that there was a compensatory increase in the level of xCT after downregulation of ASCT2 be cetuximab, which may increase intracellular GSH level via increasing cysteine uptake and lead to resistance to the combination treatment of cetuximab and PDK1 targeting. We hypothesize that adding xCT inhibitor sulfasalazine to combination treatment with cetuximab plus DCA improves the therapeutic outcome. We will confirm the inhibitory effect of sulfasalazine on the Xc(-) system by measuring the level of ^{35}S-cystine uptake with or without sulfasalazine treatment in HNSCC cells. We will examine whether the compensatory increase in xCT induced by cetuximab is accompanied by increased ^{35}S-cystine uptake. We will then determine whether addition of sulfasalazine increases the induction of ROS and apoptosis by the combination of cetuximab and DCA in cultured HNSCC cells. To determine whether sulfasalazine can significantly improve the therapeutic outcome *in vivo*, we will compare the responses of HNSCC xenografts to the combination of cetuximab and DCA, with and without sulfasalazine, as well as any treatment alone.

BIBLIOGRAPHY

1. Rothenberg, SM and Ellisen, LW. The molecular pathogenesis of head and neck squamous cell carcinoma. *J Clin Invest*, 2012. 122(6): 1951-1957.
2. Ang, KK. Multidisciplinary management of locally advanced SCCHN: optimizing treatment outcomes. *Oncologist*, 2008. 13(8): 899-910.
3. Hashibe, M, Hunt, J, Wei, M, Buys, S, Gren, L, and Lee, YC. Tobacco, alcohol, body mass index, physical activity, and the risk of head and neck cancer in the prostate, lung, colorectal, and ovarian (PLCO) cohort. *Head Neck*, 2012.
4. Maier, H, Dietz, A, Gewelke, U, Heller, WD, and Weidauer, H. Tobacco and alcohol and the risk of head and neck cancer. *Clin Investig*, 1992. 70(3-4): 320-327.
5. Mork, J, Lie, AK, Glattre, E, Hallmans, G, Jellum, E, Koskela, P, Moller, B, Pukkala, E, Schiller, JT, Youngman, L, Lehtinen, M, and Dillner, J. Human papillomavirus infection as a risk factor for squamous-cell carcinoma of the head and neck. *N Engl J Med*, 2001. 344(15): 1125-1131.
6. Induction chemotherapy plus radiation compared with surgery plus radiation in patients with advanced laryngeal cancer. The Department of Veterans Affairs Laryngeal Cancer Study Group. *N Engl J Med*, 1991. 324(24): 1685-1690.
7. Lee, J and Moon, C. Current status of experimental therapeutics for head and neck cancer. *Exp Biol Med (Maywood)*, 2011. 236(4): 375-389.
8. Cohen, EE, Lingen, MW, and Vokes, EE. The expanding role of systemic therapy in head and neck cancer. *J Clin Oncol*, 2004. 22(9): 1743-1752.

9. Pignon, JP, Bourhis, J, Domenge, C, and Designe, L. Chemotherapy added to locoregional treatment for head and neck squamous-cell carcinoma: three meta-analyses of updated individual data. MACH-NC Collaborative Group. Meta-Analysis of Chemotherapy on Head and Neck Cancer. *Lancet*, 2000. 355(9208): 949-955.

10. Forastiere, AA, Goepfert, H, Maor, M, Pajak, TF, Weber, R, Morrison, W, Glisson, B, Trotti, A, Ridge, JA, Chao, C, Peters, G, Lee, DJ, Leaf, A, Ensley, J, and Cooper, J. Concurrent chemotherapy and radiotherapy for organ preservation in advanced laryngeal cancer. *N Engl J Med*, 2003. 349(22): 2091-2098.

11. Howard, JD, Lu, B, and Chung, CH. Therapeutic targets in head and neck squamous cell carcinoma: identification, evaluation, and clinical translation. *Oral Oncol*, 2012. 48(1): 10-17.

12. Pryor, DI, Solomon, B, and Porceddu, SV. The emerging era of personalized therapy in squamous cell carcinoma of the head and neck. *Asia Pac J Clin Oncol*, 2011. 7(3): 236-251.

13. Herbst, RS. Review of epidermal growth factor receptor biology. *Int J Radiat Oncol Biol Phys*, 2004. 59(2 Suppl): 21-26.

14. Yarden, Y and Schlessinger, J. Epidermal growth factor induces rapid, reversible aggregation of the purified epidermal growth factor receptor. *Biochemistry*, 1987. 26(5): 1443-1451.

15. Downward, J, Parker, P, and Waterfield, MD. Autophosphorylation sites on the epidermal growth factor receptor. *Nature*, 1984. 311(5985): 483-485.

16. Oda, K, Matsuoka, Y, Funahashi, A, and Kitano, H. A comprehensive pathway map of epidermal growth factor receptor signaling. *Mol Syst Biol*, 2005. 1(2005 0010.

17. Ishitoya, J, Toriyama, M, Oguchi, N, Kitamura, K, Ohshima, M, Asano, K, and Yamamoto, T. Gene amplification and overexpression of EGF receptor in squamous cell carcinomas of the head and neck. *Br J Cancer*, 1989. 59(4): 559-562.

18. Grandis, JR and Tweardy, DJ. Elevated levels of transforming growth factor alpha and epidermal growth factor receptor messenger RNA are early markers of carcinogenesis in head and neck cancer. *Cancer Res*, 1993. 53(15): 3579-3584.

19. Liang, K, Ang, KK, Milas, L, Hunter, N, and Fan, Z. The epidermal growth factor receptor mediates radioresistance. *Int J Radiat Oncol Biol Phys*, 2003. 57(1): 246-254.

20. Milas, L, Mason, K, Hunter, N, Petersen, S, Yamakawa, M, Ang, K, Mendelsohn, J, and Fan, Z. In vivo enhancement of tumor radioresponse by C225 antiepidermal growth factor receptor antibody. *Clin Cancer Res*, 2000. 6(2): 701-708.

21. Nakata, E, Hunter, N, Mason, K, Fan, Z, Ang, KK, and Milas, L. C225 antiepidermal growth factor receptor antibody enhances the efficacy of docetaxel chemoradiotherapy. *Int J Radiat Oncol Biol Phys*, 2004. 59(4): 1163-1173.

22. Bonner, JA, Buchsbaum, DJ, Russo, SM, Fiveash, JB, Trummell, HQ, Curiel, DT, and Raisch, KP. Anti-EGFR-mediated radiosensitization as a result of

augmented EGFR expression. *Int J Radiat Oncol Biol Phys*, 2004. 59(2 Suppl): 2-10.

23. Bonner, JA, Harari, PM, Giralt, J, Azarnia, N, Shin, DM, Cohen, RB, Jones, CU, Sur, R, Raben, D, Jassem, J, Ove, R, Kies, MS, Baselga, J, Youssoufian, H, Amellal, N, Rowinsky, EK, and Ang, KK. Radiotherapy plus cetuximab for squamous-cell carcinoma of the head and neck. *N Engl J Med*, 2006. 354(6): 567-578.

24. Santini, J, Formento, JL, Francoual, M, Milano, G, Schneider, M, Dassonville, O, and Demard, F. Characterization, quantification, and potential clinical value of the epidermal growth factor receptor in head and neck squamous cell carcinomas. *Head Neck*, 1991. 13(2): 132-139.

25. Rubin Grandis, J, Melhem, MF, Gooding, WE, Day, R, Holst, VA, Wagener, MM, Drenning, SD, and Tweardy, DJ. Levels of TGF-alpha and EGFR protein in head and neck squamous cell carcinoma and patient survival. *J Natl Cancer Inst*, 1998. 90(11): 824-832.

26. Goldstein, NI, Prewett, M, Zuklys, K, Rockwell, P, and Mendelsohn, J. Biological efficacy of a chimeric antibody to the epidermal growth factor receptor in a human tumor xenograft model. *Clin Cancer Res*, 1995. 1(11): 1311-1318.

27. Gill, GN, Kawamoto, T, Cochet, C, Le, A, Sato, JD, Masui, H, McLeod, C, and Mendelsohn, J. Monoclonal anti-epidermal growth factor receptor antibodies which are inhibitors of epidermal growth factor binding and antagonists of epidermal growth factor binding and antagonists of epidermal growth factor-

stimulated tyrosine protein kinase activity. *J Biol Chem*, 1984. 259(12): 7755-7760.

28. Schlessinger, J. Cell signaling by receptor tyrosine kinases. *Cell*, 2000. 103(2): 211-225.

29. Fan, Z, Lu, Y, Wu, X, and Mendelsohn, J. Antibody-induced epidermal growth factor receptor dimerization mediates inhibition of autocrine proliferation of A431 squamous carcinoma cells. *J Biol Chem*, 1994. 269(44): 27595-27602.

30. Wu, X, Rubin, M, Fan, Z, DeBlasio, T, Soos, T, Koff, A, and Mendelsohn, J. Involvement of p27KIP1 in G1 arrest mediated by an anti-epidermal growth factor receptor monoclonal antibody. *Oncogene*, 1996. 12(7): 1397-1403.

31. Peng, D, Fan, Z, Lu, Y, DeBlasio, T, Scher, H, and Mendelsohn, J. Anti-epidermal growth factor receptor monoclonal antibody 225 up-regulates p27KIP1 and induces G1 arrest in prostatic cancer cell line DU145. *Cancer Res*, 1996. 56(16): 3666-3669.

32. Huang, SM, Bock, JM, and Harari, PM. Epidermal growth factor receptor blockade with C225 modulates proliferation, apoptosis, and radiosensitivity in squamous cell carcinomas of the head and neck. *Cancer Res*, 1999. 59(8): 1935-1940.

33. Petit, AM, Rak, J, Hung, MC, Rockwell, P, Goldstein, N, Fendly, B, and Kerbel, RS. Neutralizing antibodies against epidermal growth factor and ErbB-2/neu receptor tyrosine kinases down-regulate vascular endothelial growth factor production by tumor cells in vitro and in vivo: angiogenic implications for signal transduction therapy of solid tumors. *Am J Pathol*, 1997. 151(6): 1523-1530.

34. Perrotte, P, Matsumoto, T, Inoue, K, Kuniyasu, H, Eve, BY, Hicklin, DJ, Radinsky, R, and Dinney, CP. Anti-epidermal growth factor receptor antibody C225 inhibits angiogenesis in human transitional cell carcinoma growing orthotopically in nude mice. *Clin Cancer Res*, 1999. 5(2): 257-265.

35. Wu, X, Fan, Z, Masui, H, Rosen, N, and Mendelsohn, J. Apoptosis induced by an anti-epidermal growth factor receptor monoclonal antibody in a human colorectal carcinoma cell line and its delay by insulin. *J Clin Invest*, 1995. 95(4): 1897-1905.

36. Vermorken, JB, Mesia, R, Rivera, F, Remenar, E, Kawecki, A, Rottey, S, Erfan, J, Zabolotnyy, D, Kienzer, HR, Cupissol, D, Peyrade, F, Benasso, M, Vynnychenko, I, De Raucourt, D, Bokemeyer, C, Schueler, A, Amellal, N, and Hitt, R. Platinum-based chemotherapy plus cetuximab in head and neck cancer. *N Engl J Med*, 2008. 359(11): 1116-1127.

37. Vaupel, P and Mayer, A. Hypoxia in cancer: significance and impact on clinical outcome. *Cancer Metastasis Rev*, 2007. 26(2): 225-239.

38. Gray, LH, Conger, AD, Ebert, M, Hornsey, S, and Scott, OC. The concentration of oxygen dissolved in tissues at the time of irradiation as a factor in radiotherapy. *Br J Radiol*, 1953. 26(312): 638-648.

39. Thomlinson, RH and Gray, LH. The histological structure of some human lung cancers and the possible implications for radiotherapy. *Br J Cancer*, 1955. 9(4): 539-549.

40. Rankin, EB and Giaccia, AJ. The role of hypoxia-inducible factors in tumorigenesis. *Cell Death Differ*, 2008. 15(4): 678-685.

41. Reyes, H, Reisz-Porszasz, S, and Hankinson, O. Identification of the Ah receptor nuclear translocator protein (Arnt) as a component of the DNA binding form of the Ah receptor. *Science*, 1992. 256(5060): 1193-1195.

42. Whitelaw, ML, Gustafsson, JA, and Poellinger, L. Identification of transactivation and repression functions of the dioxin receptor and its basic helix-loop-helix/PAS partner factor Arnt: inducible versus constitutive modes of regulation. *Mol Cell Biol*, 1994. 14(12): 8343-8355.

43. Maxwell, PH, Wiesener, MS, Chang, GW, Clifford, SC, Vaux, EC, Cockman, ME, Wykoff, CC, Pugh, CW, Maher, ER, and Ratcliffe, PJ. The tumour suppressor protein VHL targets hypoxia-inducible factors for oxygen-dependent proteolysis. *Nature*, 1999. 399(6733): 271-275.

44. Jaakkola, P, Mole, DR, Tian, YM, Wilson, MI, Gielbert, J, Gaskell, SJ, von Kriegsheim, A, Hebestreit, HF, Mukherji, M, Schofield, CJ, Maxwell, PH, Pugh, CW, and Ratcliffe, PJ. Targeting of HIF-alpha to the von Hippel-Lindau ubiquitylation complex by O2-regulated prolyl hydroxylation. *Science*, 2001. 292(5516): 468-472.

45. Ivan, M, Kondo, K, Yang, H, Kim, W, Valiando, J, Ohh, M, Salic, A, Asara, JM, Lane, WS, and Kaelin, WG, Jr. HIFalpha targeted for VHL-mediated destruction by proline hydroxylation: implications for O2 sensing. *Science*, 2001. 292(5516): 464-468.

46. Mahon, PC, Hirota, K, and Semenza, GL. FIH-1: a novel protein that interacts with HIF-1alpha and VHL to mediate repression of HIF-1 transcriptional activity. *Genes Dev*, 2001. 15(20): 2675-2686.

47. Lando, D, Peet, DJ, Whelan, DA, Gorman, JJ, and Whitelaw, ML. Asparagine hydroxylation of the HIF transactivation domain a hypoxic switch. *Science*, 2002. 295(5556): 858-861.

48. Fukuda, R, Hirota, K, Fan, F, Jung, YD, Ellis, LM, and Semenza, GL. Insulin-like growth factor 1 induces hypoxia-inducible factor 1-mediated vascular endothelial growth factor expression, which is dependent on MAP kinase and phosphatidylinositol 3-kinase signaling in colon cancer cells. *J Biol Chem*, 2002. 277(41): 38205-38211.

49. Laughner, E, Taghavi, P, Chiles, K, Mahon, PC, and Semenza, GL. HER2 (neu) signaling increases the rate of hypoxia-inducible factor 1alpha (HIF-1alpha) synthesis: novel mechanism for HIF-1-mediated vascular endothelial growth factor expression. *Mol Cell Biol*, 2001. 21(12): 3995-4004.

50. Zhong, H, Chiles, K, Feldser, D, Laughner, E, Hanrahan, C, Georgescu, MM, Simons, JW, and Semenza, GL. Modulation of hypoxia-inducible factor 1alpha expression by the epidermal growth factor/phosphatidylinositol 3-kinase/PTEN/AKT/FRAP pathway in human prostate cancer cells: implications for tumor angiogenesis and therapeutics. *Cancer Res*, 2000. 60(6): 1541-1545.

51. Wang, GL and Semenza, GL. Purification and characterization of hypoxia-inducible factor 1. *J Biol Chem*, 1995. 270(3): 1230-1237.

52. Semenza, GL. Hypoxia-inducible factor 1: oxygen homeostasis and disease pathophysiology. *Trends Mol Med*, 2001. 7(8): 345-350.

53. Warburg, O. On respiratory impairment in cancer cells. *Science*, 1956. 124(3215): 269-270.

54. Warburg, O. On the origin of cancer cells. *Science*, 1956. 123(3191): 309-314.

55. Guppy, M, Greiner, E, and Brand, K. The role of the Crabtree effect and an endogenous fuel in the energy metabolism of resting and proliferating thymocytes. *Eur J Biochem*, 1993. 212(1): 95-99.

56. Chen, C, Pore, N, Behrooz, A, Ismail-Beigi, F, and Maity, A. Regulation of glut1 mRNA by hypoxia-inducible factor-1. Interaction between H-ras and hypoxia. *J Biol Chem*, 2001. 276(12): 9519-9525.

57. Gleadle, JM and Ratcliffe, PJ. Induction of hypoxia-inducible factor-1, erythropoietin, vascular endothelial growth factor, and glucose transporter-1 by hypoxia: evidence against a regulatory role for Src kinase. *Blood*, 1997. 89(2): 503-509.

58. Mathupala, SP, Rempel, A, and Pedersen, PL. Glucose catabolism in cancer cells: identification and characterization of a marked activation response of the type II hexokinase gene to hypoxic conditions. *J Biol Chem*, 2001. 276(46): 43407-43412.

59. Iyer, NV, Kotch, LE, Agani, F, Leung, SW, Laughner, E, Wenger, RH, Gassmann, M, Gearhart, JD, Lawler, AM, Yu, AY, and Semenza, GL. Cellular and developmental control of O2 homeostasis by hypoxia-inducible factor 1 alpha. *Genes Dev*, 1998. 12(2): 149-162.

60. Semenza, GL, Roth, PH, Fang, HM, and Wang, GL. Transcriptional regulation of genes encoding glycolytic enzymes by hypoxia-inducible factor 1. *J Biol Chem*, 1994. 269(38): 23757-23763.

61. Minchenko, O, Opentanova, I, and Caro, J. Hypoxic regulation of the 6-phosphofructo-2-kinase/fructose-2,6-bisphosphatase gene family (PFKFB-1-4) expression in vivo. *FEBS Lett*, 2003. 554(3): 264-270.

62. Firth, JD, Ebert, BL, and Ratcliffe, PJ. Hypoxic regulation of lactate dehydrogenase A. Interaction between hypoxia-inducible factor 1 and cAMP response elements. *J Biol Chem*, 1995. 270(36): 21021-21027.

63. Ullah, MS, Davies, AJ, and Halestrap, AP. The plasma membrane lactate transporter MCT4, but not MCT1, is up-regulated by hypoxia through a HIF-1alpha-dependent mechanism. *J Biol Chem*, 2006. 281(14): 9030-9037.

64. Kim, JW, Tchernyshyov, I, Semenza, GL, and Dang, CV. HIF-1-mediated expression of pyruvate dehydrogenase kinase: a metabolic switch required for cellular adaptation to hypoxia. *Cell Metab*, 2006. 3(3): 177-185.

65. Papandreou, I, Cairns, RA, Fontana, L, Lim, AL, and Denko, NC. HIF-1 mediates adaptation to hypoxia by actively downregulating mitochondrial oxygen consumption. *Cell Metab*, 2006. 3(3): 187-197.

66. Zhang, H, Gao, P, Fukuda, R, Kumar, G, Krishnamachary, B, Zeller, KI, Dang, CV, and Semenza, GL. HIF-1 inhibits mitochondrial biogenesis and cellular respiration in VHL-deficient renal cell carcinoma by repression of C-MYC activity. *Cancer Cell*, 2007. 11(5): 407-420.

67. Fukuda, R, Zhang, H, Kim, JW, Shimoda, L, Dang, CV, and Semenza, GL. HIF-1 regulates cytochrome oxidase subunits to optimize efficiency of respiration in hypoxic cells. *Cell*, 2007. 129(1): 111-122.

68. Denko, NC. Hypoxia, HIF1 and glucose metabolism in the solid tumour. *Nat Rev Cancer*, 2008. 8(9): 705-713.

69. Hamanaka, RB and Chandel, NS. Mitochondrial reactive oxygen species regulate cellular signaling and dictate biological outcomes. *Trends Biochem Sci*, 2010. 35(9): 505-513.

70. Kroemer, G and Pouyssegur, J. Tumor cell metabolism: cancer's Achilles' heel. *Cancer Cell*, 2008. 13(6): 472-482.

71. Pompella, A, Visvikis, A, Paolicchi, A, De Tata, V, and Casini, AF. The changing faces of glutathione, a cellular protagonist. *Biochem Pharmacol*, 2003. 66(8): 1499-1503.

72. Trachootham, D, Alexandre, J, and Huang, P. Targeting cancer cells by ROS-mediated mechanisms: a radical therapeutic approach? *Nat Rev Drug Discov*, 2009. 8(7): 579-591.

73. Harington, CR and Mead, TH. Synthesis of glutathione. *Biochem J*, 1935. 29(7): 1602-1611.

74. Bannai, S. Transport of cystine and cysteine in mammalian cells. *Biochim Biophys Acta*, 1984. 779(3): 289-306.

75. Maddocks, OD, Berkers, CR, Mason, SM, Zheng, L, Blyth, K, Gottlieb, E, and Vousden, KH. Serine starvation induces stress and p53-dependent metabolic remodelling in cancer cells. *Nature*, 2013. 493(7433): 542-546.

76. DeBerardinis, RJ and Cheng, T. Q's next: the diverse functions of glutamine in metabolism, cell biology and cancer. *Oncogene*, 2010. 29(3): 313-324.

77. Eagle, H. The specific amino acid requirements of a mammalian cell (strain L) in tissue culture. *J Biol Chem*, 1955. 214(2): 839-852.

78. Ko, C and Citrin, D. Radiotherapy for the management of locally advanced squamous cell carcinoma of the head and neck. *Oral Dis*, 2009. 15(2): 121-132.

79. Bonner, JA, Buchsbaum, DJ, Rogers, BE, Grizzle, WE, Trummell, HQ, Curiel, DT, Fiveash, JB, Ove, R, and Raisch, KP. Adenoviral vector-mediated augmentation of epidermal growth factor receptor (EGFr) enhances the radiosensitization properties of anti-EGFr treatment in prostate cancer cells. *Int J Radiat Oncol Biol Phys*, 2004. 58(3): 950-958.

80. Chung, CH, Zhang, Q, Hammond, EM, Trotti, AM, 3rd, Wang, H, Spencer, S, Zhang, HZ, Cooper, J, Jordan, R, Rotman, MH, and Ang, KK. Integrating epidermal growth factor receptor assay with clinical parameters improves risk classification for relapse and survival in head-and-neck squamous cell carcinoma. *Int J Radiat Oncol Biol Phys*, 2011. 81(2): 331-338.

81. Bonner, JA, Harari, PM, Giralt, J, Cohen, RB, Jones, CU, Sur, RK, Raben, D, Baselga, J, Spencer, SA, Zhu, J, Youssoufian, H, Rowinsky, EK, and Ang, KK. Radiotherapy plus cetuximab for locoregionally advanced head and neck cancer: 5-year survival data from a phase 3 randomised trial, and relation between cetuximab-induced rash and survival. *Lancet Oncol*, 2010. 11(1): 21-28.

82. Roots, R and Smith, KC. On the nature of the oxygen effect on x-ray-induced DNA single-strand breaks in mammalian cells. *Int J Radiat Biol Relat Stud Phys Chem Med*, 1974. 26(5): 467-480.

83. Quintiliani, M. Modification of radiation sensitivity: the oxygen effect. *Int J Radiat Oncol Biol Phys*, 1979. 5(7): 1069-1076.

84. Brizel, DM, Scully, SP, Harrelson, JM, Layfield, LJ, Bean, JM, Prosnitz, LR, and Dewhirst, MW. Tumor oxygenation predicts for the likelihood of distant metastases in human soft tissue sarcoma. *Cancer Res*, 1996. 56(5): 941-943.

85. Brizel, DM, Sibley, GS, Prosnitz, LR, Scher, RL, and Dewhirst, MW. Tumor hypoxia adversely affects the prognosis of carcinoma of the head and neck. *Int J Radiat Oncol Biol Phys*, 1997. 38(2): 285-289.

86. Hockel, M, Schlenger, K, Aral, B, Mitze, M, Schaffer, U, and Vaupel, P. Association between tumor hypoxia and malignant progression in advanced cancer of the uterine cervix. *Cancer Res*, 1996. 56(19): 4509-4515.

87. Nordsmark, M and Overgaard, J. A confirmatory prognostic study on oxygenation status and loco-regional control in advanced head and neck squamous cell carcinoma treated by radiation therapy. *Radiother Oncol*, 2000. 57(1): 39-43.

88. Li, X, Lu, Y, Liang, K, Pan, T, Mendelsohn, J, and Fan, Z. Requirement of hypoxia-inducible factor-1alpha down-regulation in mediating the antitumor activity of the anti-epidermal growth factor receptor monoclonal antibody cetuximab. *Mol Cancer Ther*, 2008. 7(5): 1207-1217.

89. Lu, Y, Liang, K, Li, X, and Fan, Z. Responses of cancer cells with wild-type or tyrosine kinase domain-mutated epidermal growth factor receptor (EGFR) to EGFR-targeted therapy are linked to downregulation of hypoxia-inducible factor-1alpha. *Mol Cancer*, 2007. 6(63.

90. Lu, Y, Li, X, Lu, H, and Fan, Z. 1, 9-Pyrazoloanthrones downregulate HIF-1alpha and sensitize cancer cells to cetuximab-mediated anti-EGFR therapy. *PLoS One*, 2010. 5(12): e15823.

91. Moeller, BJ, Cao, Y, Li, CY, and Dewhirst, MW. Radiation activates HIF-1 to regulate vascular radiosensitivity in tumors: role of reoxygenation, free radicals, and stress granules. *Cancer Cell*, 2004. 5(5): 429-441.

92. Kim, WY, Oh, SH, Woo, JK, Hong, WK, and Lee, HY. Targeting heat shock protein 90 overrides the resistance of lung cancer cells by blocking radiation-induced stabilization of hypoxia-inducible factor-1alpha. *Cancer Res*, 2009. 69(4): 1624-1632.

93. Li, F, Sonveaux, P, Rabbani, ZN, Liu, S, Yan, B, Huang, Q, Vujaskovic, Z, Dewhirst, MW, and Li, CY. Regulation of HIF-1alpha stability through S-nitrosylation. *Mol Cell*, 2007. 26(1): 63-74.

94. Wheeler, DL, Huang, S, Kruser, TJ, Nechrebecki, MM, Armstrong, EA, Benavente, S, Gondi, V, Hsu, KT, and Harari, PM. Mechanisms of acquired resistance to cetuximab: role of HER (ErbB) family members. *Oncogene*, 2008. 27(28): 3944-3956.

95. Harari, PM, Wheeler, DL, and Grandis, JR. Molecular target approaches in head and neck cancer: epidermal growth factor receptor and beyond. *Semin Radiat Oncol*, 2009. 19(1): 63-68.

96. Chen, LF, Cohen, EE, and Grandis, JR. New strategies in head and neck cancer: understanding resistance to epidermal growth factor receptor inhibitors. *Clin Cancer Res*, 2010. 16(9): 2489-2495.

97. Luwor, RB, Lu, Y, Li, X, Mendelsohn, J, and Fan, Z. The antiepidermal growth factor receptor monoclonal antibody cetuximab/C225 reduces hypoxia-inducible factor-1 alpha, leading to transcriptional inhibition of vascular endothelial growth factor expression. *Oncogene*, 2005. 24(27): 4433-4441.

98. Aebersold, DM, Burri, P, Beer, KT, Laissue, J, Djonov, V, Greiner, RH, and Semenza, GL. Expression of hypoxia-inducible factor-1alpha: a novel predictive and prognostic parameter in the radiotherapy of oropharyngeal cancer. *Cancer Res*, 2001. 61(7): 2911-2916.

99. Liu, J, Zhang, J, Wang, X, Li, Y, Chen, Y, Li, K, Yao, L, and Guo, G. HIF-1 and NDRG2 contribute to hypoxia-induced radioresistance of cervical cancer Hela cells. *Exp Cell Res*, 2010. 316(12): 1985-1993.

100. Unruh, A, Ressel, A, Mohamed, HG, Johnson, RS, Nadrowitz, R, Richter, E, Katschinski, DM, and Wenger, RH. The hypoxia-inducible factor-1 alpha is a negative factor for tumor therapy. *Oncogene*, 2003. 22(21): 3213-3220.

101. Harada, H, Kizaka-Kondoh, S, Li, G, Itasaka, S, Shibuya, K, Inoue, M, and Hiraoka, M. Significance of HIF-1-active cells in angiogenesis and radioresistance. *Oncogene*, 2007. 26(54): 7508-7516.

102. Kim, JW, Kim, HP, Im, SA, Kang, S, Hur, HS, Yoon, YK, Oh, DY, Kim, JH, Lee, DS, Kim, TY, and Bang, YJ. The growth inhibitory effect of lapatinib, a dual inhibitor of EGFR and HER2 tyrosine kinase, in gastric cancer cell lines. *Cancer Lett*, 2008. 272(2): 296-306.

103. Moeller, BJ, Dreher, MR, Rabbani, ZN, Schroeder, T, Cao, Y, Li, CY, and Dewhirst, MW. Pleiotropic effects of HIF-1 blockade on tumor radiosensitivity. *Cancer Cell*, 2005. 8(2): 99-110.

104. Hsu, PP and Sabatini, DM. Cancer cell metabolism: Warburg and beyond. *Cell*, 2008. 134(5): 703-707.

105. Dang, CV and Semenza, GL. Oncogenic alterations of metabolism. *Trends Biochem Sci*, 1999. 24(2): 68-72.

106. Vander Heiden, MG, Cantley, LC, and Thompson, CB. Understanding the Warburg effect: the metabolic requirements of cell proliferation. *Science*, 2009. 324(5930): 1029-1033.

107. DeBerardinis, RJ, Lum, JJ, Hatzivassiliou, G, and Thompson, CB. The biology of cancer: metabolic reprogramming fuels cell growth and proliferation. *Cell Metab*, 2008. 7(1): 11-20.

108. Deberardinis, RJ, Sayed, N, Ditsworth, D, and Thompson, CB. Brick by brick: metabolism and tumor cell growth. *Curr Opin Genet Dev*, 2008. 18(1): 54-61.

109. Grander, D. How do mutated oncogenes and tumor suppressor genes cause cancer? *Med Oncol*, 1998. 15(1): 20-26.

110. Semenza, GL. Hypoxia, clonal selection, and the role of HIF-1 in tumor progression. *Crit Rev Biochem Mol Biol*, 2000. 35(2): 71-103.

111. Semenza, GL. Involvement of hypoxia-inducible factor 1 in human cancer. *Intern Med*, 2002. 41(2): 79-83.

112. Semenza, GL. Defining the role of hypoxia-inducible factor 1 in cancer biology and therapeutics. *Oncogene*, 2010. 29(5): 625-634.

113. Jiang, BH, Agani, F, Passaniti, A, and Semenza, GL. V-SRC induces expression of hypoxia-inducible factor 1 (HIF-1) and transcription of genes encoding vascular endothelial growth factor and enolase 1: involvement of HIF-1 in tumor progression. *Cancer Res*, 1997. 57(23): 5328-5335.

114. Treins, C, Giorgetti-Peraldi, S, Murdaca, J, Semenza, GL, and Van Obberghen, E. Insulin stimulates hypoxia-inducible factor 1 through a phosphatidylinositol 3-kinase/target of rapamycin-dependent signaling pathway. *J Biol Chem*, 2002. 277(31): 27975-27981.

115. Lu, H, Liang, K, Lu, Y, and Fan, Z. The anti-EGFR antibody cetuximab sensitizes human head and neck squamous cell carcinoma cells to radiation in part through inhibiting radiation-induced upregulation of HIF-1alpha. *Cancer Lett*, 2012. 322(1): 78-85.

116. Li, X and Fan, Z. The epidermal growth factor receptor antibody cetuximab induces autophagy in cancer cells by downregulating HIF-1alpha and Bcl-2 and activating the beclin 1/hVps34 complex. *Cancer Res*, 2010. 70(14): 5942-5952.

117. Vander Heiden, MG, Locasale, JW, Swanson, KD, Sharfi, H, Heffron, GJ, Amador-Noguez, D, Christofk, HR, Wagner, G, Rabinowitz, JD, Asara, JM, and Cantley, LC. Evidence for an alternative glycolytic pathway in rapidly proliferating cells. *Science*, 2010. 329(5998): 1492-1499.

118. Zhao, Y, Liu, H, Liu, Z, Ding, Y, Ledoux, SP, Wilson, GL, Voellmy, R, Lin, Y, Lin, W, Nahta, R, Liu, B, Fodstad, O, Chen, J, Wu, Y, Price, JE, and Tan, M. Overcoming trastuzumab resistance in breast cancer by targeting dysregulated glucose metabolism. *Cancer Res*, 2011. 71(13): 4585-4597.

119. Vermorken, JB, Trigo, J, Hitt, R, Koralewski, P, Diaz-Rubio, E, Rolland, F, Knecht, R, Amellal, N, Schueler, A, and Baselga, J. Open-label, uncontrolled, multicenter phase II study to evaluate the efficacy and toxicity of cetuximab as a single agent in patients with recurrent and/or metastatic squamous cell carcinoma of the head and neck who failed to respond to platinum-based therapy. *J Clin Oncol*, 2007. 25(16): 2171-2177.

120. Goerner, M, Seiwert, TY, and Sudhoff, H. Molecular targeted therapies in head and neck cancer--an update of recent developments. *Head Neck Oncol*, 2010. 2(8.

121. Wheeler, DL, Dunn, EF, and Harari, PM. Understanding resistance to EGFR inhibitors-impact on future treatment strategies. *Nat Rev Clin Oncol*, 2010. 7(9): 493-507.

122. Fan, Z, Shang, BY, Lu, Y, Chou, JL, and Mendelsohn, J. Reciprocal changes in p27(Kip1) and p21(Cip1) in growth inhibition mediated by blockade or overstimulation of epidermal growth factor receptors. *Clin Cancer Res*, 1997. 3(11): 1943-1948.

123. Chou, JL, Fan, Z, DeBlasio, T, Koff, A, Rosen, N, and Mendelsohn, J. Constitutive overexpression of cyclin D1 in human breast epithelial cells does not prevent G1 arrest induced by deprivation of epidermal growth factor. *Breast Cancer Res Treat*, 1999. 55(3): 267-283.

124. Chandel, NS and Schumacker, PT. Cellular oxygen sensing by mitochondria: old questions, new insight. *J Appl Physiol*, 2000. 88(5): 1880-1889.

125. Droge, W. Free radicals in the physiological control of cell function. *Physiol Rev*, 2002. 82(1): 47-95.

126. Turrens, JF. Mitochondrial formation of reactive oxygen species. *J Physiol*, 2003. 552(Pt 2): 335-344.

127. Murphy, MP. How mitochondria produce reactive oxygen species. *Biochem J*, 2009. 417(1): 1-13.

128. Toyokuni, S, Okamoto, K, Yodoi, J, and Hiai, H. Persistent oxidative stress in cancer. *FEBS Lett*, 1995. 358(1): 1-3.

129. Hileman, EA, Achanta, G, and Huang, P. Superoxide dismutase: an emerging target for cancer therapeutics. *Expert Opin Ther Targets*, 2001. 5(6): 697-710.

130. Kang, D and Hamasaki, N. Mitochondrial oxidative stress and mitochondrial DNA. *Clin Chem Lab Med*, 2003. 41(10): 1281-1288.

131. Behrend, L, Henderson, G, and Zwacka, RM. Reactive oxygen species in oncogenic transformation. *Biochem Soc Trans*, 2003. 31(Pt 6): 1441-1444.

132. Pelicano, H, Carney, D, and Huang, P. ROS stress in cancer cells and therapeutic implications. *Drug Resist Updat*, 2004. 7(2): 97-110.

133. Schumacker, PT. Reactive oxygen species in cancer cells: live by the sword, die by the sword. *Cancer Cell*, 2006. 10(3): 175-176.

134. Green, DR and Reed, JC. Mitochondria and apoptosis. *Science*, 1998. 281(5381): 1309-1312.

135. Xiao, D, Powolny, AA, Moura, MB, Kelley, EE, Bommareddy, A, Kim, SH, Hahm, ER, Normolle, D, Van Houten, B, and Singh, SV. Phenethyl isothiocyanate inhibits oxidative phosphorylation to trigger reactive oxygen species-mediated death of human prostate cancer cells. *J Biol Chem*, 2010. 285(34): 26558-26569.

136. Wise, DR and Thompson, CB. Glutamine addiction: a new therapeutic target in cancer. *Trends Biochem Sci*, 2010. 35(8): 427-433.

137. Wu, MC, Arimura, GK, and Yunis, AA. Mechanism of sensitivity of cultured pancreatic carcinoma to asparaginase. *Int J Cancer*, 1978. 22(6): 728-733.

138. Ahluwalia, GS, Grem, JL, Hao, Z, and Cooney, DA. Metabolism and action of amino acid analog anti-cancer agents. *Pharmacol Ther*, 1990. 46(2): 243-271.

139. Carling, D, Zammit, VA, and Hardie, DG. A common bicyclic protein kinase cascade inactivates the regulatory enzymes of fatty acid and cholesterol biosynthesis. *FEBS Lett*, 1987. 223(2): 217-222.

140. Li, Y, Xu, S, Mihaylova, MM, Zheng, B, Hou, X, Jiang, B, Park, O, Luo, Z, Lefai, E, Shyy, JY, Gao, B, Wierzbicki, M, Verbeuren, TJ, Shaw, RJ, Cohen, RA, and Zang, M. AMPK phosphorylates and inhibits SREBP activity to attenuate hepatic steatosis and atherosclerosis in diet-induced insulin-resistant mice. *Cell Metab*, 2011. 13(4): 376-388.

141. Marsin, AS, Bertrand, L, Rider, MH, Deprez, J, Beauloye, C, Vincent, MF, Van den Berghe, G, Carling, D, and Hue, L. Phosphorylation and activation of heart PFK-2 by AMPK has a role in the stimulation of glycolysis during ischaemia. *Curr Biol*, 2000. 10(20): 1247-1255.

142. Shaw, RJ. Glucose metabolism and cancer. *Curr Opin Cell Biol*, 2006. 18(6): 598-608.

143. Inoki, K, Zhu, T, and Guan, KL. TSC2 mediates cellular energy response to control cell growth and survival. *Cell*, 2003. 115(5): 577-590.

144. Gwinn, DM, Shackelford, DB, Egan, DF, Mihaylova, MM, Mery, A, Vasquez, DS, Turk, BE, and Shaw, RJ. AMPK phosphorylation of raptor mediates a metabolic checkpoint. *Mol Cell*, 2008. 30(2): 214-226.

145. Mizrachy-Schwartz, S, Cohen, N, Klein, S, Kravchenko-Balasha, N, and Levitzki, A. Up-regulation of AMP-activated protein kinase in cancer cell lines is mediated through c-Src activation. *J Biol Chem*, 2011. 286(17): 15268-15277.

146. Zou, MH, Hou, XY, Shi, CM, Kirkpatick, S, Liu, F, Goldman, MH, and Cohen, RA. Activation of 5'-AMP-activated kinase is mediated through c-Src and phosphoinositide 3-kinase activity during hypoxia-reoxygenation of bovine aortic endothelial cells. Role of peroxynitrite. *J Biol Chem*, 2003. 278(36): 34003-34010.

147. Zou, MH, Kirkpatrick, SS, Davis, BJ, Nelson, JS, Wiles, WGt, Schlattner, U, Neumann, D, Brownlee, M, Freeman, MB, and Goldman, MH. Activation of the AMP-activated protein kinase by the anti-diabetic drug metformin in vivo. Role of mitochondrial reactive nitrogen species. *J Biol Chem*, 2004. 279(42): 43940-43951.

148. Yamada, E, Pessin, JE, Kurland, IJ, Schwartz, GJ, and Bastie, CC. Fyn-dependent regulation of energy expenditure and body weight is mediated by tyrosine phosphorylation of LKB1. *Cell Metab*, 2010. 11(2): 113-124.

149. Lu, Y, Li, X, Liang, K, Luwor, R, Siddik, ZH, Mills, GB, Mendelsohn, J, and Fan, Z. Epidermal growth factor receptor (EGFR) ubiquitination as a mechanism of acquired resistance escaping treatment by the anti-EGFR monoclonal antibody cetuximab. *Cancer Res*, 2007. 67(17): 8240-8247.

VITA

Haiquan Lu was born in Jinan, China on January 13, 1984, the son of Feng Lu and Yunmin Wu. After graduating from Shandong Experimental High School in 2002, he enrolled at Shandong Normal University in Jinan, China. There he received his Bachelor of Science degree with a major in Biological Sciences in 2006. After completing his undergraduate degree, he moved to United States of America and received his Master of Science degree in Cell Biology at Fordham University in New York city in 2008. At the same year, he entered The University of Texas Health Science Center at Houston, Graduate School of Biomedical Sciences and MD Anderson Cancer Center. He worked in Dr. Zhen Fan's lab for his Ph.D. project, focusing on the novel functions of cetuximab.

Permanent Address:

172 Jiwang Road, 1-1-202,

Jinan, Shandong, China, 250014